To the Graduate Council:

I am submitting herewith a thesis written by Charlotte M. Farmer entitled "Liquid-Liquid Extraction in a Batch Agitated Vessel with Non-Newtonian Dispersed Phase." I have examined the final copy of this thesis for form and content and recommend that it be accepted in partial fulfillment of the requirements for the degree of Master of Science, with a major in Chemical Engineering.

Dr. Trueman D. Parish, Major Professor

We have read this thesis
and recommend its acceptance:

Dr. Donald C. Bogue

Dr. George C. Frazier

Accepted for the Council:

Associate Vice Chancellor
and Dean of The Graduate School

LIQUID-LIQUID EXTRACTION IN A BATCH AGITATED VESSEL WITH A NON-NEWTONIAN DISPERSED PHASE

A Thesis

Presented for the

Master of Science

Degree

The University of Tennessee, Knoxville

Charlotte M. Farmer

December 1996

DEDICATION

This thesis is dedicated to my husband and children

Derek L. Farmer

and

G. James Farmer, Derel Charlton Farmer, Nia Dominique Taylor Farmer

who have managed with out me during Graduate studies.

ACKNOWLEDGMENTS

The author wishes to express her deep appreciation to Dr. T. D. Parish in the planning, implementation, and reporting of the work.

The author is very grateful to Dr. D. C. Bogue, Dr. G. C. Frazier, and Dr. J. S. Kanel for their guidance during the course of the study.

Appreciation is also extended to Eastman Chemical Company for their permission to perform the experimental work in the Organic Chemicals Development Lab.

Lastly, the author wishes express her appreciation to Abby Solomon and Ann Lacava for their significant contributions in formatting and editing.

ABSTRACT

Chemical industry utilizes solvent extraction as an alternative to conventional distillation, specifically for the separation of liquid mixtures with unfavorable vapor-liquid equilibria relationships and/or thermally unstable components. Common to most extraction applications (i.e., mixer settler, multistage tower extractors, rotating disc contactors, etc.) is the transfer of material taking place to or from drops of one liquid dispersed in another. Thus, a more complete knowledge of the factors affecting transfer to and from drops is essential to further understanding extraction and the development of improved design principles.

An extensive literature search indicates that much work has been done over the years to develop mass transfer coefficient models for both continuous-phase (k_c) and dispersed-phase (k_d) controlling systems. However, all of the liquid-liquid systems studied to date have included Newtonian materials with aqueous continuos phases. Industrial streams tend to be solutions containing several components with a range of Newtonian to non-Newtonian flow characteristics; thus rendering them significantly different from systems featured in mass transfer studies to date. This study is unique in that it centers on purification of a non-Newtonian industrial stream containing three major components (cellulose acetate, acetic acid, water) and a solute (sodium sulfate). Before dispersing in a predominantly aqueous solution, a solvent (isopropyl acetate) was added to the stream to prevent precipitation of the cellulose acetate (this solution is later referred to as solvated dope). The composition of the contacting solution was determined experimentally. To this end, a quaternary phase diagram was constructed for cellulose acetate, acetic acid, water, and isopropyl acetate to identify the feasible operating region where liquid-liquid phases exist without formation of a solid cellulose acetate phase. A

key requirement was to operate on a tie line, in the phase diagram described above, to deter transfer of nonsolutes across phase boundaries.

This research measured the dispersed-phase mass transfer coefficient, and the corresponding drop sizes in the system described above where the dispersed phase, solvated dope, was a viscous fluid. This was achieved by measuring solute concentration in the continuous-phase over time analytically with discrete samples. A mass balance calculation on the system was used to calculate the disappearance of solute from the dispersed-phase. In turn, the solute concentration data was used to estimate the dispersed-phase mass transfer coefficient.

The resulting correlation for dispersed-phase mass transfer was compared with expressions derived in the literature (for systems similar to the basic assumptions of this study). In conclusion:

1. Both the Penetration Theory (Higbie, 1935) and the Skelland and HuXien Model (1990) underestimate the dispersed-phase mass transfer coefficient in this kind of system. Therefore these expressions will yield a conservative extractor design.
2. The difference between the measured value of k_d and that estimated from Penetration Theory could be accounted for by errors in the physical and transport property estimations especially diffusivity, D_{AB} which is difficult to estimate for the liquid-liquid system described herein.
3. Experimentally estimated drop sizes generally agree with the Hong and Lee (1985) Sauter-mean diameter model.

4. As expected, the continuous-phase mass transfer coefficient had very little influence on the overall mass transfer coefficient as predicted by the Skelland and Moeti (1990) expression.

TABLE OF CONTENTS

LIST OF TABLES

Appendix

LIST OF FIGURES

CHAPTER 1
INTRODUCTION

Purpose and Method of the Investigation

Statement of the Problem

Garner and Hale (1955) recognized solvent extraction as a viable alternative to conventional distillation, specifically for the separation of liquid mixtures with unfavorable vapor liquid equilibrium relationships and/or thermally unstable components. Common to most extraction applications (i.e. mixer settlers, multistage tower extractors, etc.), transfer of material takes place to or from drops of one liquid dispersed in another. Thus, a more complete knowledge of the factors affecting transfer to and from drops is essential to the further understanding of extraction and the development of improved design principles (Garner and Hale, 1955).

An extensive literature search indicates that much work has been done over the years to develop mass transfer coefficients models for both continuous-phase (k_c) and disperse phase (k_d) controlling systems. However, all of the liquid-liquid systems studied to date have included Newtonian materials. Hence, there exists a need for an accurate correlation for mass transfer from a non-Newtonian droplet to a Newtonian continuous-phase.

Objective of Investigation

The objective of this work is to derive an experimental correlation for approximating k_d's in systems where the dispersed-phase is a highly viscous liquid with pseudo-plastic behavior. We will compare our correlation for k_d with expressions derived in the literature (for systems that are similar to our basic assumptions) to determine the

need for a new model. In addition, we compare the observed droplet size with the size predicted by an empirical correlation by Hong and Lee (1985).

The system investigated involves an extraction process for purifying cellulose acetate dope. Cellulose acetate dope is obtained by acetylation and subsequent hydrolysis of cellulose and consists of acetic acid, cellulose acetate, water, and ppm concentrations of sulfate salts. During extraction, the cellulose acetate dope is contacted with a predominantly aqueous-phase. Salt is preferentially soluble in the aqueous fluid and thus transferred from the organic to the aqueous-phase. A complicating factor in this process is the precipitation of the solid cellulose acetate at high aqueous levels, and the strong influence of the dissolved cellulose acetate concentration on the viscosity, and thus handling characteristics of the organic liquid-phase. As a result, co-solvents are added to both phases, an organic solvent (with low solubility in water) to the cellulose acetate dope phase and mixture of acetic acid and organic solvent to the aqueous-phase to establish concentrations within both phases such that all components are in equilibrium except the sulfate salt.

Assumptions

1. The dispersed-phase is a non-Newtonian fluid of the power law type.
2. Shear rates in the bulk phase transfer into the dispersed-phase. Per Kanel, et al. (1991), the correlation of Skelland and Hu Xien(1990) (developed for Newtonian liquid-liquid systems) may be extended to include the non-Newtonian behavior of one phase by application of the Skelland and Kanel (1990) technique. This method was used to extend correlations for the minimum impeller speed for complete dispersion of one immiscible liquid in another to include the case where the phases were non-Newtonian of the power law type. The apparent average viscosity, μ_a, of the fluid in the agitated vessel was computed as

$$\mu_a = K\left|\left(\frac{du}{dy}\right)_a\right|^{n-1} \tag{1.1}$$

where K is the fluid consistency index and n is the flow behavior index, both representative of the non-Newtonian fluid. The apparent shear rate, (du/dy), was found by Metzner and Taylor (1960) to be equivalent to the impeller speed multiplied by a constant, k_S, which was found to have an approximate value of 11 by Metzner et al. (1961) when the impeller speed, N, is in rpm. Thus,

$$\left(\frac{du}{dy}\right)_a = k_s N \tag{1.2}$$

The apparent viscosity was then substituted into the mean viscosity expression of Vermeulen et al. (1955) for the appropriate phase (either dispersed or continuous),

$$\mu_m = \frac{\mu_c}{1-\phi}\left[1 + \frac{1.5\mu_d\phi}{\mu_d + \mu_c}\right] \tag{1.3}$$

where ϕ is the volume fraction of the dispersed-phase, μ_m is the mean viscosity, and μ_c and μ_d are the continuous and dispersed-phase viscosities, respectively.

3. The solute is a sulfate salt which undergoes unimolal unidirectional diffusion through the dispersed-phase into the continuous-phase. The solute, present at low concentrations (~1700 ppm) in the dispersed-phase, is readily received by the predominantly polar continuous-phase.

4. Internal circulation does not occur within the droplets. This assumption is well founded due to the high viscosity (1,000,000 cP magnitude) of the dispersed-phase. Further still, based on photographic evidence presented by Thorton et al. (1985, 1987), Skelland and Hu Xien (1990) deduce that points on the surface of a drop newly formed (whether from a nozzle or breakage) remained undisturbed by the process of detachment. These findings prevailed at nozzle Reynolds numbers as high as 300 and actual break-off times of less than 50 milliseconds. Skelland and Hu Xien (1990) suggest that the drops are internally stagnant between consecutive breakups, and substantiate this with references to similar statements to this end by Harriott (1962) and by Calderbank (1967). In this regard, the "degree of [internal] circulation" for these drops, estimated as described by Clift et al. (1978), is around zero, in accordance with the same indications by Davies (1972). It is understood from Skelland and Lee (1981) that in order to study dispersed-phase controlled mass transfer, it is necessary to keep most of the resistance to transfer inside that phase. The theory of stagnation may be validated comparing experimentally observed dispersed-phase drop sizes with Kolmogoroff's length scale,

$$\eta = \varepsilon^{-\frac{1}{4}} \upsilon^{\frac{3}{4}} \tag{1.4}$$

which marks the upper limit of eddy sizes in the viscous sub-range. (Skelland and Moeti, 1990). In this correlation, eddy length scale, η, is related to the rate of energy dissipation per unit mass of fluid, ε, and kinematic viscosity, ν, where

$$\varepsilon = \frac{4 K_T}{\pi} \frac{d_I^5 N^3}{d_v^3} \tag{1.5}$$

and

$$\upsilon = \frac{\mu}{\rho} . \tag{1.6}$$

Please refer to the Appendix A1 for an explanation of nomenclature.

5. The droplets are small and spherical with no oscillation effects, slip or fluctuating velocity during agitation.
6. The bulk composition of the droplets will not change. Contacting of the cellulose acetate dope/isopropyl acetate mixture with an aqueous-phase, in a proper phase ratio, results in the formation of two immiscible liquid phases whose compositions lie on either side of the phase envelope boundary connected by the tie line containing the mixture point (See Figure 4.5). If the organic and aqueous-phases do not lie on the same tie line, solvents such as water, acetic acid and isopropyl acetate will transfer between the phases. Diffusion of these components will change the physical and transport properties of the resulting immiscible phases. Therefore, a contacting scheme must be devised to insure that both phases are on the same tie-line throughout each experimental run.
7. The overall mass transfer coefficient, K_d, is essentially equal to the dispersed-phase mass transfer coefficient k_d (Treybal, 1980),

$$K_d \approx k_d . \tag{1.7}$$

Based on the relationship from Hines and Maddox (1985),

$$\frac{1}{K_d} = \frac{1}{k_d} + \frac{1}{mk_c}, \tag{1.8}$$

k_C must then be much greater than k_d such that $1/mk_C$ is essentially negligible.

8. The resistance to transfer in the continuous-phase is negligible, so that the surface concentration of the sphere is constant at C_a^* in equilibrium with the entire continuous phase-the latter having constant composition. (Skelland, 1985) It is therefore assumed that the concentration C_a inside the droplet is much greater than the concentration C_a^*, at the surface of the droplet.
9. The total interfacial area available for mass transfer is essentially constant during mass transfer.

Theoretical Development

A solute mass balance for transport from the dispersed-phase to the continuous-phase can be written as

$$V_d dC_a = k_d A(C_a^* - C_a)dt \ , \tag{1.9}$$

where V_d is the volume of the dispersed-phase, t is time, and C_a is the concentration of the solute in the dispersed-phase at time t (Kanel, 1990). Based on the assumption that C_a is much greater than C_a^*, $(C_a^* - C_a)$ becomes $(-C_a)$. In Appendix Table A5.3, for example, C_a^* = 3.31E-06g/ml (at t=3960seconds) is two orders of magnitude lower than C_a during solute transfer (t<300seconds) which ranges from (8.3E-04 at t=0seconds to 3.0E-04g/ml at t=360seconds.

A is the total interfacial area available for mass transfer, and could increase as droplets separate into smaller droplets over time. Simplification of A/V_d as shown in Appendix 2 gives,

$$\frac{A}{V_d} = \frac{6}{d_p}$$

Substituting the time dependent expression for drop size, d_p, from Hong and Lee's (1985) empirical model for the Sauter-mean diameter, $d32$ (equation 5.5) gives,

$$\frac{A}{V_d} = \frac{6}{d_{32}^{*} + \alpha t^{-0.7}} \tag{1.10}$$

The constants d_{32}^{*} and α are discussed in Chapter 5.

Finally, substitution of 1.10 into 1.9 followed by variable separation and integration from concentration C_{ao} to C_a gives,

$$\ln\frac{C_a}{C_{ao}} = -6k_d \int_0 \frac{1}{\alpha(t)^{-0.7} + d_{32}^{*}} dt \tag{1.11}.$$

The right-hand side of the equation is an open-ended integral and must be solved numerically. Appendix 2 contains the numerical integration of the right-hand side of equation 1.11.

Assuming that the change in A is negligible during transfer, equation 1.9 after separation of variables and integration gives,

$$\ln\left(\frac{C_a}{C_{ao}}\right) = -\frac{k_d A}{V_d}(t - t_o) \tag{1.12}$$

Scope of Investigation

This investigation was divided into three parts: the literature survey (shown in Table 1.1), the experimental study, and the comparison of published mass transfer coefficient

correlations.

The experimental study consisted of five parts: choosing an optimal cosolvent, measuring physical and transport properties, establishing feasible experimental regions, determining mass transfer rate, and predicting the dispersed-phase mass transfer coefficient.

Literature Survey

Discussion

Table 1.1 summarizes prior experimental work gleamed from a literature search on mass transfer in agitated vessels. Like the continuous mass transfer coefficient (k_c), dispersed-phase mass transfer coefficient (k_d) in agitated vessels may be correlated with operating variables and physical properties of liquid-liquid systems. Howarth (1963) proposed two alternative mechanisms of mass transfer in an agitated vessel. The first assumption was "neither coalescence nor breakage occurs while drops are in the agitated vessel." The second assumption was "rapid coalescence and redispersion of the drops, with application of the penetration theory." Followed by Howarth, Schindler and Treybal (1968), Keey and Glen (1969), and Treybal (1971) studied liquid-liquid mass transfer rates in agitated vessels; all of these investigations were confined to single systems, so comprehensive correlations over a range of physical properties were not established. In a study by Skelland and Lee (1981), five systems were used (to measure and correlate k_c's along with corresponding drop sizes), although diffusivity varied only 1.5 fold.

Skelland and Hu Xien (1990) measured disperse-phase mass transfer rates on three agitated liquid-liquid systems (They also varied impeller speed and dispersed-phase

Table 1.1: Highlights of previous experimental work on mass transfer coefficients.

Workers	Continuous, C Batch, B	System	Cont. Phase	Disp. Droplets	*Coef.*
Garner, Hale (1955)	C	ternary	water	rigid, circulating	k_d, k_c
Rushton, Nagata, Rooney (1964)	B	ternary	water	rigid	*KA*
Boyadzhiev, Alenkov (1966)	B	ternary	water	rigid	k_c
Schindler, Treybal (1968)	C	binary	water	circulating	k_c
Keey, Glen (1969)	C	ternary	water	circulating	k_c
Mok, Treybal (1971)	C	binary	water	circulating	k_c
Skelland, Lee (1981)	B	ternary	water	circulating	k_c
Bapat, Tavlarides (1983)	C	ternary	water	circulating	k_c
Skelland, Moeti (1990)	B	ternary	water	rigid	k_c
Skelland, Hu Xien(1990)	B	ternary	water	rigid	k_d
Skelland, Kanel (1990)	B	ternary	water	rigid, circulating	k_d, k_c

volume fraction.). These exhibited 4.8-fold and 8.6-fold variations in diffusivity and viscosity, respectively, in the dispersed-phase. Building on experimental investigations, Bapat et al. (1983,1985) applied Monte Carlo simulation techniques to predict mass transfer and drop sizes in a continuous-flow agitated vessel. Following this work, Skelland and Kanel (1990) developed a simulation of mass transfer in a batch agitated liquid-liquid dispersion. Apparently, few studies have been published on mass transfer in agitated liquid-liquid systems in baffled vessels: and until recently, upon the work of Skelland and Hu Xien (1990), all have been confined to the continuous-phase.

Almost identical to the system proposed here is a study conducted by Skelland and Hu Xien (1990); the only difference is that our dispersed-phase is non-Newtonian. In their investigation, dispersed-phase mass transfer rates were measured in a baffled vessel agitated with six-flat blade turbines. Photographic techniques enabled the mass-transfer coefficients to be expressed on an area-free basis by providing information on the mean drop size as a function of time in batch operation.

CHAPTER 2
SELECTION OF OPTIMAL SOLVENT

Introduction

Several organic liquids were screened for use as a cosolvent in the cellulose acetate dope mixture. (Acetic acid was the primary solvent in the cellulose acetate dope.) The following criteria were used in the solvent selection process: 1) Cellulose acetate must be soluble in the solvent, and 2) water must be nearly insoluble in the solvent. The cosolvents examined include: methyl acetate, ethyl acetate, n-propyl acetate, isopropyl acetate, octyl acetate, methyl ethyl ketone, diisobutyl ketone, and cyclohexanone.

Literature Development

Published cellulose acetate - solvent solubility data is presented in Table 2.1 along with physical properties of each solvent (Boyd, 1977). Cellulose acetate - solvent solubility data indicates that there exists a narrow range of cellulose acetate solubility in each solvent. The mutual solubility of the solvent-acetic acid-water can be determined from ternary phase diagrams (in mole percent) provided in Figure 2.1 (Arlt and Sorensen, 1980). The heterogeneous region in the phase diagrams is smallest for methyl acetate and methyl ethyl ketone because of their high mutual solubility with water. Conversely, the heterogeneous region is largest for octyl acetate and diisobutyl ketone because of their low mutual solubility with water; the other solvents fit in between this hi-low range and follow in order of decreasing mutual solubility with water-cyclohexanone, ethyl acetate, propyl acetate, and isopropyl acetate. The aforementioned criteria favor solvents with low

Table 2.1: Cellulose acetate solubility in solvents and solvent physical properties.

SOLVENT	CA (1) SOLUBILITY	DENSITY (2) g/cc, 20C	BOILING PT. (2) degree C
Methyl ethyl ketone	Yes	0.81	80.0
Diisobutyl ketone	NA	0.81	163.0
Methyl acetate	Yes	0.93	56.9
n-Propyl acetate	NA	0.89	101.6
Ethyl acetate	Yes	0.90	77.0
Cyclohexanone	Yes	0.95	155.0
Octyl acetate	NA	0.87	210.0
Isopropyl acetate	NA	0.87	90.0

Notes:
NA indicates that solubility data was not available.
(1) Solubility data was found by E.T. Boyd, (1977).
(2) Physical property data was found in CRC Handbook, 56th ed.

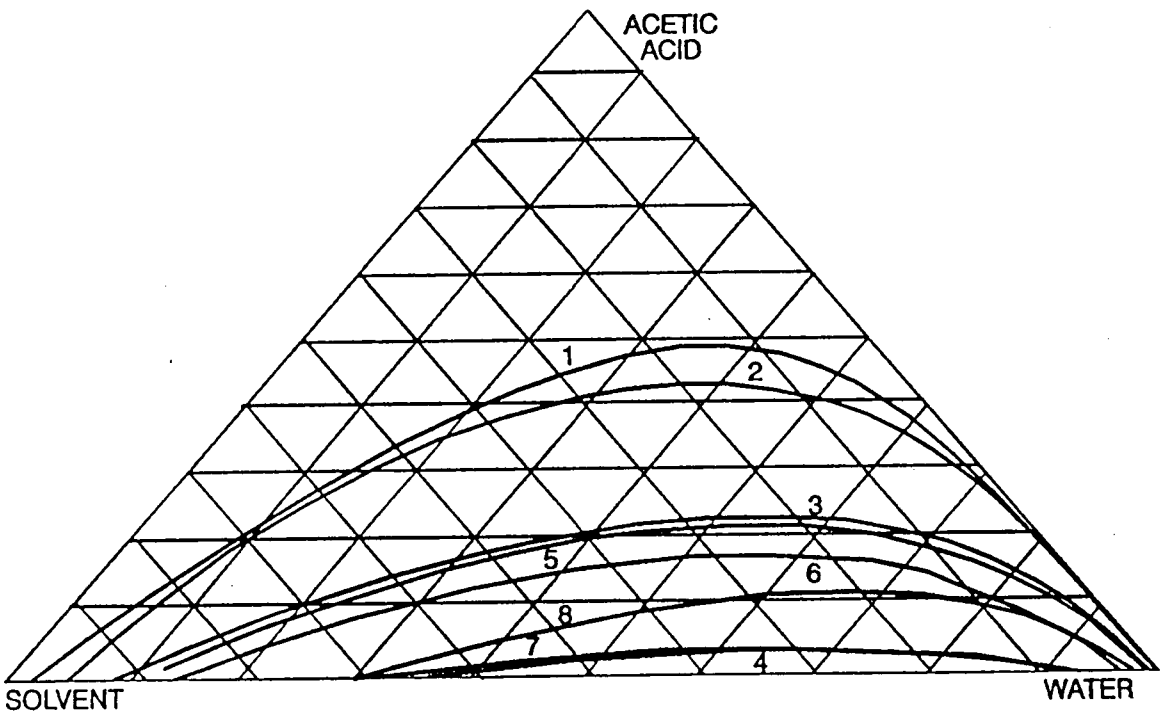

1. N-Octyl Acetate 2. Diisobutyl Ketone 3. N-Propyl Acetate 4. Methyl Ethyl Ketone
5. Isopropyl Acetate 6. Ethyl Acetate 7. Methyl Acetate 8. Cyclohexanone

Figure 2.1: Mutual Solubility Curves for Systems of Acetic Acid, Water, and Solvent.

water solubility. Next, the distribution ratio of acetic acid in organic phase and aqueous-phase (being greater than unity) for the methyl acetate-acetic acid-water system indicates that more acetic acid partitions to the aqueous layer. This is unfavorable in that acetic acid (acting as cosolvent) helps keep cellulose acetate in solution and provides control over viscosity of the organic layer. The distribution ratio is equal to unity for ethyl acetate and cyclohexanone; slightly less than unity for n-propyl acetate, and isopropyl acetate; and much less than unity for the remaining solvents (Murti, 1954 ; Othner, White and Trueger, 1941)

Experimental Procedure

Samples of cellulose acetate dope were taken directly from manufacturing lines. The analyses of these samples are summarized in Table 2.2. The major components include cellulose acetate, acetic acid, and water. Table 2.3 presents the purity of solvent lots analyzed by gas chromatography. Solvents were evaluated at incremental concentrations in 50 grams of the cellulose acetate dope. Solvent was mixed with dope (by hand stirring with a spatula) at room temperature until a homogeneous solution formed. Warm acetic acid-water wash (58^{o}C) was mixed with the solvated dope in 5-10 gram increments until either phase separation or precipitation occurred. The effect of varying acetic acid concentration in water was observed at each solvent level. Phase separation was identified as two liquid layers formed- one predominantly organic with physical form ranging from Newtonian fluid to non-Newtonian psuedoplastic, the other predominantly aqueous containing small amounts of solvent and ester. Precipitation was indicated by segregated solids which would not coalesce. For both cases, the layers were separated and weighed. The remaining organic phase was allowed to approach equilibrium for 24

Table 2.2: Composition of cellulose acetate (CA) dope sampled from manufacturing.

Experiment Set per Solvent	CA Dope Compostion		
	WATER weight%	ACETIC ACID weight%	CA weight%
Methyl ethyl ketone	15.9	81.3	2.8
Diisobutyl ketone	15.4	no sample	no sample
Methyl acetate	12.8	71.7	15.5
n-Propyl acetate	15.0	54.8	30.3
Ethyl acetate	12.9	49.2	37.9
Cyclohexanone	13.5	63.5	23.1
Octyl acetate	13.4	59.3	27.3
Isopropyl acetate	16.4	61.94	21.7

Table 2.3: Purity of solvent lots used in screening experiment set.

SOLVENT	PURITY area%
Methyl ethyl ketone	99.40
Diisobutyl ketone	98.55
Methyl acetate	99.62
n-Propyl acetate	99.83
Ethyl acetate	99.00
Cyclohexanone	99.87
Octyl acetate	99.90
Isopropyl acetate	99.00

hours; if further separation occurred the layers were separated and reweighed. Final layers, were analyzed by gas chromatography for percent water, acetic acid and solvent; cellulose acetate concentration was estimated by percent solids method.

Discussion of Experimental Results

The experimental results for the tie-lines of the cellulose acetate-solvent-acetic acid-water system are given in Tables 2.4 - 2.9. Due to sampling and analytical error, the sum of weight percents (%solvent, %acid, %water, and %CA) may total 100% ± 10%.

The solvent which yielded the broadest phase separation composition range was isopropyl acetate followed by propyl acetate, cyclohexanone, ethyl acetate, methyl acetate, and diisobutylketone, in order of decreasing phase separation range; for more detail refer to Tables 2.10 - 2.17. Small chain esters readily dissolved the cellulose acetate dope. Others were difficult to get into solution.

Phase separation is driven by volume of water present. Acetic acid is needed in the continuous-phase to prevent precipitation of the ester. Increasing acid concentration in the acid-water solution required an increase in the wash volume necessary to achieve phase separation at any given solvent level. If acid concentration is greater than or equal to 50%, a homogeneous phase forms. Increasing acetic acid concentration increases mutual solubility of solvent and water as shown in ternary phase diagram, Figure 2.1.

Table 2.4: **Composition of predominantly aqueous phase (A) and predominantly organic phase (O) for screening n-propyl acetate (nPA).**

Initial Composition , weight %		Final Composition, weight %				
Organic Phase %nPA	Aqueous Phase %acetic acid	Phase	%Water	%nPA	%Acid	%CA
16.7%	10%	aqueous	40.03	3.98	17.70	3.96
		organic	34.96	2.84	17.17	15.39
30%	10%	aqueous	40.00	10.89	19.77	no sample
		organic	28.34	14.62	15.66	no sample
	30%	aqueous	38.14	9.46	28.91	no sample
		organic	32.48	11.25	22.54	9.45
30%	10%	aqueous	40.87	10.83	25.08	1.86
		organic	29.02	14.25	18.14	14.45
	30%	aqueous	48.21	12.10	35.79	3.50
		organic	33.93	11.02	45.26	8.30
50%	0%	aqueous	70.60	4.32	20.16	1.23
		organic	31.87	37.86	17.98	9.61
	5%	aqueous	67.31	23.21	4.79	1.40
		organic	24.26	39.29	17.57	10.23
	10%	aqueous	59.46	6.22	25.53	1.76
		organic	26.03	45.42	25.85	9.27
	30%	aqueous	45.98	15.30	30.90	1.14
		organic	27.42	30.35	22.44	8.18
	50%	aqueous	26.73	21.68	42.13	5.05
		organic	26.61	21.30	42.98	5.25

Note: Composition of each phase is reported for experiment sets where phase separation occurred. Analytcial error is about 10%.

Table 2.5: Composition of predominantly aqueous phase (A) and predominantly organic (O) phase for screening cyclohexanone (CH).

Initial Composition, weight %			Final Composition, weight %			
Organic Phase	Aqueous Phase					
%CH	%acetic acid	Phase	%Water	%CH	%Acid	%CA
10%	0%	aqueous	48.59	0.00	40.36	11.05
		organic	42.32	8.09	34.72	13.50
	10%	aqueous	50.20	5.49	40.61	3.71
		organic	44.45	6.64	36.70	11.15
30%	0%	aqueous	43.70	16.45	27.73	2.20
		organic	30.92	20.81	21.61	22.90
	10%	aqueous	44.05	15.22	29.68	2.15
		organic	32.05	17.23	22.95	26.80
	30%	aqueous	40.42	11.07	34.03	3.80
		organic	37.74	11.76	28.33	7.55
50%	0%	aqueous	38.91	22.56	21.62	1.35
		organic	25.46	29.62	20.65	10.05
	10%	aqueous	36.85	23.83	22.55	1.60
		organic	27.68	27.58	20.46	11.40
	30%	aqueous	35.66	16.93	31.41	4.85
		organic	32.35	17.14	27.08	9.57

Note: Composition of each phase is reported for experiment sets where phase separating occurred. Analytcial error is about 10%.

Table 2.6: Composition of predominantly aqueous phase (A) and predominantly organic phase (O) for screening ethyl acetate (EA).

Initial Composition, weight %			Final Composition, weight %			
Organic Phas %EA	Aqueous Phase %acetic acid	Phase	%Water	%EA	%Acid	%CA
10%	10%	aqueous	46.04	1.20	24.53	no sample
		organic	39.78	3.47	24.76	no sample
30%	10%	aqueous	46.98	9.49	26.51	no sample
		organic	38.05	11.10	27.47	14.00
	30%	aqueous	38.55	3.87	21.59	no sample
		organic	34.61	4.92	17.21	8.40
	50%	aqueous	24.34	4.26	60.45	no sample
		organic	22.98	3.97	54.29	5.05
50%	10%	aqueous	45.39	15.93	13.35	no sample
		organic	33.95	18.73	10.74	9.00
	30%	aqueous	34.12	14.28	17.10	2.80
		organic	29.56	14.07	12.13	10.30

Note: Composition of each phase is reported for experiment sets where phase separation occurred. Analytcial error is about 10%.

Table 2.7: Composition of predominantly aqueous phase (A) and predominantly organic phase (O) for screening methyl acetate (MA).

Initial Concentration, weight %		Final Concentration, weight %				
Organic Phas %MA	Aqueous Phase %acetic acid	Phase	%Water	%MA	%Acid	%CA
10%	30%	aqueous	45.77	0.50	33.76	no sample
		organic	36.62	1.53	63.76	no sample
30%	10%	aqueous	47.75	8.44	38.91	2.86
		organic	40.15	7.39	33.93	10.85
	30%	aqueous	46.58	3.01	48.21	no sample
		organic	42.73	6.21	43.03	6.95
50%	30%	aqueous	35.29	10.03	13.93	1.60
		organic	30.28	8.35	11.13	12.60

Note: Composition of each phase is reported for experiment sets where phase separation occurred. Analytcial error is about 10%.

Table 2.8: Composition of predominantly aqueous phase (A) and predominantly organic phase (O) for screening isopropyl acetate (IPA).

Initial Composition, weight %			Final Composition, weight %			
Organic Phase	Aqueous Phase					
%IPA	%acetic acid	Phase	%Water	%IPA	%Acid	%CA
30%	0%	aqueous	48.73	11.39	37.26	1.90
		organic	34.92	18.65	33.33	2.25
	10%	aqueous	48.17	9.90	41.04	2.35
		organic	37.17	15.69	36.29	11.25
	30%	aqueous	44.85	9.78	40.82	4.45
		organic	41.46	10.72	39.70	10.25

Note: Composition of each phase is reported for experiment sets where phase separation occurred. Analytcial error is about 10%.

Table 2.9: Composition of predominantly aqueous phase (A) and predominantly organic phase (O) for screening Methyl ethyl ketone (MEK).

Initial Composition, weight %			Final Composition, weight %			
Organic Phas %MEK	Aqueous Phase %acetic acid	Phase	%Water	%MEK	%Acid	%CA
50%	25%	aqueous	52.51	7.46	38.10	1.14
		organic	29.38	4.66	26.05	10.50

Note: Composition of each phase is reported for experiment sets where phase separation occurred. Analytcial error is about 10%.

Table 2.10 Material Handling Data for Diisobutyl Ketone (DIBK)

%DIBK in CA Dope	Acetic acid/Water %acid	grams	Phase Separation? (liquid-liquid)	Precipitation? (solid-liquid)	Organic grams	Aqueous grams
10%	0	17.28	No	Yes	94.57	4.33
	10	57.41	No	Yes	60.05	25.57
	30	89.01	No	No		
	70	177.84	No	No		
24%	10	5.05	Yes	No	52.00	10.65
	30	10.50	Yes	No	63.40	10.80
	100	86.20	No	No		

Table 2.11 Material Handling Data for Methyl Ethyl Ketone (MEK)

%MEK in CA Dope	Acid/Water %acid	grams	Phase Separation? (liquid-liquid)	Precipitatio (solid-liquid	Organic grams	Aqueous grams
30%	4	17.28	No	Yes		
	10	57.41	No	Yes	112.20	10.05
	30	89.01	No	No		
50%	25	159.02	No	Yes	121.72	34.09

Table 2.12 Material Handling Data for Methyl Acetate (MA)

%MA in CA Dope	Acetic acid/Water %acid	grams	Phase Separation? (liquid-liquid)	Precipitatio (solid-liqui	Organic grams	Aqueous grams
10%	10	45	No	Yes	100.02	0.48
	30	90	Yes	No	144.54	1.20
	50	130	No	No		
30%	10	50.00	Yes	No	119.16	2.70
	30	90.79	Yes	No	160.22	1.86
50%	10	74.92	No	No		
	30	190.00	Yes	No	83.29	200.54

Table 2.13 Material Handling Data for Ethyl Acetate (EA)

%EA in CA Dope	Acetic acid/Water %acid	grams	Phase Separation? (liquid-liquid)	Precipitation? (solid-liquid)	Organic grams	Aqueous grams
10%	10	35	No	Yes	90.02	0.42
	30	120	No	No		
	50	110	No	No		
30%	10	40	Yes	No	87.20	18.20
	30	90	Yes	No	152.36	1.98
	50	160	No	No		
50%	10	60	Yes	No	115.35	39.00
	30	110	Yes	No	82.28	121.83
	50	175	No	No		

Table 2.14 Material Handling Data for n-Propyl Acetate (nPA)

%nPA in CA Dope	Acid/Water %acid	grams	Phase Separation? (liquid-liquid)	Precipitatio (solid-liquid	Organic grams	Aqueous grams
16.70%	10	33.21	Yes	No	79.20	9.70
30%	10	37.50	No	Yes	93.97	14.90
	30	67.50	No	No	108.00	27.58
	50	140.00	No	No		
30%	10	39.50	Yes	No	76.70	28.72
	30	69.40	Yes	No	135.50	4.65
	50	235.40	No	No		
50%	0	47.50	Yes	No	126.00	18.75
	5	45.45	Yes	No	117.20	26.50
	10	45.00	Yes	No	114.50	31.00
	30	75.00	Yes	No	140.00	33.40
	50	108.00	No	No		

Table 2.15 Material Handling Data for Cyclohexane (CH)

%CH CA Dope	Acid/Water %acid	grams	Phase Separation? (liquid-liquid)	Precipitation (solid-liquid)	Organic grams	Aqueous grams
10%	0	35.00	No	Yes	75.20	14.60
	10	47.50	No	Yes	101.80	1.10
	30	180.00	No	No		
	50	175.00	No	No		
30%	0	37.50	Yes	No	70.10	40.00
	10	50.00	Yes	No	67.60	54.10
	30	100.00	Yes	No	15.23	16.80
	50	175.00	No	No		
50%	0	50.00	Yes	No	70.15	53.20
	10	60.00	Yes	No	73.90	63.95
	30	135.00	Yes	No	30.60	172.70
	50	175.00	No	No		

Table 2.16 Material Handling Data for Isopropyl Acetate (IPA)

%IPA in CA Dope	Acid/Water %acid	grams	Phase Separation? (liquid-liquid)	Precipitation? (solid-liquid)	Organic grams	Aqueous grams
10%	10	46.20	No	Yes		
	30	46.20	Yes	No		
30%	0	27.50	Yes	No	84.03	10.20
	5	30.00	Yes	No	76.50	21.85
	10	32.50	Yes	No	89.75	10.27
	30	175.00	Yes	No	83.15	63.49
50%	0	62.50	Yes	No	113.43	49.08

Table 2.17 Material Handling Data for Octyl Acetate (OA)

%OA in CA Dope	Acid/Water %acid	grams	Phase Separation? (liquid-liquid)	Precipitation (solid-liquid)	Organic grams	Aqueous grams
10%	0	40.00	No	Yes		
	5	40.00	No	Yes		
	10	50.00	No	Yes		
	30	105.00	No	No		
22%	0	25.00	No	Yes	67.70	5.60
19%	5	22.50	No	Yes	54.60	8.40
19%	10	27.50	No	Yes	67.40	3.10
23%	30	80.00	No	Yes	112.61	12.40

CHAPTER 3
MEASUREMENT OF PHYSICAL AND TRANSPORT PROPERTIES

Introduction

In order to predict the mass transfer coefficient, several physical and transport properties of both phases need to be measured or predicted including density, viscosity, interfacial tension, the distribution coefficient of the Na_2SO_4, and molecular diffusivity of Na_2SO_4 in the solvents.

Experimental Procedure

The experimental procedure to produce fluids to measure the physical and transport properties is as follows. First, samples of cellulose acetate dope were taken directly from manufacturing lines. The cellulose acetate dope was analyzed to quantify the major components- cellulose acetate, acetic acid, and water. Accordingly, water weight percent and acid weight percent were measured by gas chromatography, while cellulose acetate weight percent was measured by percent solids. In addition, the sodium salt content was measured by inductively coupled plasma. Analytical data, summarized in Table 3.1, indicate that the cellulose acetate dope samples used in the following experiments are essentially alike.

Three sets of experiments were conducted with three identical runs within a set to check for reproducibility; the initial amount of organic solvent added to the cellulose acetate dope was varied among the sets (30%, 40%, and 50% isopropyl acetate by total weight). Experiments were conducted at room temperature and atmospheric pressure. In each set of experiments, 200 grams of cellulose acetate dope was mixed with isopropyl

Table 3.1: Composition of cellulose acetate dope samples from manufacturing.

Experiment	Run No.	%Water	%Acetic Acid	%Cellulose Acetate	Total* Weight%	ppm Na2SO4
30% IPA**	1	15.76	69.33	21.35	106.44	1500
	2	14.72	65.17	22.20	102.09	1500
	3	14.72	65.17	22.20	102.09	1500
40% IPA	1	14.72	65.17	22.20	102.09	1500
	2	13.82	63.57	21.15	98.54	1400
	3	13.82	63.57	21.15	98.54	1400
50% IPA	1	13.82	63.57	21.15	98.54	1400
	2	13.82	63.57	21.15	98.54	1400
	3	14.61	66.20	20.95	101.76	1400

Notes: * Percent of isopropyl acetate added to cellulose acetate dope for each run in the experiment set.

** See Chapter 5 for reference to analytical accuracy.

acetate in a one liter beaker at 1000 rpm (using a two inch diameter, six flat-blade impeller) for ten minutes to form a homogeneous solution. 250 grams of a 4% acetic acid in water solution was then added to the solvated dope and allowed to stir for 60 minutes at 1000 rpm. In most cases, some of the aqueous-phase was disengaged from the organic phase immediately after stirring (five minutes maximum were allowed for gravitational separation); this material was decanted and weighed. The remaining organic containing entrained aqueous phase was centrifuged for 30 minutes at 2900 rpm. The weight of each resulting layer (organic and aqueous-phase) was measured and recorded. The composition of each layer was analyzed by gas chromatography for liquid composition (acetic acid, water, and isopropyl acetate), and by percent solids for cellulose acetate.

Experimental Observations

The experimental observations for each of the three sets of experiments (on three tie-lines) are as follows.

30% Isopropyl Acetate Experiments

The average amount of aqueous-phase remaining in the organic phase after five minutes of gravitational settling was 1.87% of the total amount of aqueous-phase released from the organic phase after both settling and centrifugation with a standard deviation (SD) of 1.08%. The average equilibrium composition of the organic phase was 21.57% (SD=2.57%) isopropyl acetate, 24,13% (SD=0.48) acetic acid, 25.58% (SD=0.44%) water, and 27.95% (SD=1.59%) cellulose acetate. The average phase ratio (organic phase to aqueous-phase) was 1:2.6±0.2.

40% Isopropyl Acetate Experiments

The average amount of aqueous-phase remaining in the organic phase after five minutes of gravitational settling was 10.44% of the total amount of aqueous-phase released from the organic phase after both settling and centrifugation with a SD of 7.01%. The average equilibrium composition of the organic phase was 35.10% (SD=5.40%) isopropyl acetate, 23.99% (SD=0.53%) acetic acid, 26.60% (SD=1.30%) water, and 17.20% (SD=0.99%) cellulose acetate. The average phase ratio (organic phase to aqueous-phase) was 1:1.2±0.1.

50% Isopropyl Acetate Experiments

The average amount of aqueous-phase remaining in the organic phase after five minutes of gravitational settling was 44.66% of the total amount of aqueous-phase released from the organic phase after both settling and centrifugation with a SD of 11.43%. The average equilibrium composition of the organic phase was 36.58% (SD=3.65%) isopropyl acetate, 23.15% (SD=1.22%) acetic acid, 29.49% (SD=1.07%) water, and 9.73% (SD=0.76%) cellulose acetate. The average phase ratio (organic phase to aqueous-phase) was 1:0.4±0.1.

Physical Property Measurements for the Two Phases

The measurement of each physical property for both aqueous and organic phases resulting from the aforementioned experiments are now addressed.

Density

The density of the aqueous-phase was measured via a specific gravity chain balance device. However, the organic phase was so viscous that a calibrated centrifuge tube was required to measure its density. According to the measured data shown in Table 3.2, the

Table 3.2: Composition of each phase on opposite sides of an equilibrium tie-line at 25C used in experiments to determine molar volume.

Expt. Set		O=Org	Weight		Weight Percent			
%IPA		A=Aqu	grams	ppmNa	IPA	Acid	Water	CA
30%	Run 1	O	135.43	149	18.59	24.80	26.20	29.05
		A	368.57	871	6.28	30.25	62.03	0.90
	Run 2	O	160.25	135	24.85	23.70	25.22	25.70
		A	361.25	807	7.50	28.47	63.18	1.15
	Run 3	O	137.50	133	21.27	23.89	25.31	29.10
		A	373.00	789	4.44	23.77	68.30	1.15
			Avg. Organic wgt%		21.60	24.10	25.60	composite
			Avg. Organic mol.frac.		0.10	0.20	0.70	**Vb**
			Organic Molar Vol., Vb		13.83	2.92	47.81	**64.56**
40%	Run 1	O	233.00	212	29.45	24.27	26.54	17.85
		A	309.30	855	6.58	26.87	64.92	0.85
	Run 2	O	234.90	151	33.48	24.46	25.03	17.95
		A	319.00	800	6.79	26.82	65.05	0.90
	Run 3	O	276.20	191	42.38	23.25	28.22	15.80
		A	289.80	803	6.56	26.90	67.90	0.90
			Avg. Organic wgt%		35.10	24.00	26.60	composite
			Avg. Organic mol.frac.		0.16	0.18	0.67	**Vb**
			Organic Molar Vol., Vb		20.62	2.67	45.53	**68.81**
50%	Run 1	O	293.35	205	31.73	24.82	28.07	10.80
		A	174.25	853	5.82	23.03	69.57	0.90
	Run 2	O	347.15	255	40.55	22.70	30.65	9.15
		A	131.30	882	4.97	24.15	73.93	1.00
	Run 3	O	352.40	265	37.44	21.93	29.76	9.25
		A	129.60	904	4.75	23.79	72.46	1.00
			Avg. Organic wgt%		36.60	23.10	29.50	composite
			Avg. Organic mol.frac.		0.15	0.16	0.69	**Vb**
			Organic Molar Vol., Vb		20.05	2.39	47.10	**69.55**

phase containing cellulose acetate (organic phase) is more dense than the predominantly aqueous-phase for the 30% IPA set of experiments. In contrast, for the 40% IPA and 50% IPA set of experiments the organic phase was indeed less dense than the aqueous-phase. This phenomena is referred to as density inversion and is discussed in detailed by Sink, (1990).

Interfacial Tension

Interfacial tension was measured via the duNouy ring technique. The force required to pull a platinum-iridium ring through the interface was converted to interfacial tension and read from a dial. The estimated interfacial tension for the organic phase was 1.6, 1.8, and 2.0 dynes/cm for the 30% , 40% , and 50% isopropyl acetate experiments, respectively. Interfacial tension was measured in order to calculate the Sauter-mean diameter of the dispersed-phase droplets using equation 5.5.

Viscosity

The viscosity of the aqueous phase was Newtonian, and was measured using a Brook Field Viscometer. However, the organic phase was pseudoplastic in nature, and the flow curves were measured by a cup and bob or a cone and plate viscometer depending on the apparent viscosity. The Cox-Mertz empiricism was used to convert the radian frequency to frequency. Thus, for a pseudoplastic fluid the constitutive equation is

$$\tau = K\dot{\gamma}^{n}, \tag{3.1}$$

where $\dot{\gamma}$ is the shear rate, τ is the shear stress, and K and n are material constants.

Distribution Coefficient

The distribution coefficient for the sodium sulfate salt, defined as

$$m = \frac{[ppmNa]_{aqueous}}{[ppmNa]_{organic}} \tag{3.2}$$

was determined via inductively coupled plasma analysis testing for sodium in each phase. The dispersion was allowed to completely separate (i.e., stand for 24 hours) before each phase was sampled.

Diffusivity

Molecular diffusivity was calculated for the sulfate salt in the organic phase by the Lusis and Ratcliff (1968) correlation for organic solvents,

$$\frac{D_{AB}\mu_B}{T} = 8.52X10^{-10}(V_{bB})^{-1/3}\left[1.40\left(\frac{V_{bB}}{V_{bA}}\right)^{1/3} + \left(\frac{V_{bB}}{V_{bA}}\right)\right], \tag{3.3}$$

where D_{AB} is the mutual diffusion coefficient, μ_B is the dispersed-phase viscosity, T is temperature, V_{bA} is the molar volume of the solute, sodium sulfate; while, V_{bB} is the composite molar volume of the dispersed-phase. This correlation is based on a binary liquid system at infinite dilution. and is recommended for diffusion in organic solvents. It assumes that the difference between the motion of a molecule in the pure solvent B (characterized by the diffusion coefficient D_{AB}), and the motion of a solute molecule at infinite dilution of A in B (characterized by the mutual diffusion coefficient), should be a function of the ratio of the molar volumes of A and B; for both the frictional forces involved in the sliding motion, and the energy required to open up a hole for the moving molecule to occupy, are functions of the volume of the molecule involved. Possible complications introduced by steric factors or other forms of strong solute-solvent

interaction (e.g. association) are neglected. This correlation was used to estimate the diffusion coefficient of Na^- in the dispersed-phase instead of the Nernst (1888) equation due to the lack of measured thermodynamic properties including limiting ionic conductance and activity coefficients to relate conductivity to diffusivity (Payne, 1995). A sample calculation for the Na^- diffusion coefficient in the organic dispersed-phase is provided in Appendix A3.

The alternative, physical measurement using a diaphragm diffusion cell is not feasible due to the high viscosity of the dispersed-phase (Wilke and Chang, 1955; Holmes, et.al., 1963; and Skelland and Hu Xien, 1990). With the diaphragm cell approach, the material must migrate over time through a sintered disk having porosity of 3 to 8 microns; the viscosity of the dispersed-phase would retard any such migration.

The diffusivity of the salt in the aqueous-phase was estimated by the strong electrolyte at infinite dilution expression of Nernst (1888) (Hines and Maddox, 1985),

$$D^o_{AB} = 8.931E-10T\frac{\lambda^o_+\lambda^o_-}{\lambda^o_+ + \lambda^o_-}\frac{|Z_-|+|Z_+|}{|Z_+Z_-|}, \qquad (3.4)$$

where F is the Faraday constant, D^oAB is the diffusion coefficient at infinite dilution, λ^o_+ is the cationic conductance at infinite dilution, λ^o_- is anionic conductance at infinite dilution, $\lambda^o_+ + \lambda^o_-$ is the electrolyte conductance at infinite dilution, Z_+ is the cation valence, Z_- is the anionic valence, R is the gas constant and T is absolute temperature. This correlation, which relates diffusivity to electrical conductivities, is valid for dilute solutions. The ionic conductances in water, readily available, were used since water is the major component of the continuous-phase (i.e., composition is 71% water, 24% acetic acid, and 5% isopropyl acetate). A sample calculation of the diffusion coefficient for Na- in the predominantly aqueous-phase is provided in Appendix A3.

These physical and transport properties are summarized in Tables 3.3 through 3.5, and their variation with position on the isopropyl acetate, water, acetic acid face of the quaternary phase diagram is qualitatively illustrated in Figure 3.1. All data were collected or predicted at 25°C.

Table 3.3 Physical and transport properties for both dispersed and continuous-phases on opposite sides of a tie-line taken at 25°C.

Expt. Set	Continuous-phase		σ	Dispersed-phase			
	μ_c, cP	ρ_c, g/ml	dyne/cm	n	K	$\mu_d = \frac{K}{\sec}\dot{\gamma}_o$	ρ_d, g/ml
30%IPA							
Run 1	1.7643	1.00	1.60	0.24	10,600,000	203,668	1.062
Run 2	1.7253	1.00	1.60	0.28	7,100,000	169,885	1.067
Run 3	1.6178	1.00	1.60	0.28	11,200,000	262,323	1.061
40%IPA							
Run 1	1.6614	1.02	1.80	0.81	154,000	58,209	1.029
Run 2	1.6401	1.02	1.80	0.82	105,000	40,587	0.990
Run 3	1.6463	1.02	1.80	0.80	64,800	22,853	0.996
50%IPA							
Run 1	1.6537	1.03	2.00	0.80	18,200	6,286	0.948
Run 2	1.6405	1.03	2.00	0.79	10,400	3,555	0.957
Run 3	1.6685	1.03	2.00	0.77	12,200	3,661	0.953

Note: The density of the continuous-phase may be determined as follows:

$$\rho_c = x_{IPA}\rho_{IPA} + x_{H2O}\rho_{H2O} + x_{acid}\rho_{acid}$$

where x is weight fraction of the given component.

Table 3.4: Calculation of Na_2SO_4 Diffusivity in the organic phase using the physical properties from Table 3.2 and Table 3.3 (Skelland, 1985).

Experiment Set		$\frac{D_{AB}\mu_B}{T} = 8.52X10^{-10}(V_B)^{-1/3}\left[1.40\left(\frac{V_B}{V_A}\right)^{1/3} + \left(\frac{V_B}{V_A}\right)\right]$
30%IPA	Run 1	5.88E-09 cm^2/s
	Run 2	7.05E-09 cm^2/s
	Run 3	4.56E-09 cm^2/s
40%IPA	Run 1	2.09E-08 cm^2/s
	Run 2	2.99E-08 cm^2/s
	Run 3	5.32E-08 cm^2/s
50%IPA	Run 1	1.97E-07 cm^2/s
	Run 2	3.43E-07 cm^2/s
	Run 3	3.33E-07 cm^2/s

Note: Solute, Na_2SO_4, molar volume is 96.8 $cm^3/gmol$.

Table 3.5: Calculation of the Distribution Ratio using the Na2SO4 Concentration data from Table 3.2.

Experiment Set		$m = \frac{[ppmNa]_{aqueous}}{[ppmNa]_{organic}}$
30%IPA	Run 1	5.850
	Run 2	5.980
	Run 3	5.930
40%IPA	Run 1	4.030
	Run 2	5.300
	Run 3	4.200
50%IPA	Run 1	4.160
	Run 2	3.460
	Run 3	3.410

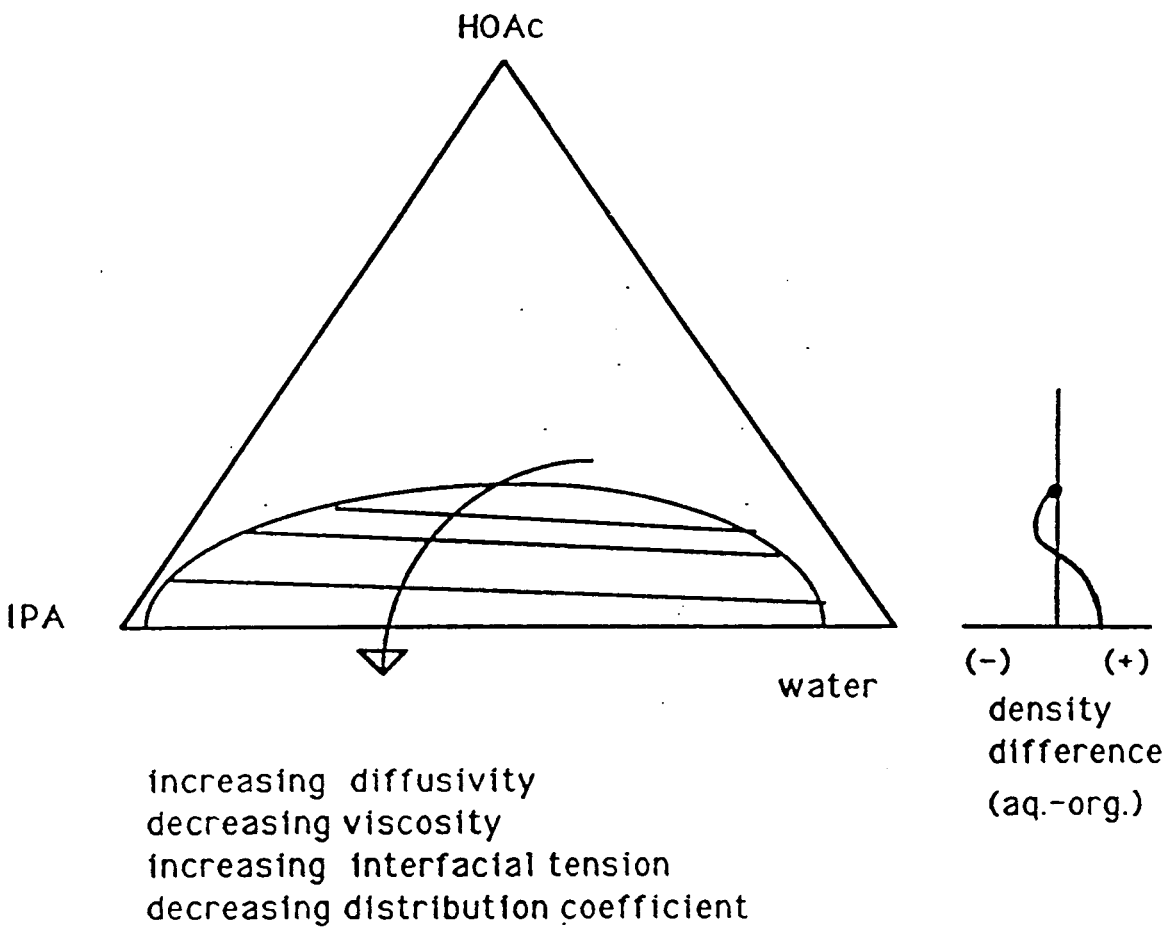

Figure 3.1: Variation of Physical and Transport properties of the organic phase with position on the isopropyl acetate, water, acetic acid face of the quaternary phase diagram. This phase diagram is a general representation; it is not drawn to scale.

CHAPTER 4
FEASIBLE EXPERIMENTAL REGIONS

Phase Equilibrium Study

The system studied herein contained five components; namely acetic acid, water, isopropyl acetate, cellulose acetate (not truly a single component due to its polymeric nature), and Na_2SO_4. The Na_2SO_4 was present in ppm levels and was therefore not included in the phase diagram. Thus, a three dimensional representation (tetrahedron) could be constructed with the first four compounds. It should be noted that the phase diagram for this system is not like those typified by Treybal (1963) where the transferring component (the salt in this case) is included on the diagram. Instead, this diagram illustrates various phase regions for the non-solute. The presence of cellulose acetate as a solid with potential for solid-liquid-liquid dispersion made phase equilibrium predictions difficult and of questionable accuracy. Equilibrium data for the acetic acid, isopropyl acetate, water system was available in the DECHEMA Chemistry Data Series. Thus, the phase behavior was experimentally measured for the other three faces of the tetrahedral shaped phase diagram. Three faces (water, acetic acid, cellulose acetate; isopropyl acetate, acetic acid, cellulose acetate; and water, isopropyl acetate, and acetic acid) exhibited type one behavior as discussed by Treybal (1963), and the other face displayed type three behavior. These faces are provided in Figures 4.1, 4.2, 4.3, and 4.4. As shown in Figure 4.5, five different phase regions were identified at 25°C, and they are described as follows: Region I is a single liquid-phase rich in acetic acid; Region II is a two phase solid-liquid system where cellulose acetate is the solid and the liquid-phase is predominantly isopropyl acetate; Region III consists of a two phase solid-liquid system where cellulose acetate is the solid and water is the predominant liquid component;

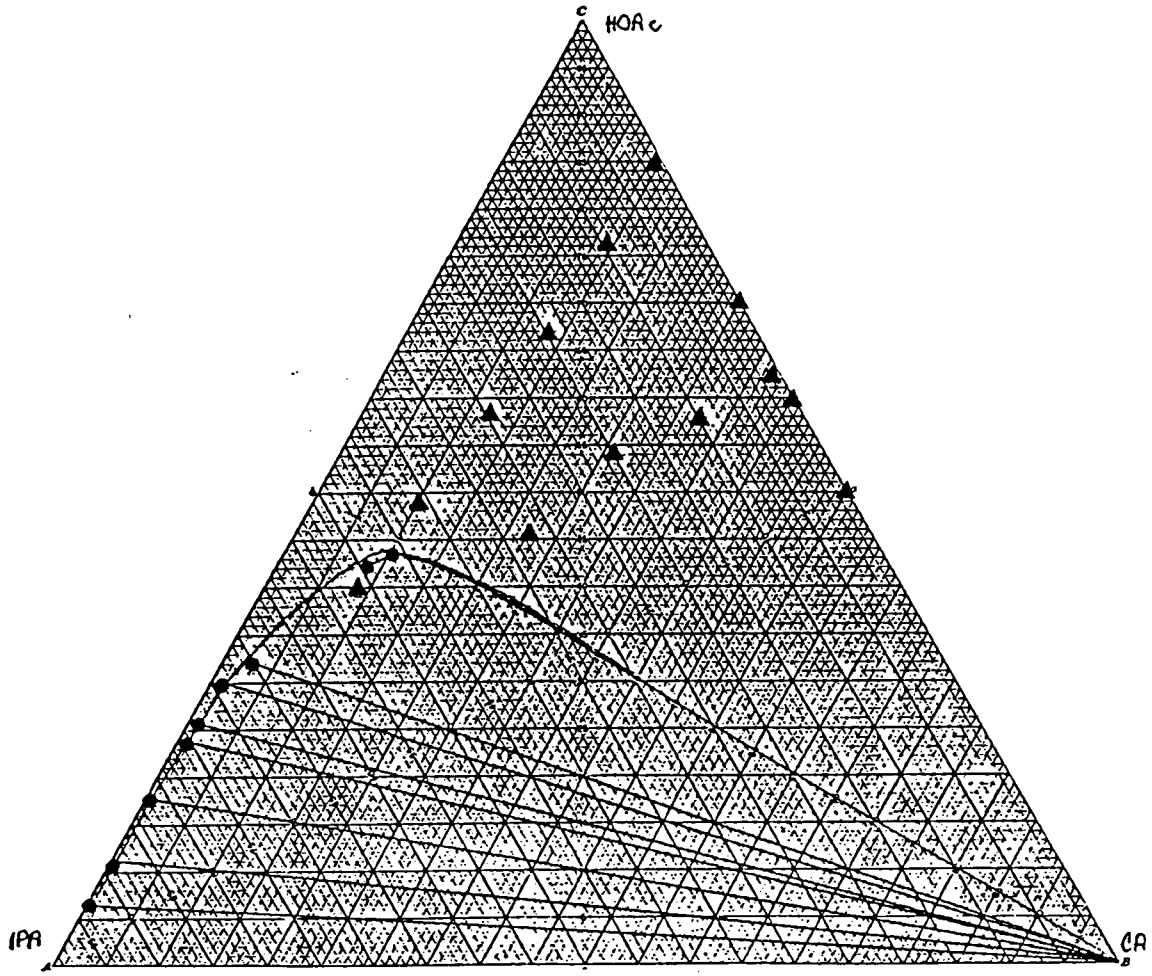

Figure 4.1: Ternary Diagram for the CA-IPA-Acetic Acid system experimentally determined at 25°C. Triangles indicate compositions that produced a single phase, while circles indicate that two phases were formed.

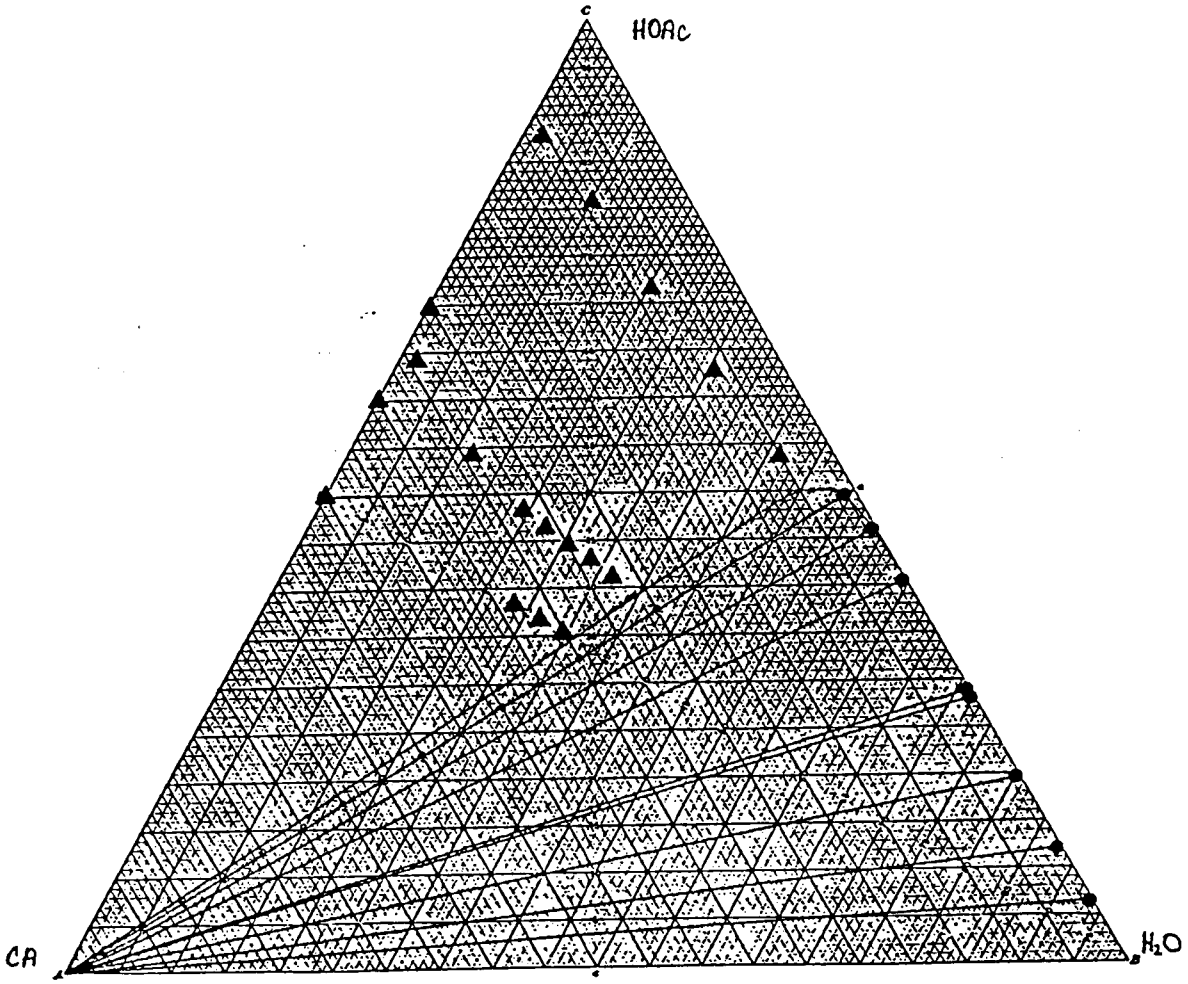

Figure 4.2: Ternary Diagram based on mass fractions for the CA-Water-Acetic Acid system experimentally determined at 25°C. Triangles indicate compositions that produced a single phase, while circles indicate that two phases were formed.

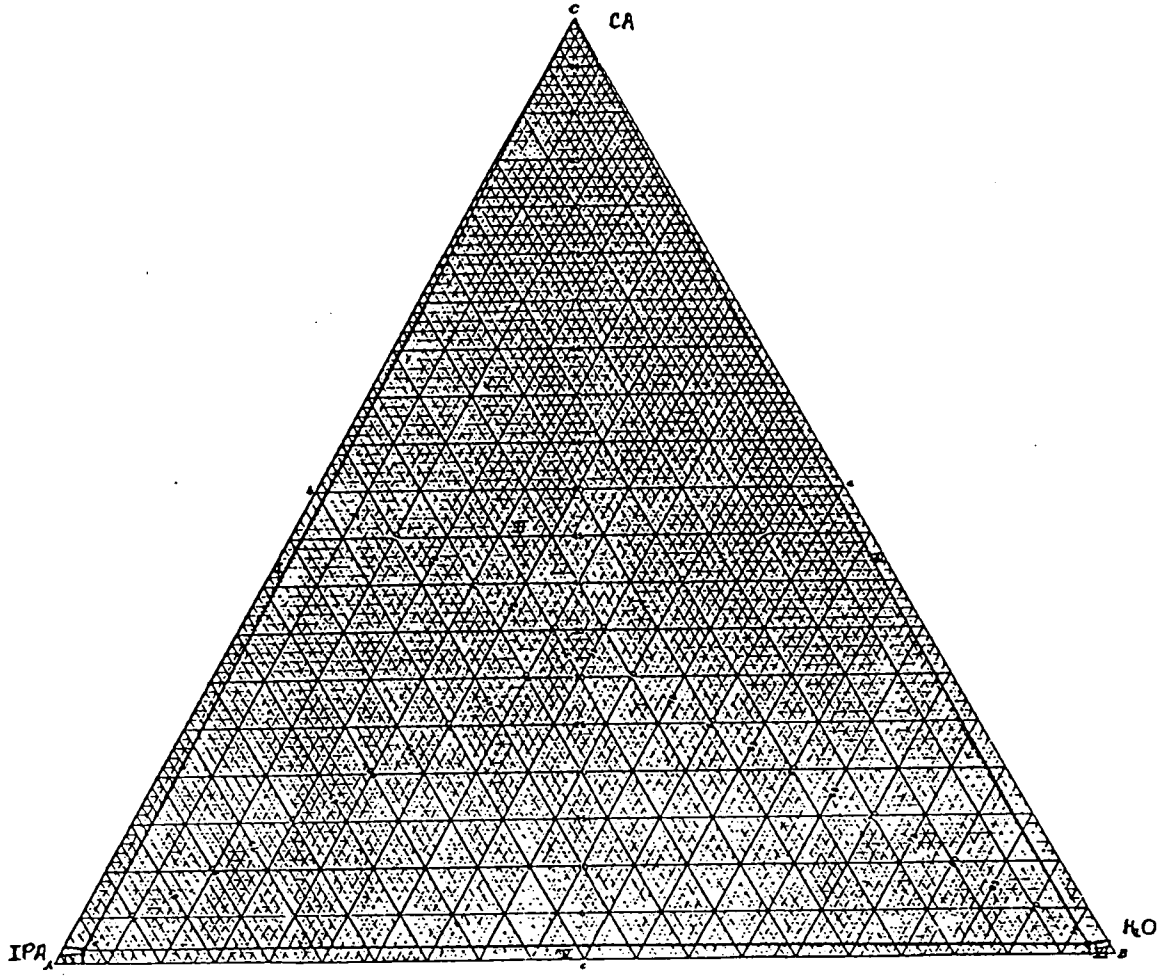

Figure 4.3: Ternary Diagram based on mass fractions for the CA-Water-IPA system experimentally determined at 25°C.

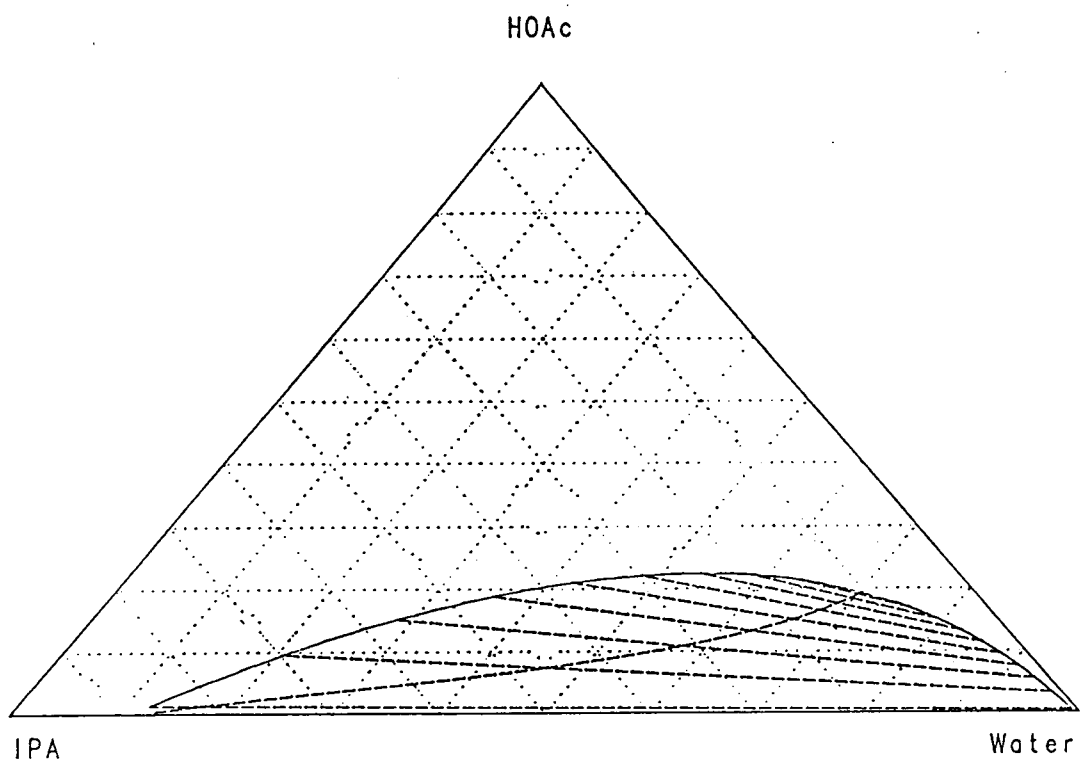

Figure 4.4: Ternary Diagram based on mass fractions for the IPA-Water-Acetic Acid system experimentally determined at 25°C.

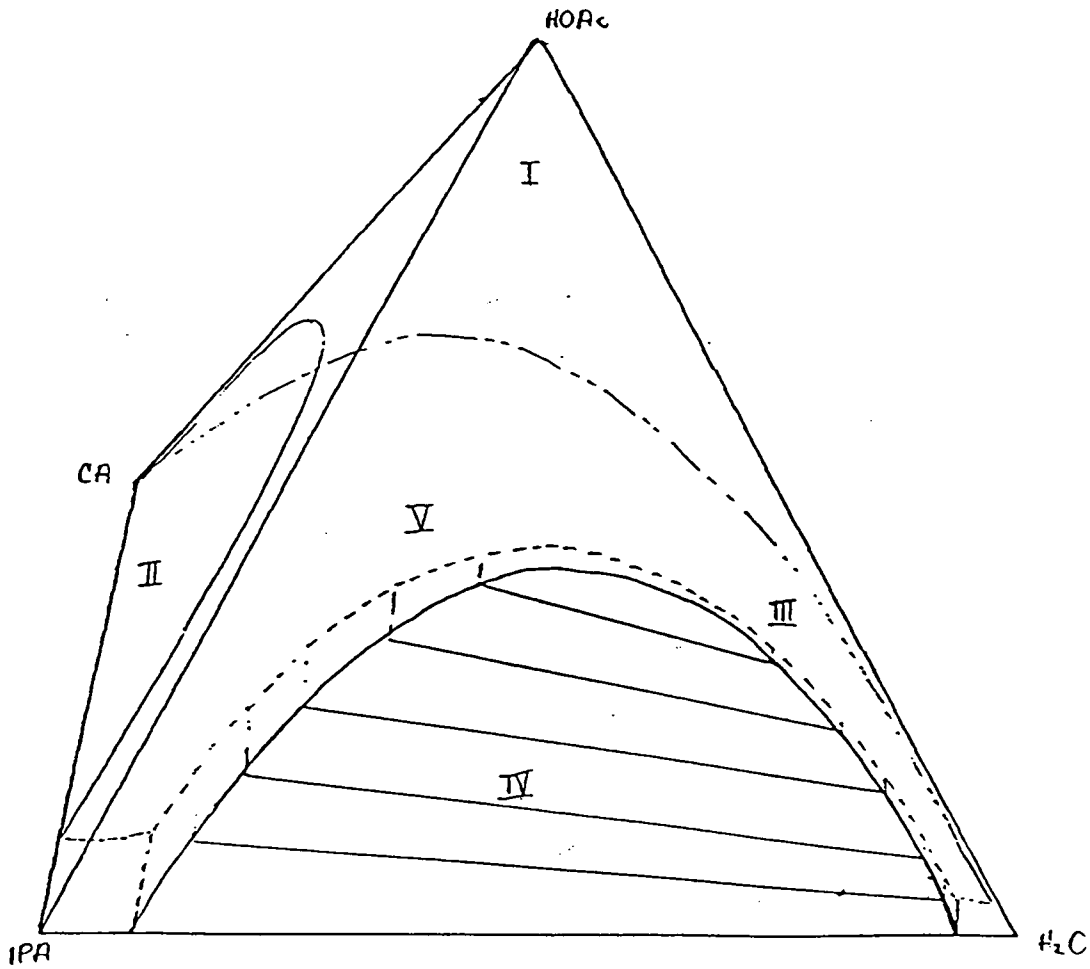

Figure 4.5: Quaternary Phase Diagram for the CA-Water-Acetic Acid-IPA system experimentally determined at 25°C.

Region IV exhibits two immiscible liquid-phase behavior where aqueous and organic phases are in equilibrium; and Region V is a three phase region where cellulose acetate is the solid in equilibrium with two immiscible liquids of aqueous and organic nature. Experimental details concerning the development of the diagram are discussed by Kanel and Moncier (1990).

Each region of the phase diagram represents a possible operating zone for salt removal. However, liquid-liquid dispersions that exist without the precipitation of solid cellulose acetate are possible only in region IV of the phase diagram.

Contact of the cellulose acetate dope - isopropyl acetate mix with an aqueous-phase, in a proper phase ratio to place the mixing point in region IV [based on the inverse lever-arm rule, see Treybal (1963, pp. 7,8)] , would result in the formation of two immiscible liquid phases whose compositions lie on either side of the phase envelope boundary connected by the tie line containing the mixture point. Thus, various areas of region IV can be experimentally obtained by changing the phase ratio of the same aqueous and organic feeds. However, unless the organic and aqueous feed compositions lie on the same tie line, there will not only be transfer of solute between the phases, but solvents such as water, acetic acid, and isopropyl acetate will also be transferred. Diffusion of these components will significantly change the physical and transport properties of the resulting immiscible phases such as viscosity, density, equilibrium distribution coefficient of the sodium sulfate salt, interfacial tension, and molecular diffusivity.

Determination of the Optimal Phase to Disperse

Determination of the optimal phase to disperse has historically been a difficult question to answer. Skelland (1985) suggests that when equal amounts of each phase are present, it may be best to disperse the phase that offers the least resistance to mass transfer based on the hypothesis that even if trace amounts of surfactant are present, interruption of internal circulation of the drop would have a less deleterious effect. Another consideration in selecting the dispersed-phase is the viscosity of the continuous-phase. If very viscous materials are made continuous, droplet interactions may be significantly reduced, thus reducing the rate of mass transfer. Also a significant increase in the viscosity of the fluid to be agitated would result in increasing mixing and pumping requirements. Based on the latter argument, the viscous dope phase (i.e., the cellulose acetate dope - isopropyl acetate mixture) was chosen to be dispersed.

Agitator Speed Necessary to Maintain Dispersion

As discussed in Chapter 3, Measure of Physical and Transport Properties, the predominantly aqueous-phase is a Newtonian fluid; while, the cellulose acetate dope phase is a non-Newtonian fluid with pseudoplastic behavior.

As discussed in the previous section, the viscous cellulose acetate dope phase will be dispersed in the predominantly aqueous-phase. Accordingly, the Skelland and Ramsay (1987) correlation combined with Metzner and Otto's (1957) definition of apparent viscosity and Vermuelen et al's (1955) viscosity expression may be used to estimate the impeller speed needed to completely disperse a pseudoplastic in a Newtonian fluid. The Skelland and Ramsay (1987) correlation predicts the Froude number as such

$$\left(N_{Fr}\right)_{\min} = C^2\left(\frac{d_v}{d_i}\right)^{2\alpha} \phi^{0.106}\left(N_{Bo}N_{Ga}\right)^{-0.084}, \tag{4.1}$$

where C and α are constants relating to impeller type and location (the values of C and α are given by Skelland and Ramsay, (1987) for a flat-blade turbines); d_v is vessel diameter; d_i is impeller diameter; ϕ is volume fraction of the dispersed-phase; N_{Fr} is the Froude number ($d_i N^2 \rho_m/\Delta\rho g$); N_{Bo} is the Bond number ($d_i^2 g\Delta\rho/\sigma$); and N_{Ga} is the Galileo number ($d_i^3 g\rho_m\Delta\rho/\mu_m^2$). Substituting values of N_{Fr}, N_{Bo}, and N_{Ga} and simplification (as per Skelland and Kanel, 1990) gives,

$$N_{\min} = C\left(\frac{d_v}{d_i}\right)^{\alpha} \frac{g^{0.42}\Delta\rho^{0.42}\mu_m^{0.08}\sigma^{0.04}\phi^{0.05}}{d_i^{0.71}\rho_m^{0.54}}, \tag{4.2}$$

where from Laity and Treybal (1957); Vermeulen et al. (1955) the mean density is

$$\rho_m = \phi\rho_d + (1-\phi)\rho_c, \tag{4.3}$$

and mean viscosity is

$$\mu_m = \frac{\mu_c}{1-\phi}\left(1+\frac{1.5\mu_d\phi}{\mu_d+\mu_c}\right). \tag{1.3}$$

If the dispersed-phase is non-Newtonian, μ_d becomes the apparent viscosity (Skelland and Kanel, 1990),

$$\mu_d = \mu_A = K\left(k_s N\right)^{n-1} \tag{4.4}$$

where K is the flow consistency index, n is the flow behavior index, N is the impeller speed and k_s is a constant with recommended value 11±5 (Metzner et al., 1961). Based on the correlation of Skelland and Kanel (1990), the minimum impeller speed for complete dispersion (using the vessel geometry data in Table 5.5 and physical property data in Table 3.3) is 265 rpm when the dispersed-phase volume fraction, ϕ , is 0.10 and the %IPA-CA dope is 50%. A sample calculation for the minimum impeller speed is provided in Appendix A4.

CHAPTER 5
PRELIMINARY MASS TRANSFER KINETICS STUDY

Introduction

Preliminary batch experiments were conducted to establish mass transfer kinetics for extracting sodium sulfate salt from cellulose acetate dope into a predominantly aqueous solution containing acetic acid and isopropyl acetate. These experiments were designed to measure the period of time between initial dispersion of the cellulose acetate dope in the aqueous solution and the point at which the sulfate salt concentration in the aqueous solution reaches equilibrium. A dispersed-phase mass transfer coefficient may be derived from the [Na^-] versus time data. In this experiment set, solvent concentration (both in the dispersed-phase and continuous-phase), was varied to study its effect on the cellulose acetate dope behavior and to determine its effect on the period of time between initial contact and phase equilibria.

Theoretical Development

Skelland -HuXien Model

Skelland and Hu Xien (1990) developed a model for mass transfer from droplets based upon the "continuous" generation of new surface due to droplet breakup. They developed an empirical correlation for the dispersed-phase mass transfer coefficient as

$$\frac{k_d}{\left[D_{AB} / t_{95\%}\right]^{1/2}} = 5.0(10^{-6})\phi^{-0.0204}\left(\frac{d_I^2 N\rho_m}{\mu_m}\right)^{1.140}\left(\frac{\rho_c}{\Delta\rho}\right)^{0.518} \qquad (5.1)$$

which predicted k_d with a mean absolute deviation of 9.8% for 55 experimental runs.

Chapter 6 provides a detailed discussion of the assumptions applied in the development of the Skelland - HuXien (1990) model.

Dispersed-phase Mass Transfer Coefficient from Experimental **[Na^+]** ***and*** d_p ***Data***

Driving force calculations (in Appendix A5) indicate that the dominant transfer resistance resides in the organic phase. Accordingly, if the organic phase is dispersed, the mass transfer coefficient may be estimated using the expression developed in Chapter 1: Substitution of A, total transfer area, into equation 1.12 with aV gives,

$$\ln\left(\frac{C_a}{C_{ao}}\right) = -\frac{k_d a V}{V_d}(t - t_o), \tag{5.2}$$

where a is the interfacial area per unit volume of the system and V is the total liquid volume. Thus, a plot of the left hand side of equation 5.2 versus t-t_O gives a straight line with slope equal to $-\frac{k_d a V}{V_d}$. The mass transfer coefficient, k_d, can then be determined from

$$k_d = -\frac{V_d}{aV}(slope). \tag{5.3}$$

Simplification of $\frac{aV_d}{V}$ in equation 5.3 as shown in Appendix 2 gives,

$$k_d = -\frac{d_p}{6}(slope). \tag{5.4}$$

Sample calculations for the dispersed mass transfer coefficient using equation 5.4 are provided in Appendix A5.

Sauter-mean Diameter, d_{32}, from Physical Property Data

The Sauter-mean diameter,

$$d_{32} = t^{-\beta}\alpha + d_{32}^{*}\ , \tag{5.5}$$

was used in equation 5.1 by Skelland and Hu Xien (1990) to approximate k_d in cases where the droplet diameter was less than 1 millimeter after time t_o when all of the dispersed-phase was added to the mixing vessel.

The dimensionless variables in equation 5.5, α, β, and d^{*}_{32} require knowledge of the vessel geometry in terms of impeller diameter, vessel diameter, and vessel fill height and may be evaluated from,

$$\alpha = 29.7 d_{32}^{*} \left(\frac{d_I}{d_v}\right)^{-2.015} \left(\frac{N_{Wec}}{N_{Rec}}\right)^{0.5508} N^{-0.7} \tag{5.6}$$

$$\frac{d_{32}^{*}}{d_I} = 0.05(1 + 2.316\phi)\left(\frac{d_I}{d_v}\right)^{-0.75} N_{Frc}^{-0.13} N_{Wec}^{-0.6} \tag{5.7}$$

as developed by Hong and Lee (1985). In this paper, Hong and Lee developed the general correlation equations 5.5-5.7 for the changes of the Sauter-mean droplet diameter

(d_{32}) with respect to time during the initial period of liquid-liquid dispersion in agitated vessels where the steady state droplet size (d^*_{32}) and α were correlated with operating variables and physical properties of liquid-liquid systems. Unlike α, β remained constant with changes in d_I/d_V and systems. β, the slope of $(d_{32}-d^*_{32})/d^*_{32}$ versus (Nt), equals 0.7. The absolute relative deviation ($|d_{32,observed}-d_{32,predicted}| / d_{32,observed}$) was 11.1%. Hong and Lee dispersed ethyl acetate or dimethylsiloxanes in sucrose water. In order to provide a point of reference, the physical properties for a few of the Hong and Lee systems as well as one of the systems studied here-in (taken from Table 3.3) are summarized in Table 5.1. The vessel geometry data used in the Sauter-mean diameter expression are summarized in Table 5.2. Sample calculations for d_{32} may be found in Appendix A5.

***Dispersed-phase Mass Transfer Coefficient from Experimental* [Na] *Data with* d_{32}**

The Sauter-mean diameter may be used to approximate the total interfacial area available for transfer, A, over time. In turn, the total transfer area may be used in the mass balance relationship, defined by equation 1.11, to estimate the dispersed-phase mass transfer coefficient.

$$\ln\frac{C_a}{C_{ao}} = -6k_d\int_0^t \frac{1}{\alpha(t)^{-0.7}+d^*_{32}}dt \qquad (1.11)$$

The values of α and d_{32}^* are calculated in Appendix 5 for each experimental run.

Table 5.1: Comparison of Physical Properties with those used as the basis of developing the Sauter-mean Diameter Expression (equation 5.5).

System	interfacial tension,	Density, g/cc		Viscosity cP:kg/m-s	
	dynes/cm	cont.	disp.	cont.	disp.
Hong&Lee- 1	32	1.087	0.920	2.9	4.6
Hong&Lee- 2	23	1.131	0.920	2.0	4.6
Hong&Lee- 3	42	1.000	0.787	1.0	1.7
50% IPA-CA	2	1.033	0.957	1.6	3,555

Table 5.2: Specifications of the experimental apparatus and Operating Conditions

Symbol		Description	Dimension
d_v	-	internal diameter of vessel	0.1302m
H_v	-	height of vessel	0.3175m
H	-	liquid height in vessel	0.2117m
d_I	-	diameter of impeller	0.0508m
ϕ	-	volume fraction	0.10
N	-	impeller speed	1000rpm

Experimental Apparatus

The apparatus employed in these experiments is shown in Figure 5.1. A three liter cylindrical vessel equipped with four vertical baffles at 90^{o} angles, an Applikon™ magnetic drive, and a two inch diameter six-flat-blade turbine was used as the mixing vessel configuration. A Liquid-Flow™ gear pump was used to transfer the dispersed-phase from an agitated two liter round bottom reservoir to the mixing vessel; the calibration data for this pump is supplied in Table 5.3.

Experimental Procedure

A total of eleven experiments were carried out; each experiment was conducted at room temperature and atmospheric pressure. Material handling dictated the composition of each phase; see Chapter 4 for more detail on establishing experimental range. For the bulk of the experiments, cellulose acetate dope in solution with 50% by weight isopropyl acetate (i.e., solvated dope) was dispersed in a predominantly aqueous solution such that there was no solvent transfer between phases. To facilitate handling the viscous cellulose acetate dope solution, a small volume fraction (1:9 dispersed to continuous ratio) was used.

The same method was used at lower solvent concentrations; however, instead of forming the desired liquid-liquid dispersion, a solid-liquid dispersion resulted. For example, experiments conducted using a 40% by weight isopropyl acetate - cellulose acetate dope solution resulted with precipitation of the cellulose acetate. Likewise, an experiment conducted using a 30% by weight isopropyl acetate - cellulose acetate dope solution resulted in precipitation of the cellulose acetate.

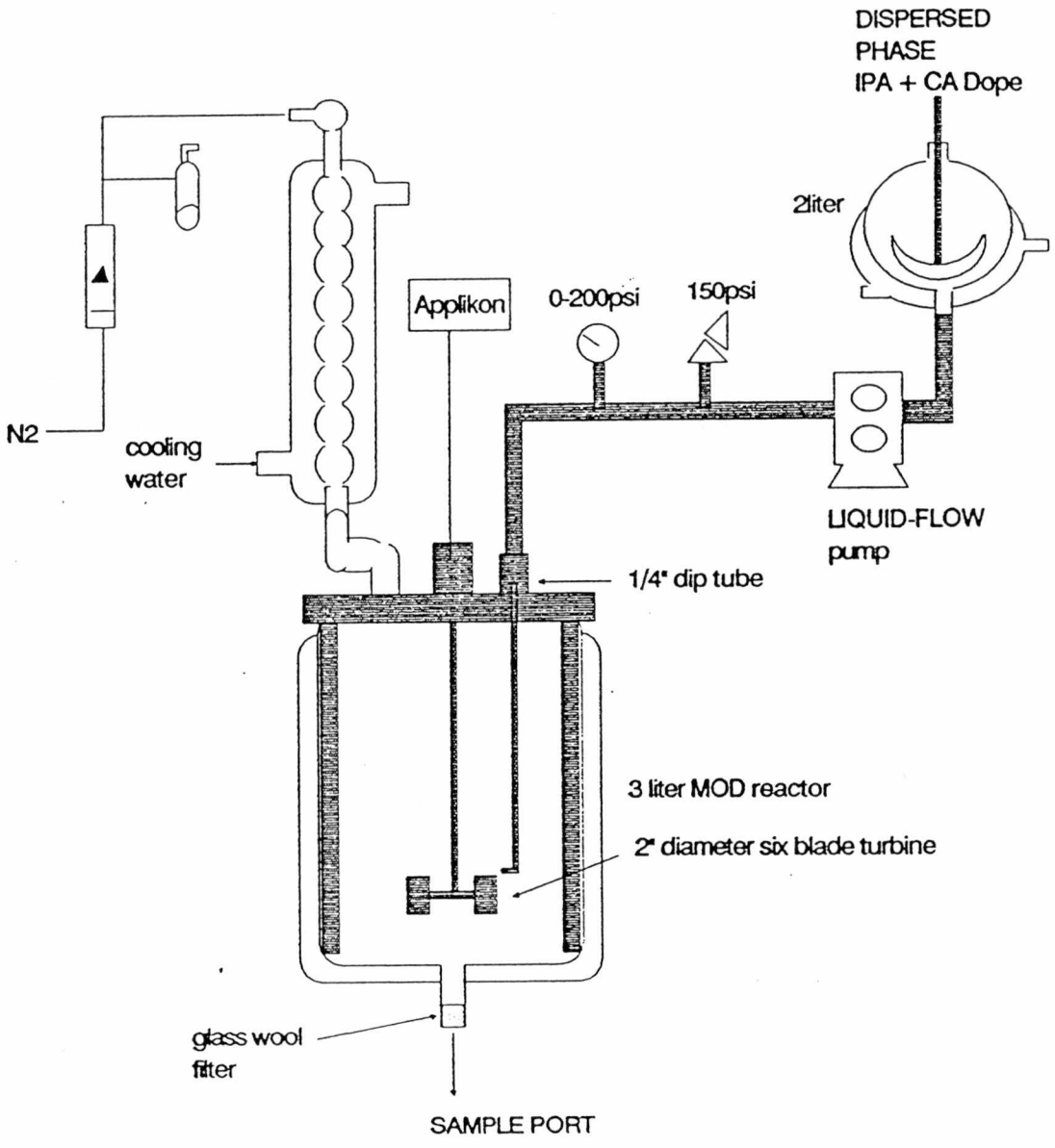

Figure 5.1: Apparatus for Experimental Estimation of Sodium Sulfate Transfer rate from Solvated Cellulose Acetate Dope.

Table 5.3: Calibration of Liquid-Flow TM Gear Pump

%IPA in CA Dope	Run Number	Elaspsed Time seconds	Amount Collected grams	Rate grams/sec	Pump Setting rpm	Grams per Revolution
10%	1	60	28.2	0.5	30	0.9
	2	60	30.2	0.5	40	0.8
	3	60	33.3	0.6	30	1.1
	4	60	35.0	0.6	40	0.9
	5	60	37.7	0.6	40	0.9
	6	60	35.1	0.6	30	1.2
	7	120	74.0	0.6	35	1.1
	8	60	69.1	1.2	35	2.0
30%	1	46	131.4	2.9	30	5.7
	2	46	148.1	3.2	40	4.8
	3	46	157.3	3.4	50	4.1
	4	20	52.7	2.6	50	3.2
	5	46	142.8	3.1	30	6.2
	6	46	157.3	3.4	40	5.1
	7	46	131.4	2.9	30	5.7
	8	46	135.8	3.0	40	4.4
	9	60	166.0	2.8	35	4.7
	10	60	169.8	2.8	35	4.9
40%	1	23	90.0	3.9	40	5.9
	2	50	176.0	3.5	40	5.3
	3	26	79.5	3.1	40	4.6
50%	1	39	210.0	5.4	40	8.0
	2	63	371.5	5.9	40	8.8
	3	49	310.0	6.3	40	9.4
	4	38	218.0	5.7	40	8.6
	5	57	265.0	4.6	40	6.9
	6	29	175.5	6.1	40	9.0

Each experiment was performed using the following procedure:

1. Samples of cellulose acetate dope were taken directly from manufacturing lines. The composition of each sample was determined by gas chromatography for the liquid components, percent solids for the cellulose acetate, and inductively coupled plasma for the sodium sulfate content. Resulting analyses of these samples are summarized in Table 5.4. The major components of the cellulose acetate dope include cellulose acetate, acetic acid, and water.
2. The cellulose acetate dope was added to a given amount isopropyl acetate necessary to achieve 30%, 40% or 50% by weight of isopropyl acetate and then mixed for 20 minutes at 300 rpm to form a homogeneous solution.
3. Meanwhile, the continuous-phase solution was mixed in graduated cylinders and added directly through the charge port in the reactor head.
4. The agitator was then set at 1000 rpm well above the minimum value needed for uniform dispersion, as defined by Skelland and Kanel (1989). Applying the Skelland and Kanel model to this experiment as shown in Appendix A4 Sample Calculations, gives a minimum impeller speed of 265 rpm if ϕ is 0.1.
5. The solvated dope was pumped in at a rate sufficient to charge the total amount in less than a minute.
6. The continuous-phase was sampled every five minutes from the time of dispersion for two hours and again 16 hours later for half of the experiments conducted. In a second set of experiments, in order to refine the estimated mass transfer rate range, the continuous phase was sampled one minute from the point of dispersion , again after 3 minutes and then every five minutes for two hours and again 16 hours later. Continuous-phase samples were selected from a given time interval (e.g., 1, 5, 15, 30, ..., 970 minutes) and then analyzed for ppm sodium sulfate by inductively coupled

Table 5.4 Composition of cellulose acetate (CA) dope sampled from manufacturing.

Experiment Initial Conditions		CA dope Sample Composition			
Dispersed	Continuous	weight percent			ppm
Phase	Phase	%H2O	%Acid	%CA	Na2SO4
40%IPA-CA dope	4%Acid	16.33	64.91	23.75	2100
40%IPA-CA dope	4%Acid	16.33	64.91	23.75	2100
50%IPA-CA dope	25.5%acid 6.3%IPA 68.2%H2O	16.33	64.91	23.75	2100
50%IPA-CA dope	30%acid/H2O sat. with IPA	16.33	64.91	23.75	2100
50%IPA-CA dope	30%acid/H2O sat. with IPA	16.33	64.91	23.75	2100
50%IPA-CA dope	27.4%acid 7.6%IPA 65.1%H2O	15.78	71.78	21.4	1300
50%IPA-CA dope	25.5%acid 7.6%IPA 68.2%H2O	15.40	68.18	21.25	1700
50%IPA-CA dope	26.5%acid 6.3%IPA 69.6%H2O	15.40	68.18	21.25	1700
50%IPA-CA dope	26.1%acid 5.3%IPA 68.4%H2O	15.40	68.18	21.25	1700
40%IPA-CA dope	8.6%acid 1.7%IPA 89.6%H2O	15.40	68.18	21.25	1700
30%IPA-CA dope	9.5%acid 2.4%IPA 88.6%H2O	14.08	67.10	21.10	1700

plasma within 10% accuracy. The sodium sulfate concentration in the continuous-phase over time is summarized for each experiment in Table 5.5. After 16 hours (arbitrarily designated as point of equilibrium) of mixing, the dispersed-phase was allowed to coalesce. The two phases were then separated and analyzed for liquid composition (acetic acid, water, and isopropyl acetate) by gas chromatography within 0.1% accuracy and cellulose acetate by percent solids within 0.31% accuracy. The phase equilibria data are shown in Table 5.5.

Discussion of Experimental Observations

Effect of Varying Solvent Concentration on CA Dope Behavior

The physical form of the dispersed-phase varied distinctively with the water concentration in the continuous-phase. As such, the tendency for the cellulose acetate in the dispersed-phase to precipitate increased when the concentration of water in the continuous-phase increased. For example, the 50% isopropyl acetate - cellulose acetate dope solution (50%IPA solvated dope), did not precipitate when dispersed in an aqueous solution containing 65% water, 27% acetic acid, and 8% isopropyl acetate; but instead, formed a *fluid gel*. Next, a dispersion of *viscous gel* spheres formed when mixing the 50%IPA solvated dope into a solution containing a slightly lower concentration of solvent- 26% acetic acid, 6% isopropyl acetate, and 68% water. Finally, the 50%IPA solvated dope precipitated into a *solid mass* when contacted with an aqueous solution containing 89% water, 9% acetic acid, and 2% isopropyl acetate.

The behavior of solvated dope during dispersion in the predominantly aqueous solution may be described using traditional phase diagrams. Refer to Chapter 4, Feasible experimental Regions, for a detailed discussion of phase characteristics with respect to variation in component concentrations. Table 5.6 summarizes dispersed-phase

Table 5.5: (continued)

Expt Run No.	Initial Conditions Dispersed	Continuous	Physical Form	Time minutes	Na2SO4 ppm	Phase Equilibrium Data C=continuous, D=dispersed	%IPA	%Acid	%H2O	%CA
8	50%IPA-	26.5%acid	viscous gel	1	35					
	CA dope	6.3%IPA	3mm sphere	5	45					
		69.6%H2O		15	44					
				35	38					
				65	45					
				125	47					
				970	66	C	8.11	27.58	64.13	0.10
						D	30.16	24.02	22.62	24.65
9	*50%IPA-	26.1%acid	viscous gel	1	19					
	CA dope	5.3%IPA	3mm sphere	5	51					
		68.4%H2O		15	46					
				35	50					
				65	45					
				85	45					
				125	54					
				970	64	C	7.38	27.66	65.21	0.10
						D	22.66	23.19	25.19	26.00
10	40%IPA-	8.6%acid	Precipitated:	1	12					
	CA dope	1.7%IPA	agglomerate	25	30					
		89.6%H2O		45	35					
				970	59	C	2.67	12.26	84.12	0.10
						D	25.88	11.54	47.54	18.90
11	30%IPA-	9.5%acid	Precipitated:	0.5	4					
	CA dope	2.4%IPA	agglomerate	2	24					
		88.6%H2O		45	26					
				985	46	C	3.56	14.23	81.18	0.5
						D	9.87	12.85	64.23	9.15

Table 5.5: Sodium sulfate concentration in the continuous-phase during extraction from cellulose acetate (CA) dope.

Expt. Run No.	Initial Conditions Dispersed	Continuous	Physical Form	Time minutes	Na2SO4 ppm	Phase Equilibrium Data C=continuous, D=dispersed	%IPA	%Acid	%H2O	%CA
1	40%IPA-CA dope	4%Acid	Precipitated: noodles 13mmx2mm	5	19					
				15	28					
				25	32					
				40	39					
				60	39					
				1020	46	C	1.22	4.42	91.29	0.00
						D	1.23	3.71	77.74	13.05
2	40%IPA-CA dope	4%Acid	Precipitated: agglomerate	5	47					
				15	45					
				25	51					
				50	78	D NO SAMPLE				
				70	75	C	2.14	6.68	88.36	0.00
3	50%IPA-CA dope	25.5%acid 6.3%IPA 68.2%H2O	Precipitated: flake 10-20mm	5	26					
				15	28					
				25	25					
				50	27					
				60	26					
				975	26	C	6.47	26.54	66.26	0.00
						D	4.09	13.74	29.63	22.15
4	50%IPA-CA dope	30%acid/H2O sat. with IPA	fluid gel 0.5 mm sphere	5	30					
				15	28					
				25	28					
				50	28					
				90	29	D NO SAMPLE				
				985	36	C	8.01	27.91	63.41	0.00

Table 5.5: (Continued)

Expt. Run No.	Initial Conditions Dispersed	Continuous	Physical Form	Time minutes	Na2SO4 ppm	Phase Equilibrium Data C=continuous, D=dispersed	%IPA	%Acid	%H2O	%CA
5	50%IPA-	30%acid/H2O	fluid gel	5	48					
	CA dope	sat. with IPA	0.5 mm sphere	15	53					
				25	55					
				50	56					
				60	55					
				978	57	C	9.24	28.52	61.95	0.00
						D	27.75	23.92	26.00	21.75
6	*50%IPA-	27.4%acid	fluid gel	1	54					
	CA dope	7.6%IPA	0.5 mm sphere	3	68					
		65.1%H2O		6	59					
				36	68					
				66	92					
				96	110					
				126	79					
				970	89	C	9.02	29.46	61.45	0.10
						D	38.17	21.03	24.14	17.90
7	50%IPA-	25.5%acid	viscous gel	1	84					
	CA dope	7.6%IPA	3mm sphere	5	70					
		68.2%H2O		15	70					
				35	67					
				55	73					
				85	75					
				125	70					
				970	80	C	7.97	28.52	63.25	0.10
						D	19.86	22.06	23.24	32.05

Table 5.6: Organic Phase Composition at Phase Equilibrium

Dispersion Form	%IPA	%Acid	%H2O	%CA
Fluid droplets	45	21	19	15
Viscous droplets	30	22	23	25
Small solids	4	39	24	33
Large solid mass	14	13	10	64

Note: The characteristic of the organic phase and its respective composition range after 16 hours of mixing in the predominantly aqueous continuous-phase is provided below. This information is summarized from thirteen experiments where the phase ratio was 1:9 dispersed to continuous.

composition at phase equilibrium for each system (i.e., where the dispersed-phase ranges from fluid droplets to viscous droplets to small solids).

Fluid Droplets. Per visual observation, the organic phase dispersed into minuscule spheres less than 0.5 mm in diameter suspended by agitation. With out agitation the droplets gradually settled to the bottom of the vessel and coalesced. At equilibrium, the composition of the fluid gel phase was about 45% isopropyl acetate, 28% acetic acid, 12% water, and 15% cellulose acetate. The low solids and high solvent concentration accounts for the fluid nature of the dispersed-phase.

Viscous Droplets. Per visual observation, the organic phase dispersed into viscous gel spheres which were about 3 mm in diameter. With out agitation the droplets quickly settled to the bottom of the vessel and coalesced. This is expected since the viscous droplets are less buoyant than the fluid gel droplets. At equilibrium, the composition range of the viscous gel was 20-30% isopropyl acetate, 22-24% acetic acid, 22-25% water, and 25-32% cellulose acetate. The higher solids concentration accounts for the more viscous nature of the dispersed-phase.

Small Solids. The precipitated solids ranged in shape from spaghetti-like noodles 13 millimeters long by 2 millimeters diameter to irregular flakes 2 millimeters in diameter. The final composition ranged from 1-4% isopropyl acetate, 4-15% acetic acid, 13-22% water, and 30-78% cellulose acetate.

Large Solid Mass. In contrast to the fluid gel and the viscous gel, the solvent immediately transferred from the solvated dope phase to the predominantly aqueous-phase. As a result, an agglomerated mass formed upon contact.

Effect of Solvent Concentration on Residence Time

Fluid Droplets. Analytical results for ppm sodium sulfate in the continuous-phase indicate that 95% of mass transfer was achieved within 1 to 3 minutes for a fluid

gelatinous droplet. The initial composition of the continuous-phase was 27% acetic acid, 8% isopropyl acetate and 65% water, while the equilibrium composition was 29% acetic acid, 9% isopropyl acetate and 62% water. The slight increase in solvent concentration in the continuous-phase suggests that along with the sulfate salt, a small amount of solvent and cosolvent may have transferred to the continuos phase. However, since there is negligible solubility of sodium sulfate in isopropyl acetate and acetic acid, it can be deduced that diffusion is the major proponent of sulfate salt transport into the continuous-phase rather than solvent flux. Other plausible explanations for the difference in initial and equilibrium compositions include analytical error and sampling error.

Viscous Droplets. Analytical results for ppm sodium sulfate in the continuous-phase indicate that 95% of mass transfer was achieved within 5 minutes for a viscous gelatinous droplet. The initial composition of the continuous-phase was about 26% acetic acid, 8% isopropyl acetate and 68% water, while the final composition ranged from 27.6-28.5% acetic acid, 7.4-8.1% isopropyl acetate and 63.3-65.2% water,. The slight increase in acetic acid concentration in the continuous-phase suggests that along with the sulfate salt, a small amount of solvent and cosolvent may have transferred to the continuos phase (see Table 5.4). However, since there is negligible solubility of sodium sulfate in acetic acid, it can be deduced that diffusion is the major proponent of sulfate salt transport into the continuous-phase rather than solvent flux. As stated above, analytical error and sampling error may account for the difference between the initial acetic acid concentration and the equilibrium acetic acid concentration in the continuous-phase.

Small Solids. Analytical results for ppm sodium sulfate in the continuous-phase indicate that equilibrium was achieved within 15 to 50 minutes for precipitated flakes roughly 2 millimeters in diameter. At equilibrium, the composition range of the continuous-phase was 3-4% isopropyl acetate, 14-42% acetic acid, 24-30% water, and 22-33% cellulose acetate. The initial composition of the continuous-phase, 6.3%

isopropyl acetate, 25.5% acetic acid, 68.2% water, suggests a definite flux of solvent and water from the dispersed-phase. As discussed in Chapter 4, there is a narrow region between a fluid gel and a precipitated solid.

Large Solid Mass. Analytical results for ppm sodium sulfate in the continuous-phase indicate that equilibrium was not achieved after 120 minutes for these large solids. At equilibrium, the solid mass composition ranged from 10-26% isopropyl acetate, 12-13% acetic acid, 9-19% water, and 48-64% cellulose acetate.

Data Analysis

Three values for the dispersed-phase mass transfer coefficient have been approximated.

- $k_{d\,\text{experimental}}$, determined from equation 5.4 using experimentally observed droplet diameter and analytically measured Na ion concentration data;
- $k_{d\,\text{prediction}}$, found using equation 1.11 (derived from Hong and Lee's (1985) empirical model) with analytically measured Na ion concentration data
- $k_{d\,\text{prediction}}$, calculated using the Skelland and HuXien (1990) model (represented as equation 5.1) with experimentally measured viscosity, density, and interfacial tension (summarized in Table 3.3) and diffusivity data (shown in Table 3.4).

First, the experimental dispersed-phase mass transfer coefficient ($k_{d\,exp}$) was calculated by using the slope, $Ln(C_d/C_{dO}) / (t-t_O)$, obtained from linear regression of experimentally measured Na ion concentrations in equation 5.2. Table 5.7 summarizes experimentally derived dispersed-phase mass transfer coefficients. The concentration of

Table 5.7: Calculation of the Dispersed-phase Mass Transfer Coefficient using Experimental Data

Form of Dispersion	Observed droplet diameter, cm	SLOPE: $\frac{\ln\left(\frac{Ca}{Cao}\right)}{t-t_o}$	Dispersed-phase Mass Transfer Coef., cm/min $k_d = -\frac{d_p}{6} Slope$
Fluid Spheres	0.03	-0.0012	6.0E-06
	0.04±0.01	-0.0012	8.0E-06
	0.02	-0.0012	1.0E-05
Viscous Spheres	0.28	-0.0001	4.7E-06
	0.29±0.01	-0.0001	4.8E-06
	0.30	-0.0001	5.0E-06

Na ions in the dispersed-phase was calculated via a mass balance on the continuous-phase sodium content. An example of the mass balance calculation is provided in Appendix A5.

Figure 5.2 shows a typical plot of sodium concentration in the continuous-phase over time. The [Na-]-versus-time curves for experimental Runs 2-11 are provided in Appendix A5 as Figures A5.1-A5.10. Typical $Ln(C_d/C_{do})$ versus $(t-t_o)$ plots are shown in Figure 5.3 and 5.4.

Second, the Sauter-mean diameter was estimated with equation 5.5 using vessel geometry data in Table 5.2. Sample calculations for the Sauter-mean diameter are provided in Appendix A5. For the fluid droplet case, the calculated Sauter-mean diameter, 0.019 cm, was in the same order of magnitude as the experimentally observed, 0.05 cm, droplet diameter. In contrast, the viscous droplet case, the Sauter-mean diameter, 0.008 cm, was two orders of magnitude smaller. This may be attributed to the fact that the droplet viscosity is not accounted for by the expression. Recall from Table 3.3 that the viscosity for the viscous droplet (23,000cP- 58,000cP) is an order of magnitude larger than viscosity for the fluid droplet (3,500-6,300cP). The Froude number does account for the density difference between both phases; but, it has a small impact on the d_{32} expression, equations 5.5 through 5.7.

Lastly, k_d was predicted with the Skelland and HuXien (1990) model using experimentally measured viscosity and density (from Table 3.3), calculated diffusivity (from Table 3.4), and experimentally measured $t_{95\%}$ (in Table 5.8). Sample calculations for k_d are provided in Appendix A5. Table 5.8 summarizes predicted k_d's for all systems. The predicted k_d's do not fall within the range of experimentally derived k_d's.

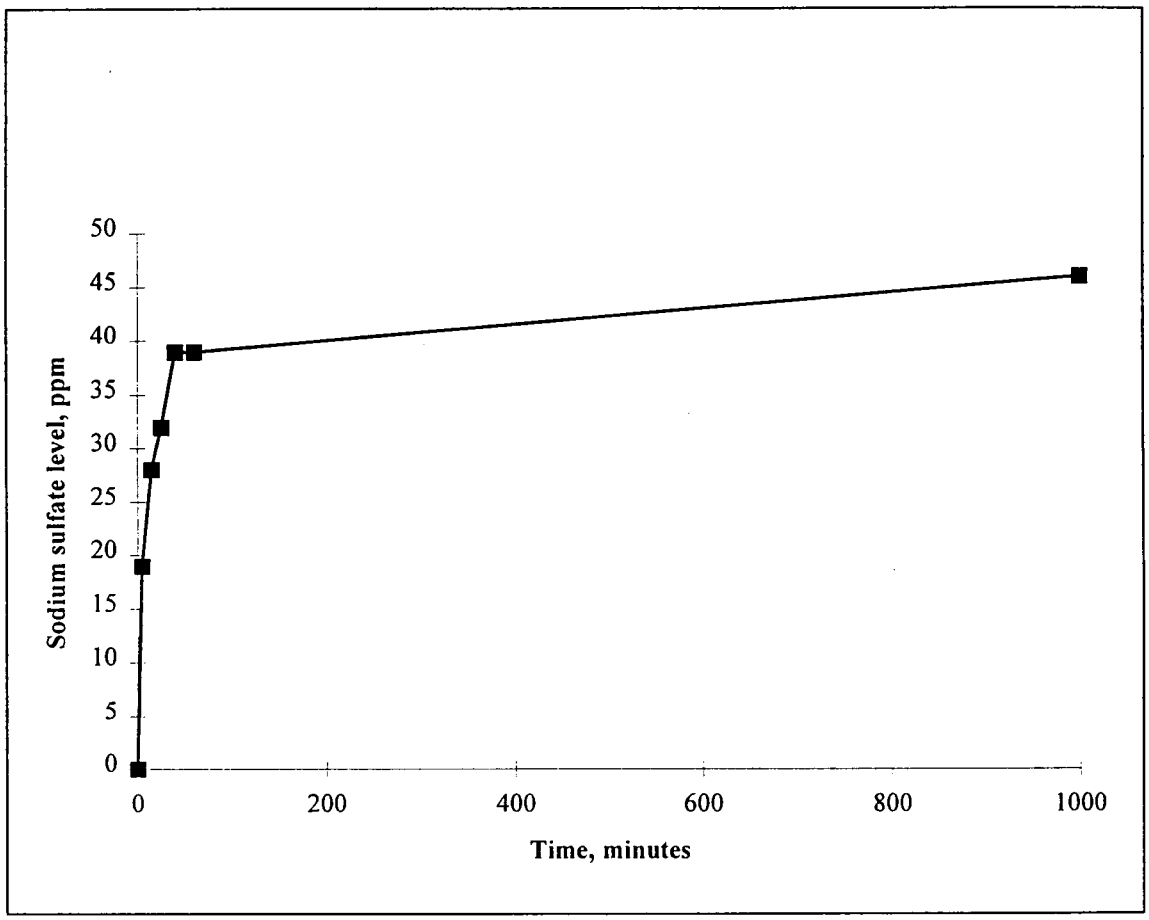

Figure 5.2: Time required for Sodium sulfate concentration in the continuous-phase to reach equilibrium for Run 1.

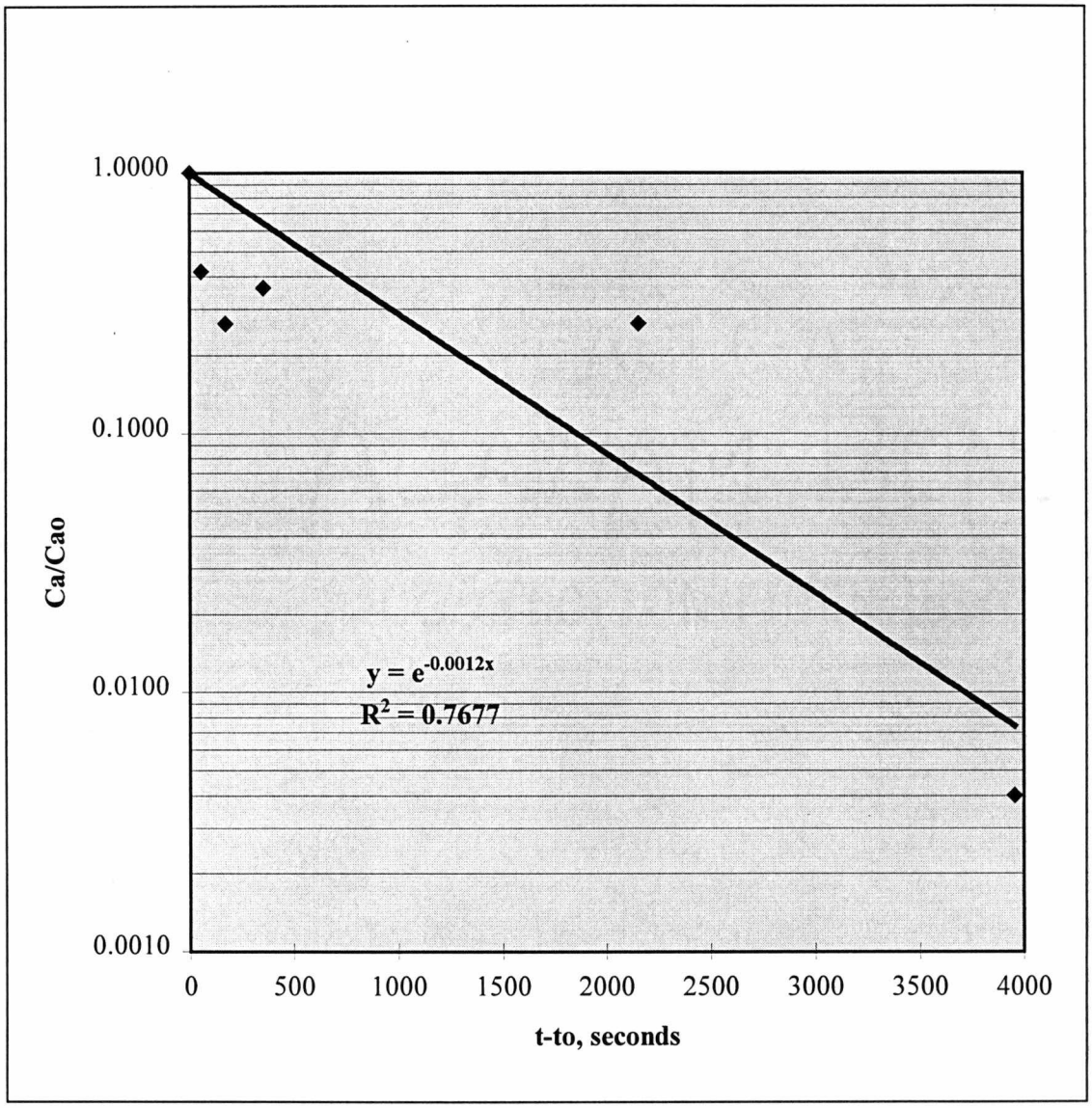

Figure 5.3: Plot of $Ln(C_a/C_{ao})$ vs $t\text{-}t_o$ for Fluid Droplet. The slope of the line, $\frac{Ln\left(\frac{C_a}{C_{ao}}\right)}{t-t_o}$, is used in Table 5.7 to calculate the dispersed-phase mass transfer coefficient, k_d.

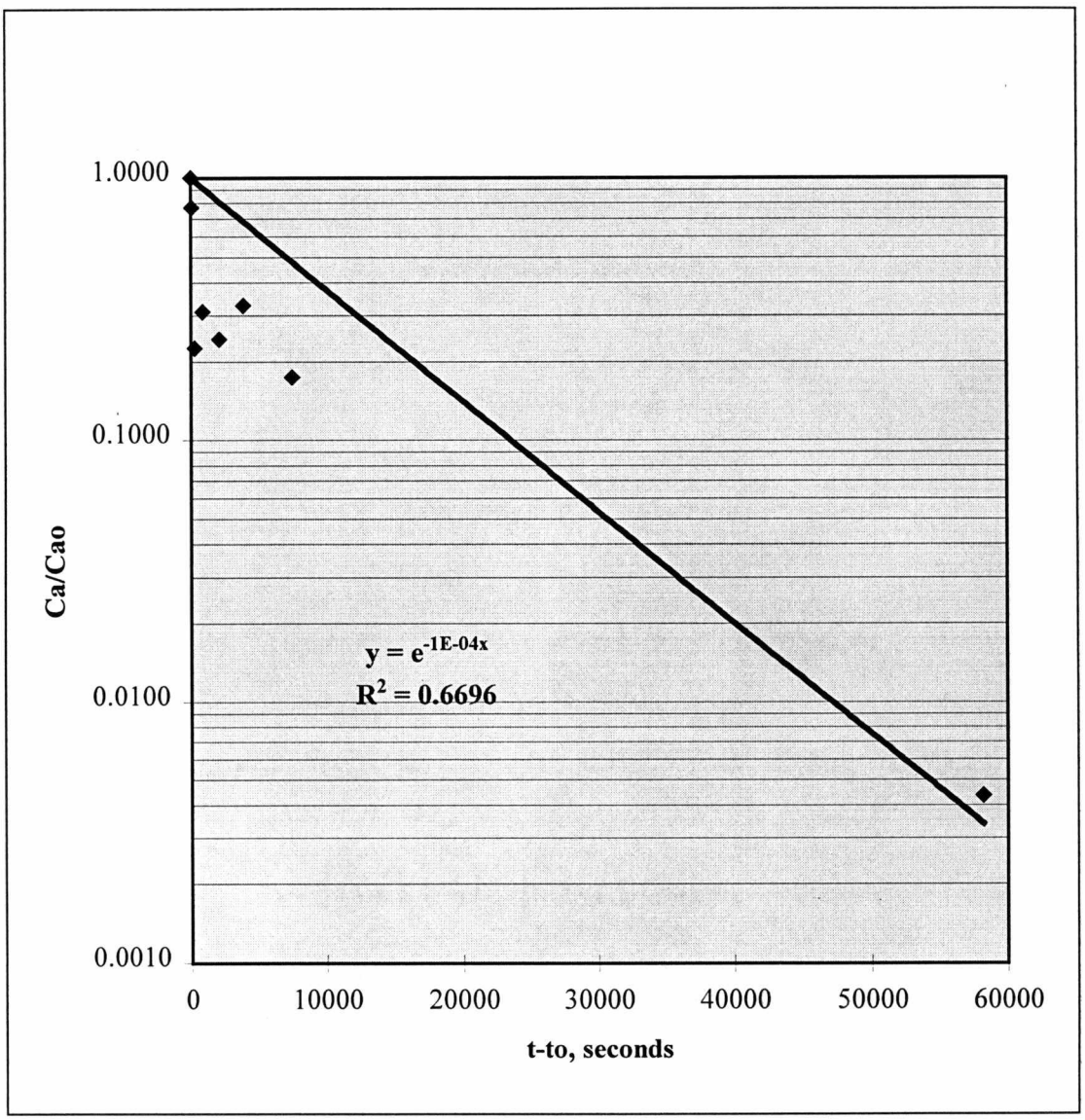

Figure 5.4: Plot of $Ln(C_a/C_{ao})$ vs $t\text{-}t_o$ for Viscous Droplet. The slope of the line, $\frac{Ln\left(\frac{C_a}{C_{ao}}\right)}{t-t_o}$, is used in Table 5.7 to calculate the dispersed-phase mass transfer coefficient, k_d.

Table 5.8: Dispersed-phase Mass Transfer Coefficient Calculation using physical property data from Table 3.3 with the Skelland and HuXien (1990) Expression.

Expt. Set	Run No.	Mean Density, ρ_m g/cc	Mean Viscosity, μ_m P: g/cm-sec	Time to reach 95% mass transfer $t_{95\%,\ seconds}$	k_d cm/sec
30%IPA	1	1.04	0.035	900	5.89E-07
	2	1.01	0.034	900	3.63E-07
	3	1.00	0.032	900	3.00E-07
40%IPA	1	1.02	0.033	180	4.19E-06
	2	1.02	0.032	180	2.84E-06
	3	1.02	0.032	180	4.29E-06
50%IPA	1	1.00	0.033	120	5.91E-06
	2	1.01	0.032	120	8.40E-06
	3	1.00	0.033	120	8.08E-06

Note: Equation (1.3) becomes , $\mu_m = \frac{\mu_c}{1-\phi}[1+1.5\phi]$, where $\mu_d >> \mu_c$

$$\rho_m = \phi\rho_d + (1-\phi)\rho_c$$

$$\frac{k_d}{\left[D_{AB}/t_{95}\right]^{1/2}} = 5.0(10^{-6})\phi^{-0.0204}\left(\frac{d_I^2 N\rho_m}{\mu_m}\right)^{1.140}\left(\frac{\rho_c}{\Delta\rho}\right)^{0.518}$$

Conclusions

Three major conclusions resulted from this preliminary study of mass transfer characteristics for three solvated dope systems ranging in viscosity from 200,000 centipoise to 4,000 centipoise.

1. The bulk of the mass transfer occurred within 3 minutes for liquid-liquid systems (where the dispersed-phase is a cellulose acetate solution containing 50% by weight isopropyl acetate). Therefore, additional experiments are needed to focus on the time period between 0 and 3 minutes to improve the characterization of mass transfer from the dispersed-phase. The additional experiments should include a range of volume fractions to determine the effect on dispersed-phase controlled mass transfer.

2. Internal circulation may be eliminated as a consideration in predicting the dispersed-phase mass transfer coefficient. The theory of stagnation was validated by comparing the experimentally observed dispersed-phase drop sizes with Kolmogoroff's length scale,

$$\eta = \varepsilon^{-\frac{1}{4}} \upsilon^{\frac{3}{4}} \tag{1.4}$$

which marks the upper limit of eddy sizes in the viscous sub-range. Dispersed-phase droplets were clearly within the inertial sub-range of eddy sizes, 0.0118m, as calculated in Appendix A2. (Skelland and Moeti, 1990)

3. Eliminate future study of solvent levels below 50% by weight in cellulose acetate dope. Mass transfer data is unreliable due to the narrow operating region where the

cellulose acetate in dispersed-phase has a high tendency to precipitate out of solution. In addition, it is difficult to focus in on the first 60 seconds of transfer due to the extended addition periods associated with high viscosity of the solvated dopes systems containing less than 50% isopropyl acetate (by weight).

CHAPTER 6

MASS TRANSFER KINETICS

Introduction

The previous chapter established a baseline for a more focused study of mass transfer kinetics. The experimental study discussed in Chapter 5 centered on an analytical approach to measuring the solute concentration. It was determined that the bulk of the transfer occurred within the first 2-3 minutes; yet, only five data points were available in this period of transfer. This chapter attempts to refine the sodium concentration-time data by focusing on the first 5 minutes of mass transfer with more frequent [Na^+] measurements. Accordingly, a portable conductivity meter will be used to record the solute concentration in the continuous-phase as the solute transfers from dispersed-phase droplets.

First, the dispersed-phase mass transfer coefficient, k_d, will be derived experimentally and compared to k_d's predicted by the Skelland HuXien (1990) model and the Penetration Theory, Higbie(1935). The visually measured droplet size will be compared to the Sauter-mean diameter (Hong and Lee, 1985).

Second, the continuous-phase mass transfer coefficient, k_c, will be estimated using the Skelland and Moeti (1990) expression. In turn, the dispersed-phase mass transfer

coefficient and the continuous-phase mass transfer coefficient will be used to estimate an overall mass transfer coefficient for liquid-liquid extraction in an agitated vessel.

Theoretical Development

Mass Transfer Coefficient Models for k_d

There have been two recent publications on prediction of mass transfer coefficients in agitated liquid-liquid dispersions that allow one to predict the mass transfer kinetics. If the dispersed-phase controls the rate of solute transfer (in this case when the organic phase is dispersed), the mass transfer coefficient can be computed by the Skelland and Hu Xien (1990) semitheoretical correlation. If, on the other hand, the continuous-phase is controlling, the continuous-phase mass transfer may be calculated by the Skelland and Moeti (1990) expression. Both of these models were developed for Newtonian liquid-liquid systems, but in this case the cellulose acetate rich organic phase is non-Newtonian of pseudoplastic nature. The correlations, therefore, strictly do not apply, but they may be extended to include the non-Newtonian behavior of one phase by application of the Skelland and Kanel (1990) technique. This method was used to extend correlations for the minimum impeller speed for complete dispersion of one immiscible liquid in another to include the case where one of the phases was non-Newtonian of the power law type. The apparent viscosity, μ_a, of the fluid in the agitated vessel was computed as

$$\mu_a = K\left|\left(\frac{du}{dy}\right)_a\right|^{n-1} \tag{1.2}$$

where K is the fluid consistency index and n is the flow behavior index, both representative of the non-Newtonian fluid. These qualities are tabulated in the physical property data table (Table 3.3). The apparent shear rate, $(du/dy)_a$, was found by Metzner and Taylor (1960) to be equivalent to the impeller speed multiplied by a constant, k_s, which was found to have an approximate value of 11 by Metzner et al. (1961) when the impeller speed, N, is in rpm. Thus,

$$\left(\frac{du}{dy}\right)_a = k_s N.$$

The apparent viscosity was then substituted into the mean viscosity expression of Vermeulen et al. (1955) for the appropriate phase (either dispersed or continuous)

$$\mu_m = \frac{\mu_c}{1-\phi}\left[1+\frac{1.5\mu_d\phi}{\mu_c+\mu_d}\right] \tag{1.3}$$

where ϕ is the volume fraction of the dispersed-phase, μ_m is the mean viscosity, and μ_c and μ_d are the continuous and dispersed-phase viscosities, respectively.

Penetration theory (Higbie, 1935). The penetration theory predicts a mass transfer coefficient for the transfer across a gas-liquid interface proportional to $(D_{AB})^{0.5}$,

$$k_d = 2\sqrt{\frac{D_{AB}}{\pi t_s}} \tag{6.1}$$

where t_S is the exposure time of the new surface. Hines and Maddux (1985) capture Higbie's (1935) assumptions best by stating, "..this theory assumes that the liquid surface consists of small fluid elements that contact the gas phase for an average time, after which they penetrate into the bulk liquid. Each element is then replaced by another element from the bulk liquid phase." At face value, this approximation implies that the mass transfer coefficient is independent of drop size. Hines and Maddux (1985) described the model as "the unsteady-state diffusion [or penetration] of a solute into a liquid phase of infinite thickness." Skelland (1985) as with Treybal (1955) suggest that the indicated dependence on diffusivity is typical of short exposure times, where depth of solute penetration is small relative to the depth of the absorbing pool.

Skelland -HuXien Model. Skelland and Hu Xien (1990) were pioneers in the study of dispersed-phase controlled mass transfer in batch liquid-liquid systems (Skelland and Kanel, 1990). They developed a model for mass transfer from droplets based upon the "continuous" generation of new surface due to droplet breakup. They developed an empirical correlation, equation 5.1, for the dispersed-phase mass transfer coefficient.

Substituting time t_f (the point at which 99% of solute has transferred to the continuous-phase) in equation 5.1 for t_{95} gives,

$$\frac{k_d}{\left[D_{AB}/t_f\right]^{1/2}} = 5.0(10^{-6})\phi^{-0.0204}\left(\frac{d_I^2 N\rho_M}{\mu_M}\right)^{1.140}\left(\frac{\rho_c}{\Delta\rho}\right)^{0.518} \tag{6.2}$$

The empirical model, equation 5.1, predicted k_d with a mean absolute deviation of 9.8% for 55 experimental runs. From Laity and Treybal (1957); Vermeulen et al. (1955) the mean density follows:

$$\rho_M = \phi\rho_d + (1-\phi)\rho_c. \tag{6.3}$$

This model builds on the Penetration theory accounting for the effect of drop breakage and the change in drop size over time in the Reynold's number and density ratio terms. In addition, entrance effects between time t_0 and time t_1 are included in the t_f term. Similar to the experiment set to follow, six-flat-blade turbines were centrally placed in a baffled vessel. Following are the conditions under which the model, equation 5.1, was developed:

- Impeller speed ranged between 3.2-12 rps. The impeller speed used herein , 4.2 rps, falls within the range.
- Low volume fractions, 0.14-0.09, were used to insure little to no droplet coalescence. Volume fraction in this experiment set range from 0.05 to 0.20.

- The droplets were treated as internally stagnant between breakage.
- Low total transfer (ppm level) was used causing driving force, C_a-$C_a{}^*$ to be linear with C_a.
- Exposure times ranged between 0.26-1.31 minutes.
- Aqueous continuous-phase

Experimental k_d. As in Chapter 5, the mass-transfer process will be analyzed between time t_0, when the initial disturbance due to dispersed-phase addition has ceased and time t_f, when 99% of solute has been transferred. The experimental k_d will be estimated using equation 5.4 with the visually measured drop size, d_p.

Hong and Lee (1985) Sauter-mean Diameter Relationship. The slope of the $\ln C_a/C_{ao}$ versus $\int_{20s} \frac{1}{\alpha(t)^{-0.7} + d_{32}^*} dt$ will be used in equation 1.11,

$$\ln \frac{C_a}{C_{ao}} = -6k_d \int_0 \frac{1}{\alpha(t)^{-0.7} + d_{32}^*} dt \qquad (1.11)$$

to calculate the dispersed-phase mass transfer coefficient. The integral will be evaluated numerically between time t_0= 20 seconds (since Hong and Lee's (1985) model is valid after 20 seconds) and time t_f at 30 second intervals. For example, in the ϕ=0.05 case, there are three intervals- 20 to 30 seconds, 20 to 60 seconds, and 20 to 90 seconds. As shown in Appendix Table A6.19, time t_f increases with the dispersed-phase volume fraction.

The Sauter-mean diameter will be estimated using equations 5.5-5.7 and then compared to visually measured drop size, d_p. Similarly, the k_d determined from the Hong and Lee (1985) Sauter-mean diameter relationship, equation 1.11, will be compared to the k_d determined from d_p.

Reducing terms in equation 1.11 gives,

$$k_d = -\frac{slope}{6}. \tag{6.4}$$

The resulting slope will be used in equation 6.4 to calculate k_d.

Mass Transfer Coefficient Model for k_c

Presented below is a correlation for the continuous-phase mass transfer coefficient, k_c, in a batch agitated liquid-liquid dispersion as developed by Skelland and Moeti (1990).

Skelland and Moeti (1990) investigated the mass transfer mechanisms by varying molecular diffusivity over an eight fold range. They determined that k_c was proportional to the molecular diffusivity raised to the 2/3 power. The resulting expression was found to be

$$\frac{k_c d_p}{D_c} = 1.237(10^{-5})\left(\frac{\mu_c}{\rho_c D_c}\right)^{1/3}\left(\frac{d_I^2 N \rho_c}{\mu_c}\right)^{2/3}\left(\frac{d_I N^2}{g}\right)^{5/12}\left(\frac{d_I}{d_p}\right)^{2}\left(\frac{d_p}{T}\right)^{1/2}\left(\frac{\rho_d d_p^2 g}{\sigma}\right)^{5/4}\phi^{-1/2} \tag{6.5}$$

based on 180 experiments with an average absolute deviation of 19.71%.

Prediction Of Overall Mass Transfer Coefficient

The overall mass transfer coefficient, K_d is written in terms of k_c and k_d as

$$\frac{1}{K_d} = \frac{1}{k_d} + \frac{1}{mk_c} \quad ; \tag{6.6}$$

where, m is defined as

$$m = \frac{[Na_2SO_4]_{Aqueous}}{[Na_2SO_4]_{Organic}} \tag{6.7}$$

In this experiment set, the organic phase is dispersed. Recall that in Chapter 1, it was assumed that K_d=k_d; since, k_c is expected to be much greater than k_d.

Description of Apparatus

Experiments were carried out in a cylindrical glass vessel fitted with four equally spaced, radial, vertical wall baffles, and whose dimensions are listed in Table 5.5.

An agitator equipped with a 316 stainless steel six-flat-blade turbine impeller was used since this type impeller showed the best dispersion performance during the solvent screening experiments discussed in Chapter 2.

The change of Na^+ concentration in the continuous-phase was measured analytically by sampling and continuously by monitoring electrical conductivity as recommended by Rushton et al. (1964). Accordingly, a portable Fischer™ Model 4070 conductivity meter was braced against one of the vessel baffles. The meter did not have a port for record connection; so, micro Siemen (μS) readings were recorded manually every 15 seconds.

A calibration curve giving the conductivity versus solute concentration was made as follows. First, the relation between the conductivity and solute concentration was obtained without the organic dispersed-phase. This was achieved by measuring the conductivities of progressively diluted aqueous solutions. Then the effect of the presence of the isopropyl acetate and acetic acid was found in solutions of known concentration. A summary of calibration data is provided in Appendix Table A6.1. In addition, a plot and regression of ppmNa - μS data are provided in Appendix Figures A6.1 and A6.2.

A Toledo Scale was placed under the mixing vessel to measure the amount of material added.

Experimental Procedure

The continuous and dispersed-phases of each system were prepared separately. In making the dispersed-phase, CA dope was combined with 50 percent by weight isopropyl acetate to form a homogeneous solution. In making up the predominantly aqueous phase, 547.8 grams of acetic acid, 151.8 grams of isopropyl acetate and 1301.8 grams of deionized water were mixed until a homogeneous solution resulted.

The continuous-phase was placed in the cylindrical mixing vessel and a ruler with millimeter scale was attached to one of the baffles. The agitator was started with the impeller speed, N, above the minimum impeller speed for the 98% gross uniformity (Skelland and Kanel, 1989). A sample calculation for estimating the minimum impeller speed is provided in Appendix A4.

The conductivity meter was turned on and the first micro mho reading was recorded. After the continuous-phase reached a fully developed flow pattern, the prepared solution of dispersed-phase was rapidly poured into the continuous-phase near the tip of the impeller blades. Addition time was short relative to the time where the fractional mass transferred (FMT) approaches unity, say less than 10%. Thus, if FMT $\approx$1 in three minutes as suggested by experimental results in Chapter 5 (see Figures 2 through 12), the dispersed-phase must be added in less than 18 seconds.

The conductivity was measured and recorded 15 seconds from the moment the dispersed-phase was added. Depending on the dispersed-phase volume fraction, ϕ, it took about 1 to 3 seconds to completely disperse the organic phase throughout the vessel. Samples of the continuous-phase were taken exclusively at 30 second intervals after dispersed-phase addition for a total of 5 minutes.

Design of Experiments

For a full factorial design, 6 experimental runs (including two replicate runs) were used to study the effect of volume fraction (ϕ= 0.05, 0.10, 0.15, and 0.20) on the dispersed-phase mass transfer coefficient.

Other variables could have been explored such as dispersed-phase viscosity, direction of dispersion, temperature, vessel geometry, impeller type, and impeller speed.

Varying the viscosity of the dispersed-phase would be limited by material handling. The more viscous the dispersed-phase, the more difficult it becomes to transfer it into the mixing vessel. More important, increase in viscosity increases the addition period; recall from the Experimental Procedure that the addition period should be no more than 10% of the fractional mass transfer.

Similarly, the direction of dispersion (i.e., dispersing aqueous phase in organic phase versus dispersing organic phase in the aqueous phase) was not studied further due to difficulty associated with transferring and agitating the viscous solvated dope as indicated in Chapter 5.

Temperature was eliminated as a variable because of its influence on physical and transport properties. Measure of sulfate salt transfer from the dispersed-phase would become unreliable as solvents transfer between phases.

Vessel geometry, impeller type, and impeller speed were not varied since models have already been established by Skelland and his protégées for the relationship of these variables to mass transfer coefficients in batch agitated vessels. (Skelland and Kanel,1991; Skelland and HuXien, 1990; Skelland and Moeti, 1989). Impeller speed will vary the power input per unit mass, ε. Thus experimental results may be applied to a variety of possible extraction devices, including various impeller types (from Power number versus Reynolds number plots). The influence of ε and the physical properties (in the Schmidt group) on k_c is illustrated by Calderbank (1967),

$$k_c = (N_{Sc})^{-2/3}\left(\mu\frac{P}{\upsilon\rho_c}\right)^{1/4} = (N_{Sc})^{-2/3}(\mu\varepsilon)^{1/4} \qquad (6.1)$$

Discussion of Experimental Results

Measure of Sodium Sulfate in the Continuous-phase

Conductivity Measure. Typical curves showing the change in continuous-phase conductivity with time appears in Appendix Figure A6.2. The data for this curve is provided in Appendix Table A6.2. Calibration data shows that increases in the continuous-phase sodium concentration yield only slight increases in conductivity. This could be due to the acetic acid presence in the continuous-phase. Acetic acid is highly conductive (conductivity =2,000 μS versus deionized water at 0μS and 100ppm sodium

at 1400 μS) and masks the measurement of sodium transferring into the continuous-phase.

Analytical Measure. Typical curves showing the change of ppm Na in the continuous-phase with time appear in Figure 6.1. A summary of the ppm Na-time data is provided in Table 6.1. Mass balances shown in Tables A6.3, A6.5, A6.7, A6.9, A6.11, and A6.13 were used to represent the disappearance of sodium from the dispersed-phase over time. Dispersed-phase ppmNa-time profile is shown for each run in Appendix Figures A6.3, A6.5, A6.7, A6.9, A6.11, and A6.13.

Estimation of Experimental Dispersed-phase Mass Transfer Coefficient

Experimental disperse-phase mass transfer coefficients were estimated using droplet size, and the slope defined by equation 5.4.

Droplet size. Droplets were visually approximated to within ± 0.10mm of 0.30mm. Visually measured droplet diameters, d_p, generally agree with the Sauter-mean diameters (d_{32} predicted by equations 5.5-5.7). A sample calculation for predicting d_{32} is provided in Appendix Table A6.17. Comparing d_p to d_{32} offers a basis for establishing the validity of equation 1.11 (which was derived using the Sauter-mean diameter relationship with time) in estimating k_d.

Slope. Non-linear regression of C_a versus t data was used to estimate the sodium concentration and time at which C_a/C_{ao}=1. Table A6.15 provides a summary of estimated C_{ao} and t_o for the systems ranging in ϕ=0.05 to 0.20. In Figures 6.2 through 6.7, the initial condition data was used in conjunction with C_a and t data from Table 6.1

Table 6.1: Sodium Sulfate Content As Measured Analytically In The Continuous-phase Over Time.

	ppmNa in Continuous-phase					
TIME, s	Run 1 phi=0.10	Run 2 phi=0.10	Run 3 phi=0.05	Run 4 phi=0.20	Run 5 phi=0.15	Run 6 phi=0.05
0	0.0	0.0	0.0	0.00	0.0	0.0
30	52.4	57.4	26.1	60.75	52.0	27.4
60	69.4	73.4	34.7	95.26	78.1	35.6
90	75.8	79.0	37.2	112.54	92.4	38.5
120	81.1	81.5	39.0	125.76	105.6	39.3
150		82.8	39.3	135.42	112.7	39.4
180	82.7	83.1	39.4	146.50	117.9	39.5
210	83.0	83.2	39.4	151.92	123.5	39.5
240	83.2	83.3	39.5	159.37	126.9	39.5
270	83.3	83.3	39.5	167.89	129.8	39.5
300	83.3	83.3	39.5	175.75	132.0	39.5

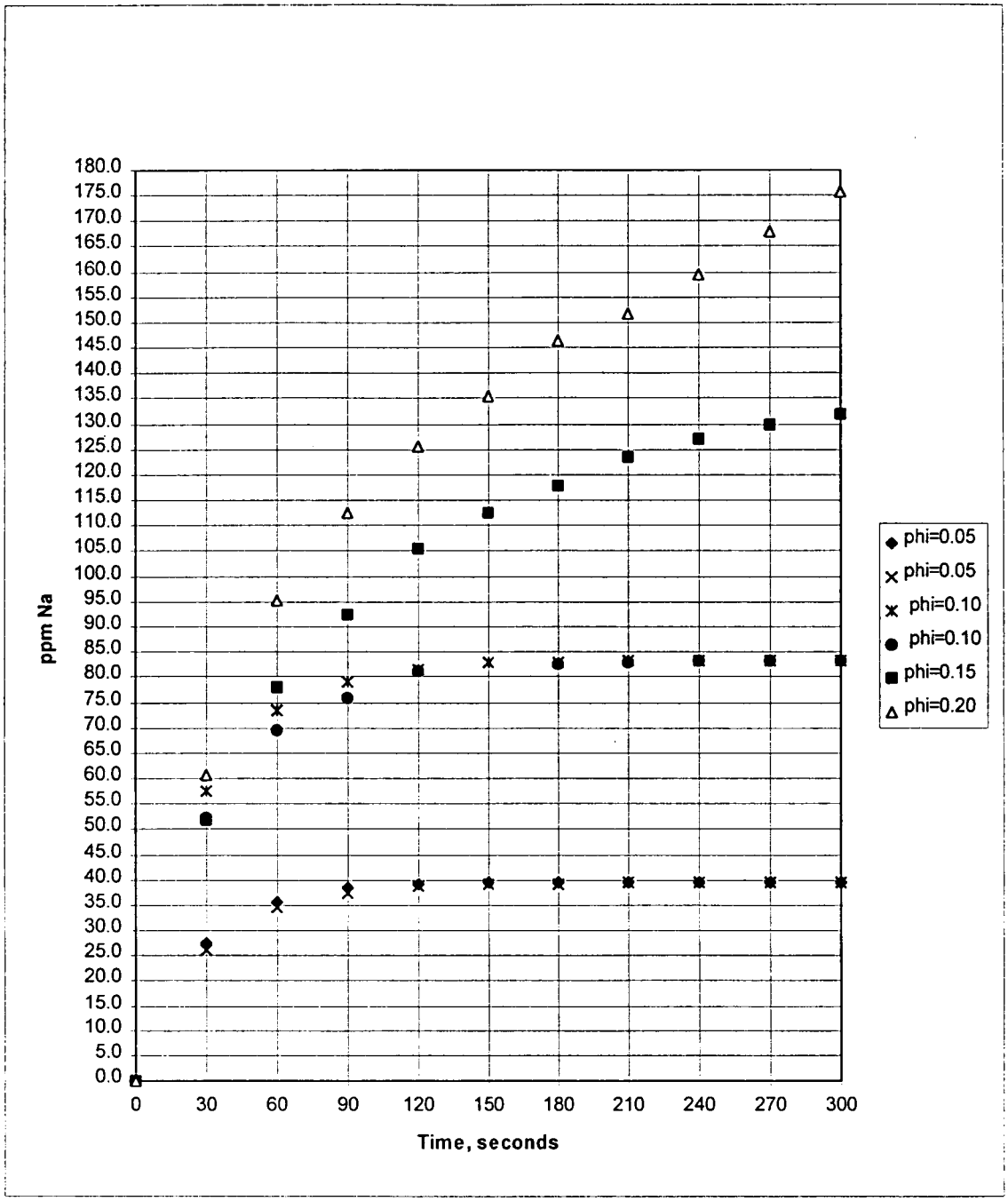

Figure 6.1: Summary of Sodium Sulfate profiles over time in the continuous-phase for systems with volume fraction, phi, ranging from 0.05 to 0.20.

to plot $\ln C_d/C_{ao}$ versus t-t_o. Appendix Table A6.18 summarizes dispersed-phase volume fractions and corresponding slopes. This data indicates that the slope increases as volume fraction decreases. For example, the slope corresponding to ϕ=0.05 is 0.0359, while the slope corresponding to ϕ=0.15 is 0.0134.

Experimental Dispersed-phase Mass Transfer Coefficient. The slope of the $\ln C_d/C_{ao}$ versus t-t_o curves (as shown in equation 5.2) from Figures 6.2 through 6.7 were used to estimate the dispersed-phase mass transfer coefficient. Sample calculations for estimating the dispersed-phase mass transfer coefficient using equation 5.4 are provided in Appendix A6. Table A6.18 summarizes k_d calculated using d_p = 0.02cm, 0.03cm, and 0.04cm for each experimental run where the dispersed-phase volume fraction, ϕ, ranges from 0.05 to 0.20. Figures 6.8 through 6.10 show that for any given drop size, k_d increases as dispersed-phase volume fraction decreases. For example, ϕ=0.05 yields k_d (d_p=0.03cm)=1.8E-04 cm/s, while ϕ=0.15 yields k_d (d_p=0.03cm) =6.7E-05 cm/s.

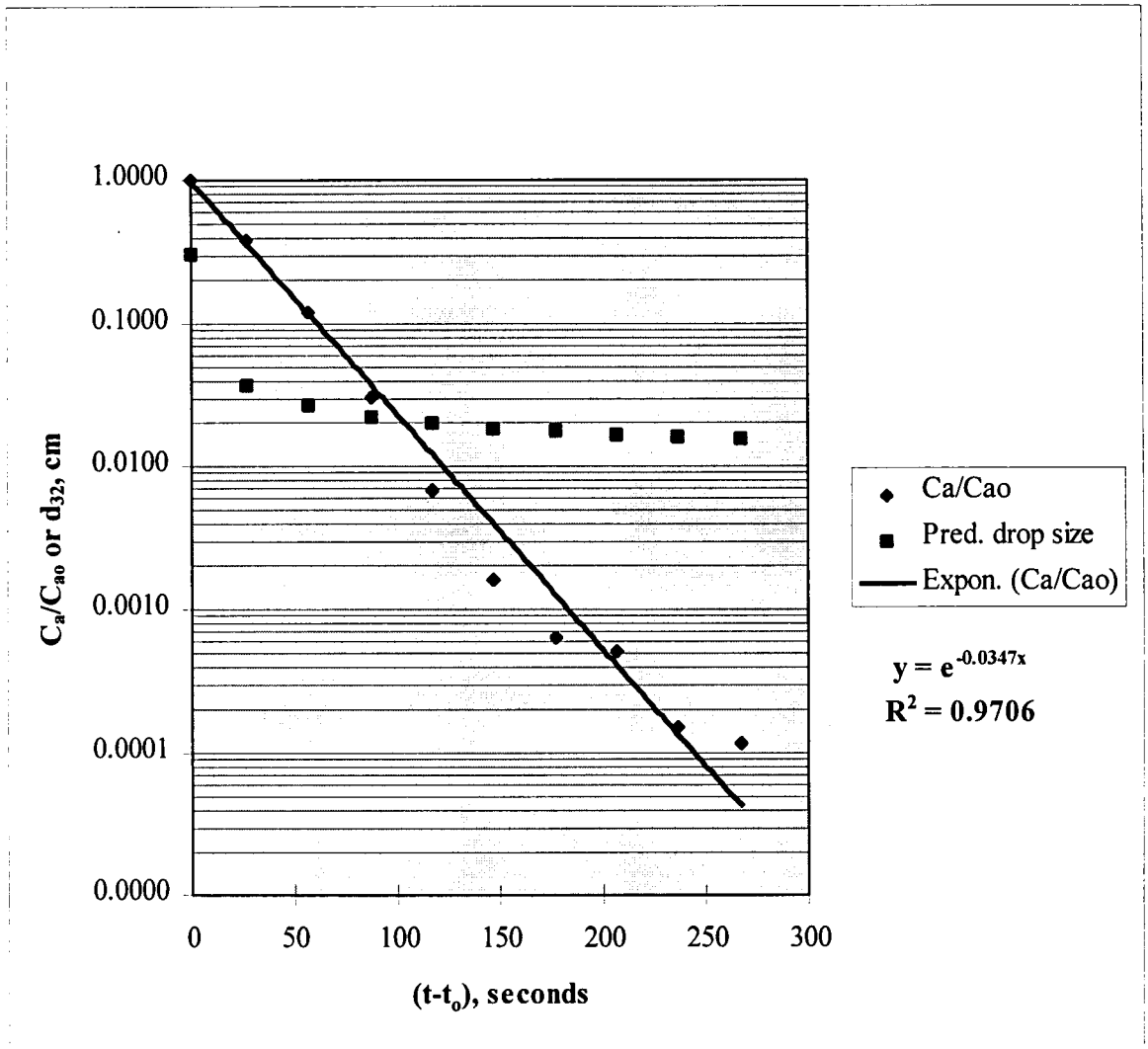

Figure 6.2 : Experimental Run 1 where Volume Fraction, $\phi = V_d/V_T = 0.10$. The concentration and drop size profile of the dispersed-phase over time. The drop size was calculated by the Sauter-mean diameter approximation (Hong and Lee, 1985).

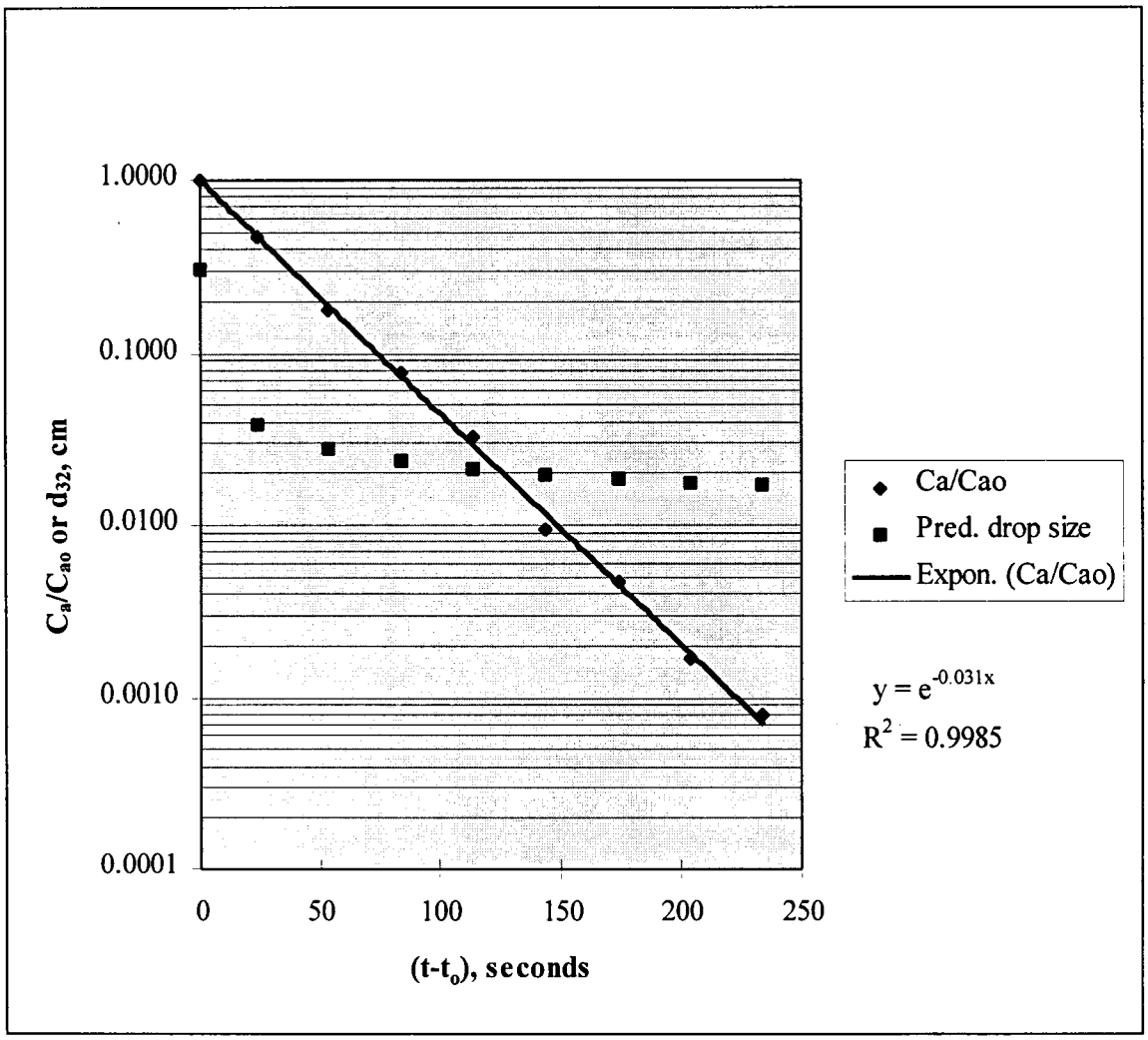

Figure 6.3 : Experimental Run 2 where Volume Fraction, $\phi = V_d/V_T = 0.10$. The concentration and drop size profile of the dispersed-phase over time. The drop size was calculated by the Sauter-mean diameter approximation (Hong and Lee, 1985).

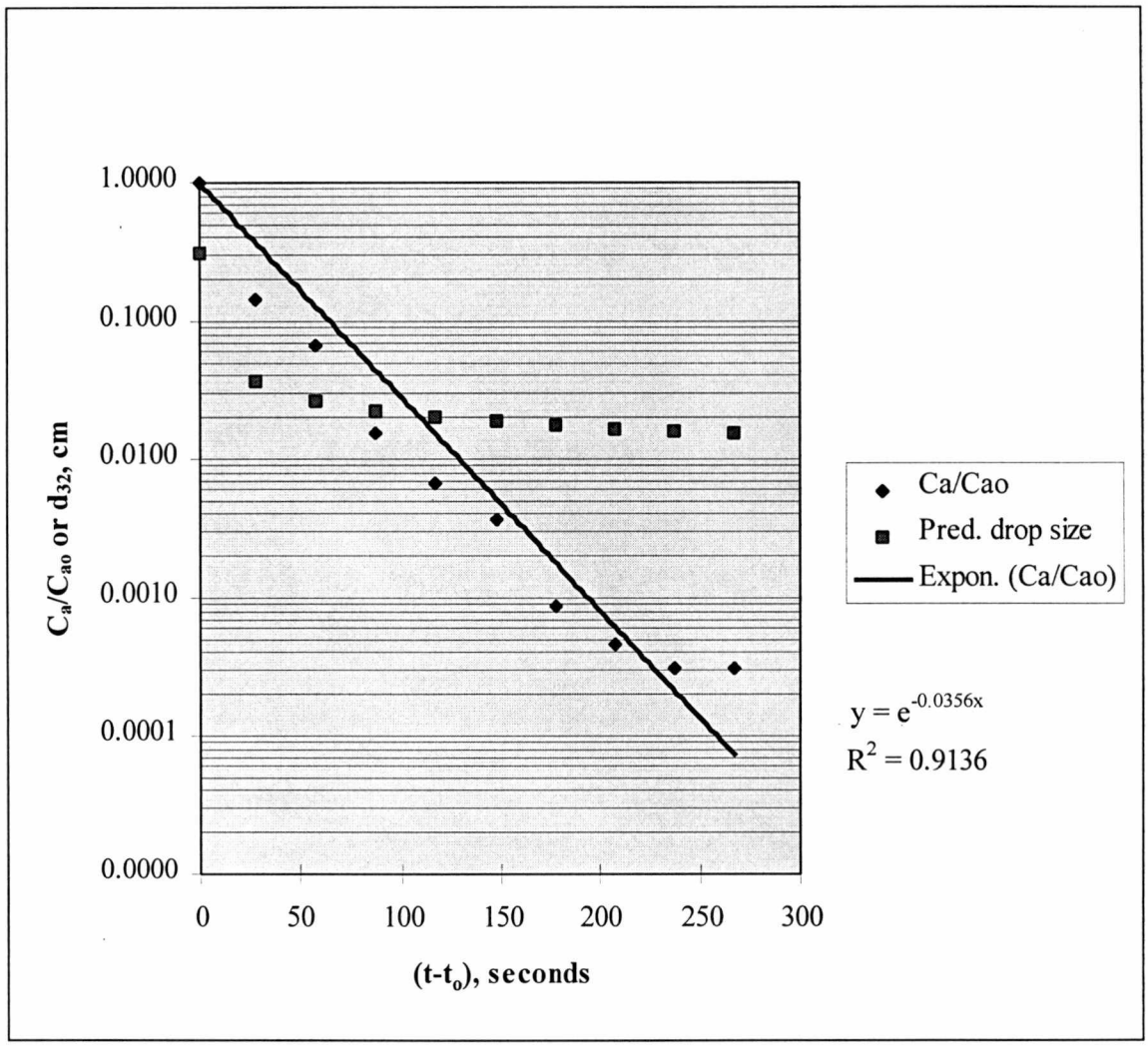

Figure 6.4 : Experimental Run 3 where Volume Fraction, $\phi = V_d/V_T = 0.05$. The concentration and drop size profile of the dispersed-phase over time. The drop size was calculated by the Sauter-mean diameter approximation (Hong and Lee, 1985).

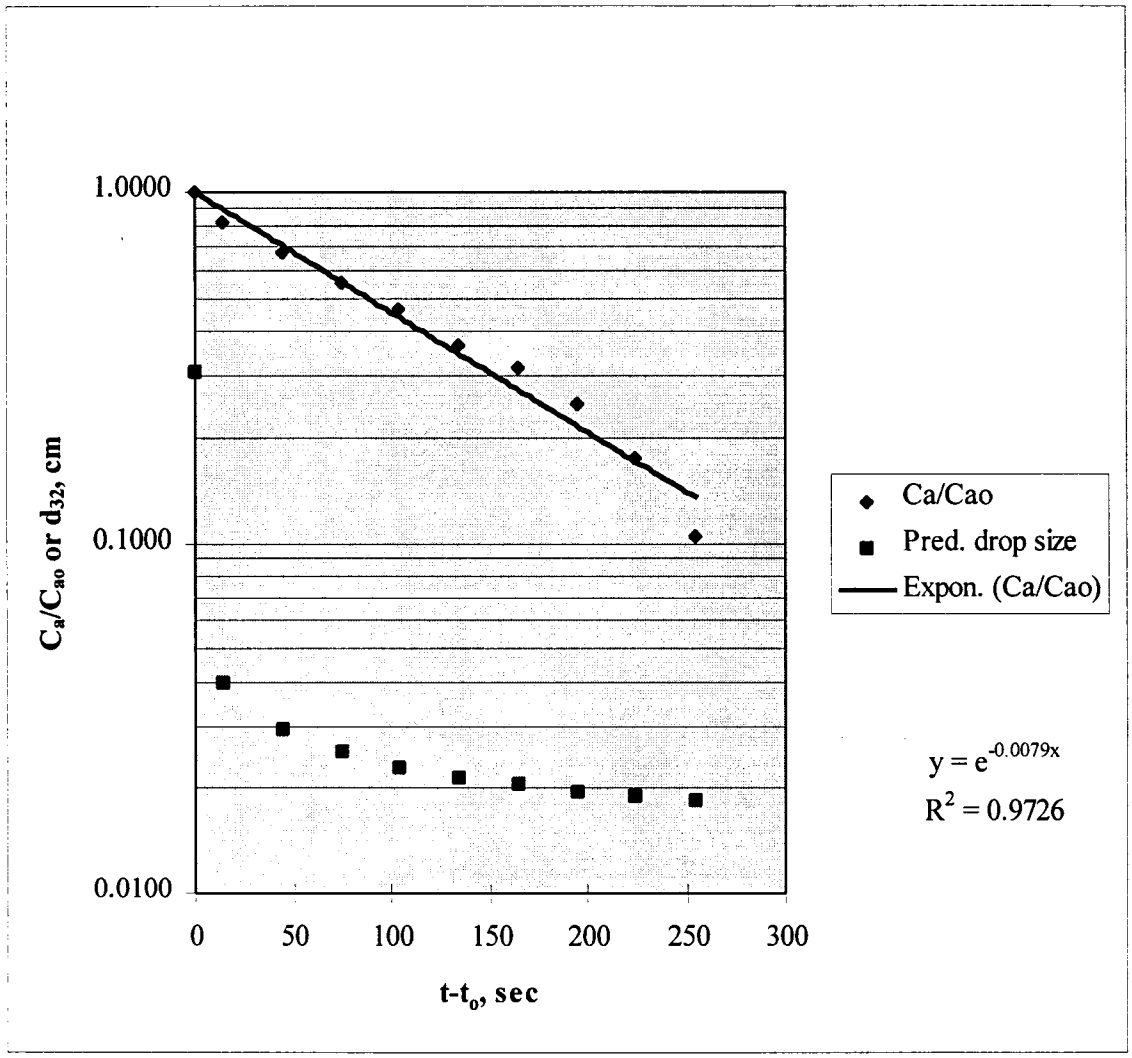

Figure 6.5 : Experimental Run 4 where Volume Fraction, $\phi = V_d/V_T = 0.20$. The concentration and drop size profile of the dispersed-phase over time. The drop size was calculated by the Sauter-mean diameter approximation (Hong and Lee, 1985).

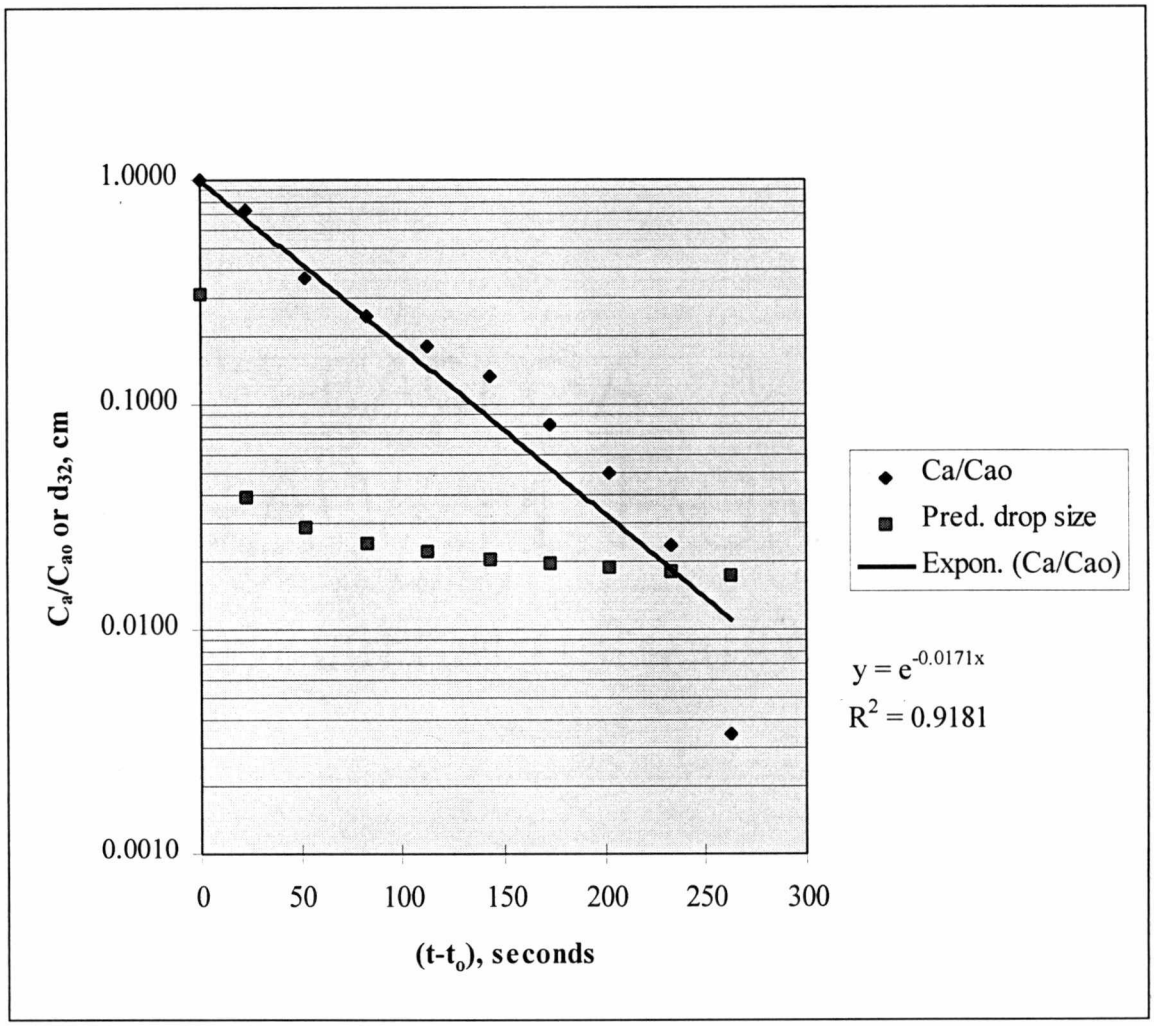

Figure 6.6 : Experimental Run 5 where Volume Fraction, $\phi = V_d/V_T = 0.15$. The concentration and drop size profile of the dispersed-phase over time. The drop size was calculated by the Sauter-mean diameter approximation (Hong and Lee, 1985).

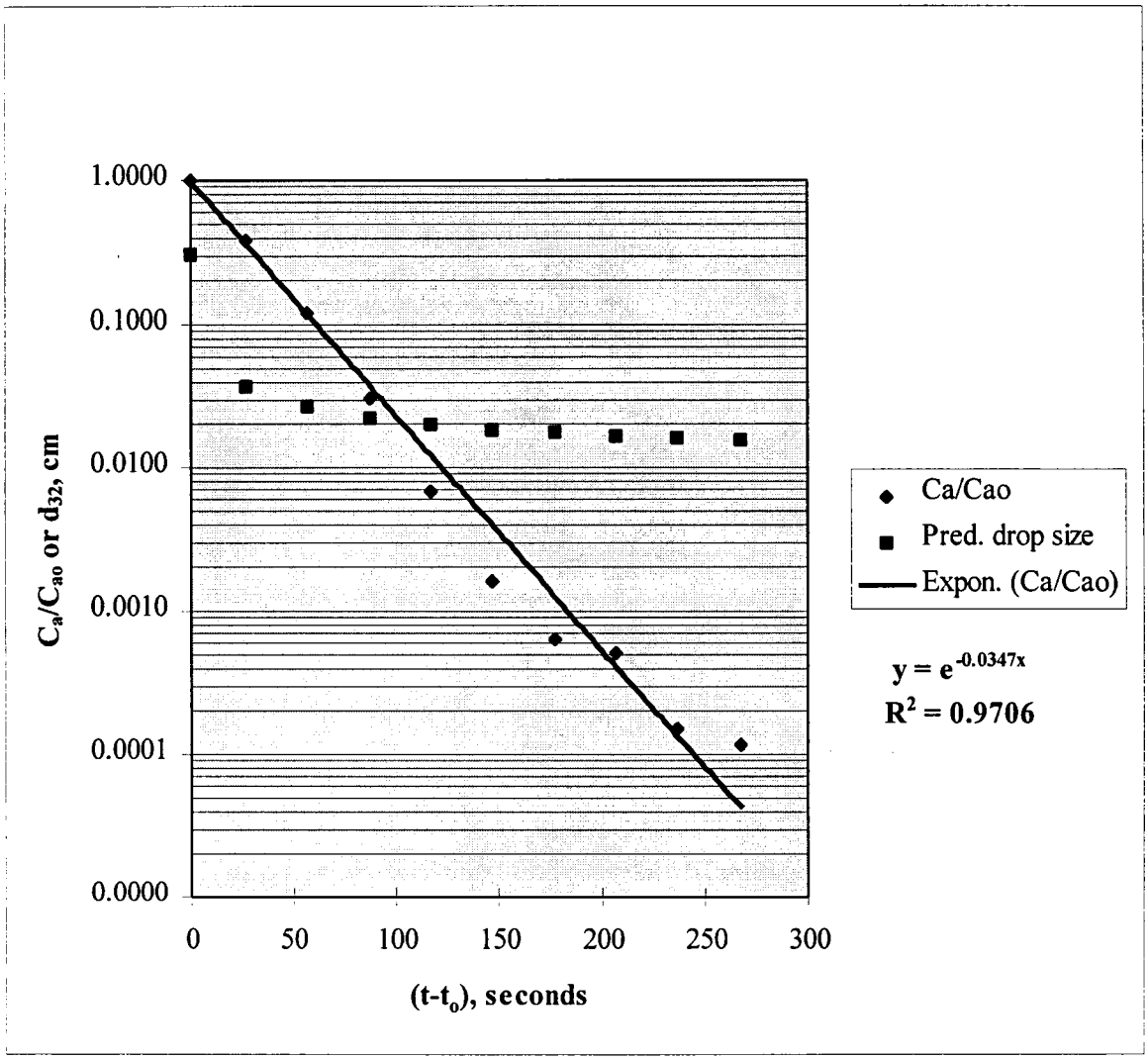

Figure 6.7 : Experimental Run 6 where Volume Fraction, $\phi = V_d/V_T = 0.05$. The concentration and drop size profile of the dispersed-phase over time. The drop size was calculated by the Sauter-mean diameter approximation (Hong and Lee, 1985).

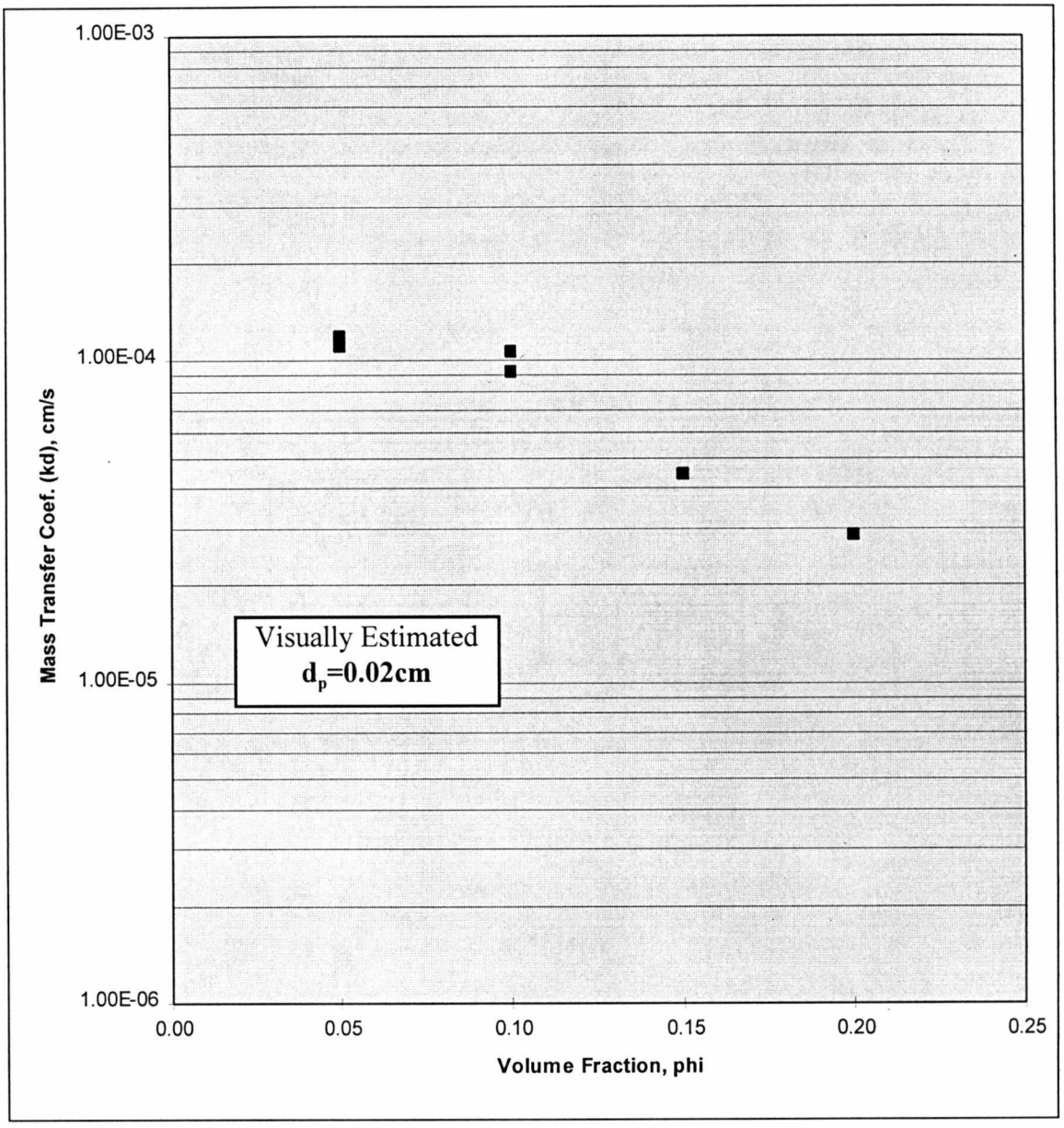

Figure 6.8: Effect of dispersed-phase volume fraction, ϕ, on dispersed-phase mass transfer coefficient estimated using a solute mass balance for transport from the dispersed-phase to the continuous-phase: $\ln\left(\frac{C_a}{C_{ao}}\right) = -\frac{k_d a V}{V_d}(t - t_o)$, rather $k_d = -\frac{d_p}{6}(slope)$, with experimentally measured C_a and d_p where d_p= 0.02 cm.

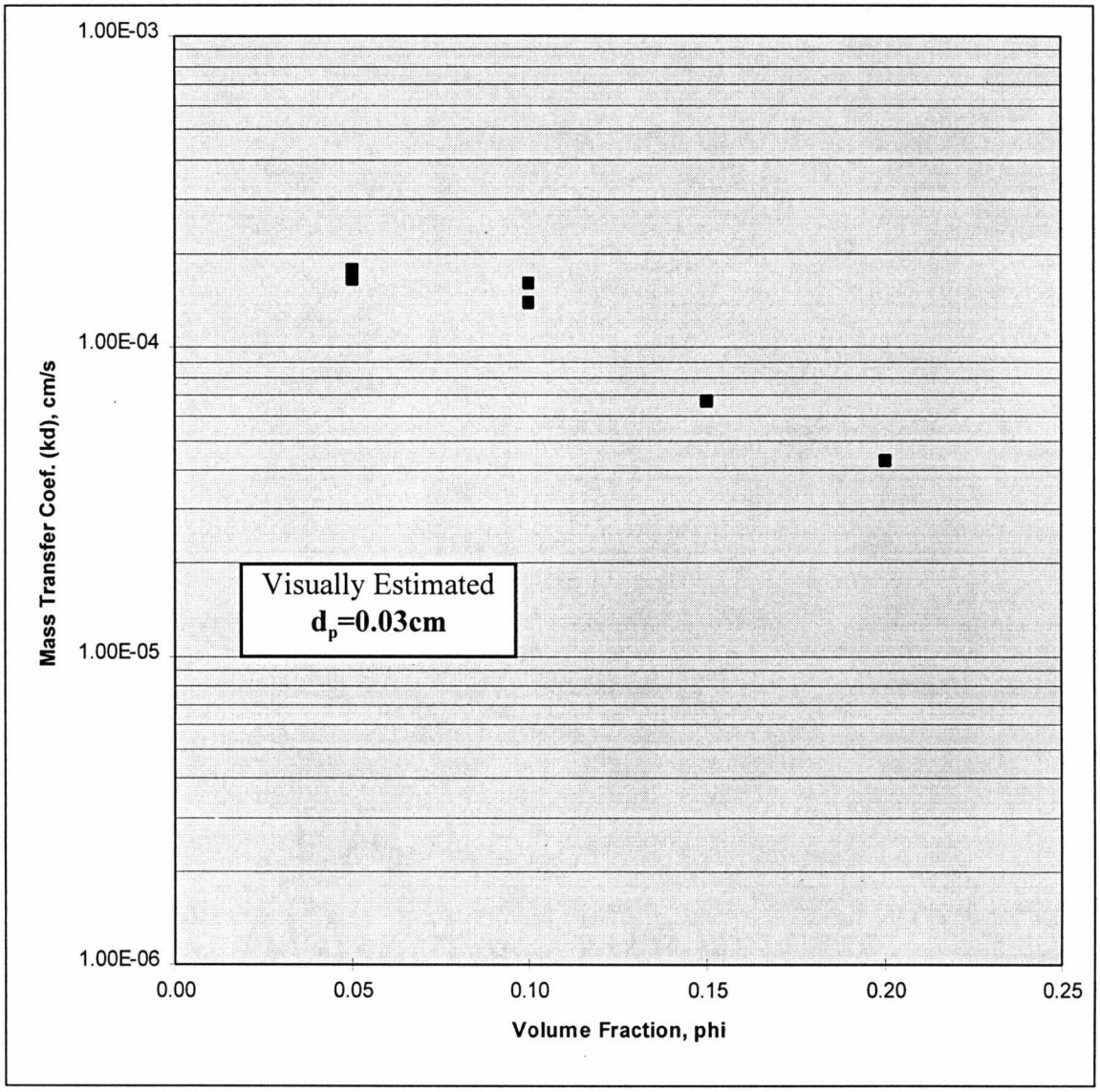

Figure 6.9: Effect of dispersed-phase volume fraction, ϕ, on dispersed-phase mass transfer coefficient estimated using a solute mass balance for transport from the dispersed-phase to the continuous-phase: $\ln\left(\frac{C_a}{C_{ao}}\right) = -\frac{k_d a V}{V_d}(t - t_o)$, rather $k_d = -\frac{d_p}{6}(slope)$, with experimentally measured C_a and d_p where d_p= 0.03 cm.

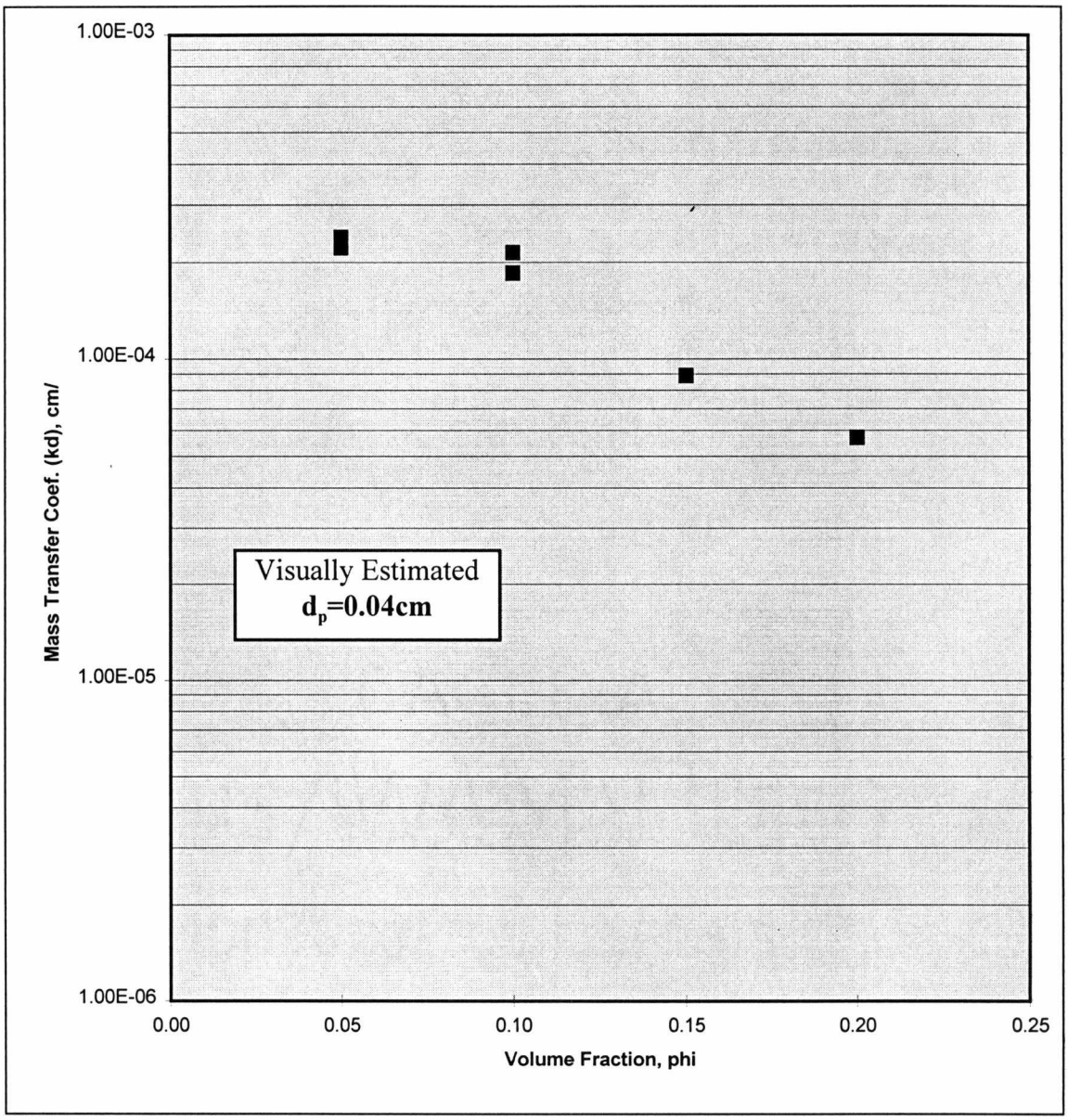

Figure 6.10: Effect of dispersed-phase volume fraction, ϕ, on dispersed-phase mass transfer coefficient estimated using a solute mass balance for transport from the dispersed-phase to the continuous-phase: $\ln\left(\frac{C_a}{C_{ao}}\right) = -\frac{k_d a V}{V_d}(t - t_o)$, rather $k_d = -\frac{d_p}{6}(slope)$, with experimentally measured C_a and d_p where d_p= 0.04 cm.

Prediction of Dispersed-phase Mass Transfer Coefficient

Table 6.2 summarizes the effect of volume fraction on both dispersed-phase mass transfer coefficients estimated with empirical models (i.e. Higbie (1935), Skelland-HuXien (1990), and Equation 1.11) and dispersed-phase mass transfer coefficients estimated using a solute mass balance- Equation 5.2, with experimentally measured solute concentration-time data and visually estimated droplet size data (equal to 0.02cm, 0.03cm and 0.04cm, respectively).

Penetration Theory (Higbie, 1935). Appendix Table A6.19 summarizes k_d as approximated by the Penetration Theory. It may be noted from Figure 6.11 that k_d increases as exposure time decreases. For example, when exposure time is 90 seconds (ϕ=0.05), $k_d \cong$ 7.0E-05 cm/s; but, when exposure time increases to 300 seconds (ϕ=0.15) decreases to $k_d \cong$ 3.0E-05 cm/s. Note that from equation 5.1, k_d is proportional to $(t_s)^{-0.5}$.

Skelland and HuXien (1990). Appendix Table A6.20 summarizes k_d as approximated by the Skelland and HuXien's empirical correlation, equation 6.2. It may be noted from Figure 6.12 that k_d decreases as volume fraction increases. It follows that (since volume fraction increases with tf, Table A6.20) k_d decreases as tf increases. Data from Appendix Table A6.22 indicate that k_d increases as the Reynolds number increases. For example, when the impeller Reynolds number is about 5800 (where ϕ=0.05) $k_d \cong$ 2.5E-05 cm/s; however, when the impeller Reynolds number is around 4600 (where ϕ=0.15), k_d decreases to less than half, ~1.0E-05 cm/s. Note that from equation 6.2, k_d is proportional to $(N_{Re})^{1.14}$.

Table 6.2: Predicted Mass Transfer Coefficients based on Experimental and Calculated Physical and Transport Properties.

Expt. Run	Volume Fraction ϕ	DISPERSED-PHASE MASS TRANSFER COEFFICIENT, cm/s EXPERIMENTAL (1) dp: 0.20mm	0.3mm	0.40mm	EQUATION 1.11 (2)	PENETRATION THEORY (3)	SKELLAND HU XIEN (4)
1	0.10	9.300E-05	1.395E-04	1.860E-04	1.667E-04	4.134E-05	1.241E-05
2	0.10	1.073E-04	1.610E-04	2.147E-04	1.667E-04	4.145E-05	1.241E-05
3	0.05	1.113E-04	1.670E-04	2.227E-04	1.833E-04	5.313E-05	1.875E-05
4	0.20	2.867E-05	4.300E-05	5.733E-05	6.667E-05	2.848E-05	6.317E-06
5	0.15	4.467E-05	6.700E-05	8.933E-05	1.167E-05	2.907E-05	7.557E-06
6	0.05	1.197E-04	1.795E-04	2.393E-04	1.833E-04	5.331E-05	1.875E-05

Notes:

(1)

$$k_d = -\frac{d_p}{6}(slope)$$

(2)

$$\ln\frac{C_a}{C_{ao}} = -6k_d\int_{t_o}^{t}\frac{1}{\alpha(t)^{-0.7}+d_{32}^{*}}dt$$

(3)

$$k_d = 2\sqrt{\frac{D_{AB}}{\pi t_s}}$$

(4)

$$\frac{k_d}{\left[D_{AB}/t_f\right]^{1/2}} = 5.0(10^{-6})\phi^{-0.0204}\left(\frac{d_I^2 N\rho_M}{\mu_M}\right)^{1.140}\left(\frac{\rho_c}{\Delta\rho}\right)^{0.518}$$

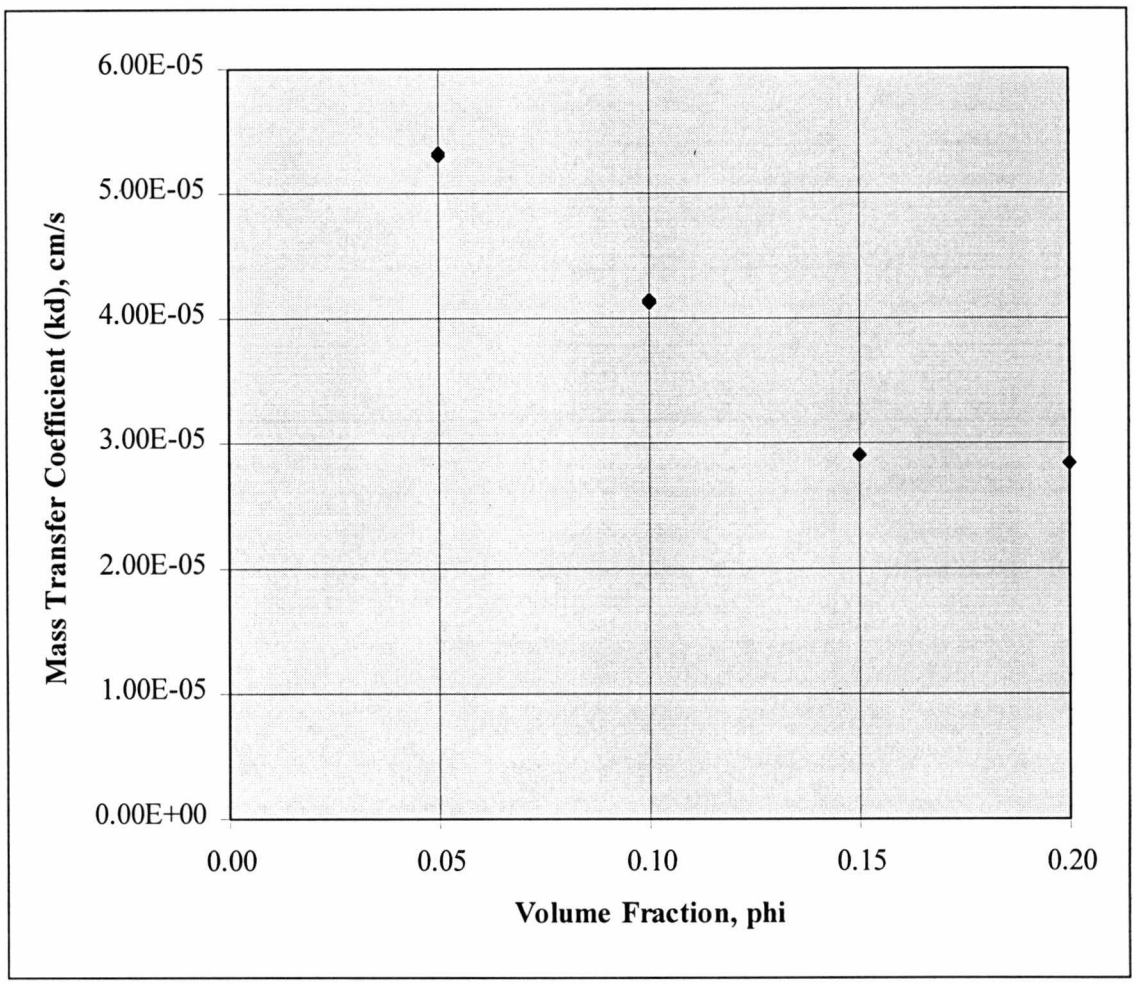

Figure 6.11: Effect of dispersed-phase volume fraction, ϕ, on dispersed-phase mass transfer calculated using the Penetration Theory (Higbie, 1935): $k_d = 2\sqrt{\frac{D_{AB}}{\pi t_s}}$.

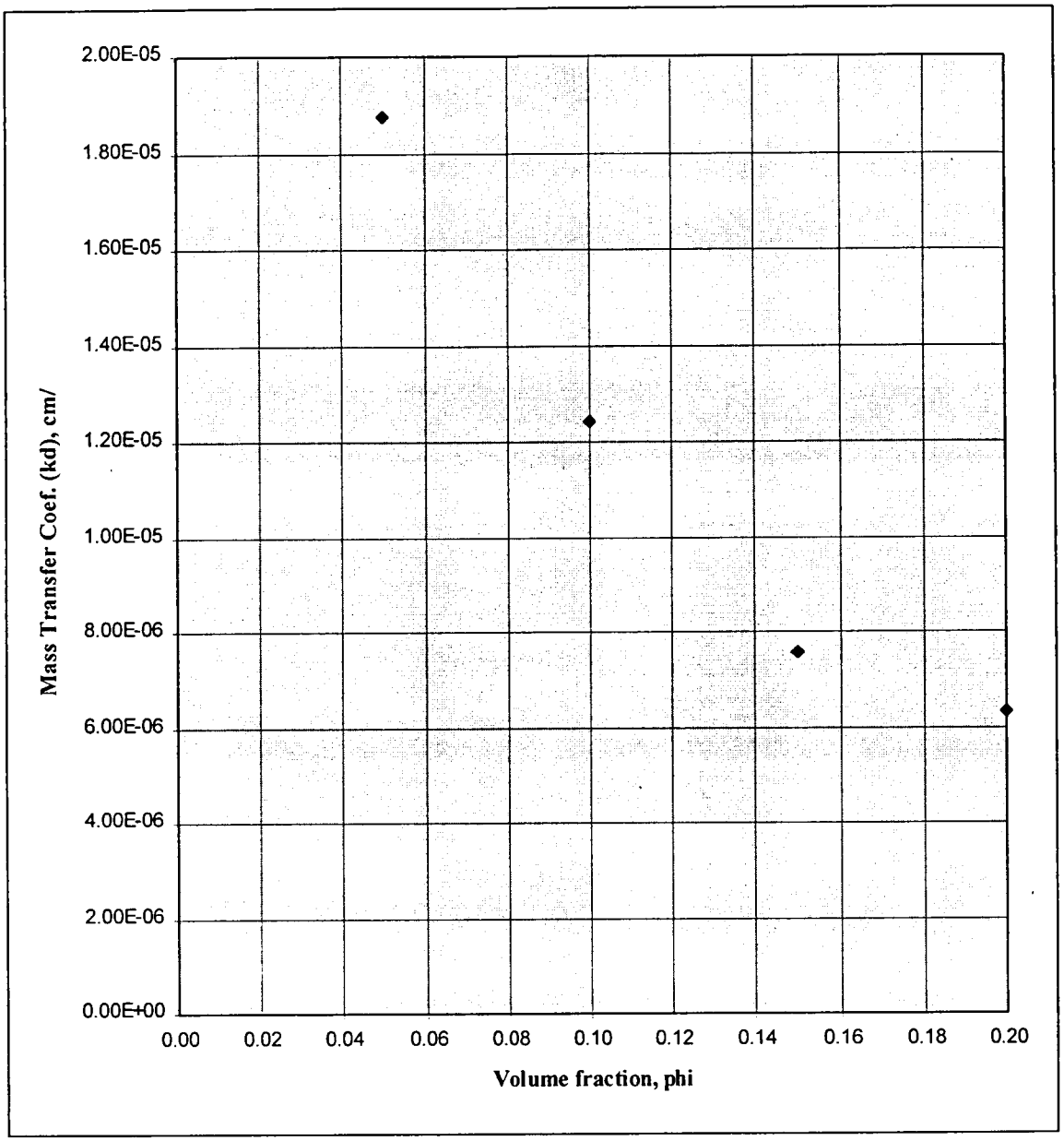

Figure 6.12: Effect of dispersed-phase volume fraction, ϕ, on dispersed-phase mass transfer coefficient calculated using the Skelland and HuXien (1990) Empirical Expression: $\frac{k_d}{\left[D_{AB}/t_f\right]^{1/2}} = 5.0(10^{-6})\phi^{-0.0204}\left(\frac{d_I^2 N\rho_M}{\mu_M}\right)^{1.140}\left(\frac{\rho_c}{\Delta\rho}\right)^{0.518}$.

Hong and Lee (1985) Sauter-mean Diameter Relationship. Slopes from Figures 6.13 through 6.16 were used in equation 1.11 to estimate the mass transfer coefficient. As shown in Figures 6.17, k_d increases as the dispersed-phase volume fraction, ϕ, decreases. For example, at ϕ=0.05 k_d = 1.83E-04 cm/s, while at ϕ=0.20 k_d = 0.67E-04 cm/s. Sample calculations for estimating the dispersed-phase mass transfer coefficient using equation 1.11 are provided in Appendix A6. Figures A6.15 through A6.17 contain a plot of the relationship between I(t) and t.

Overall Mass Transfer Coefficient. As expected from Table A6.21, k_c's ranging from ~0.2 to ~0.4 cm/s was much greater than experimental k_d's ranging from 2.9E-05 cm/s to 2.4E-05cm/s. This validates the assumption that $K_d \cong k_d$.

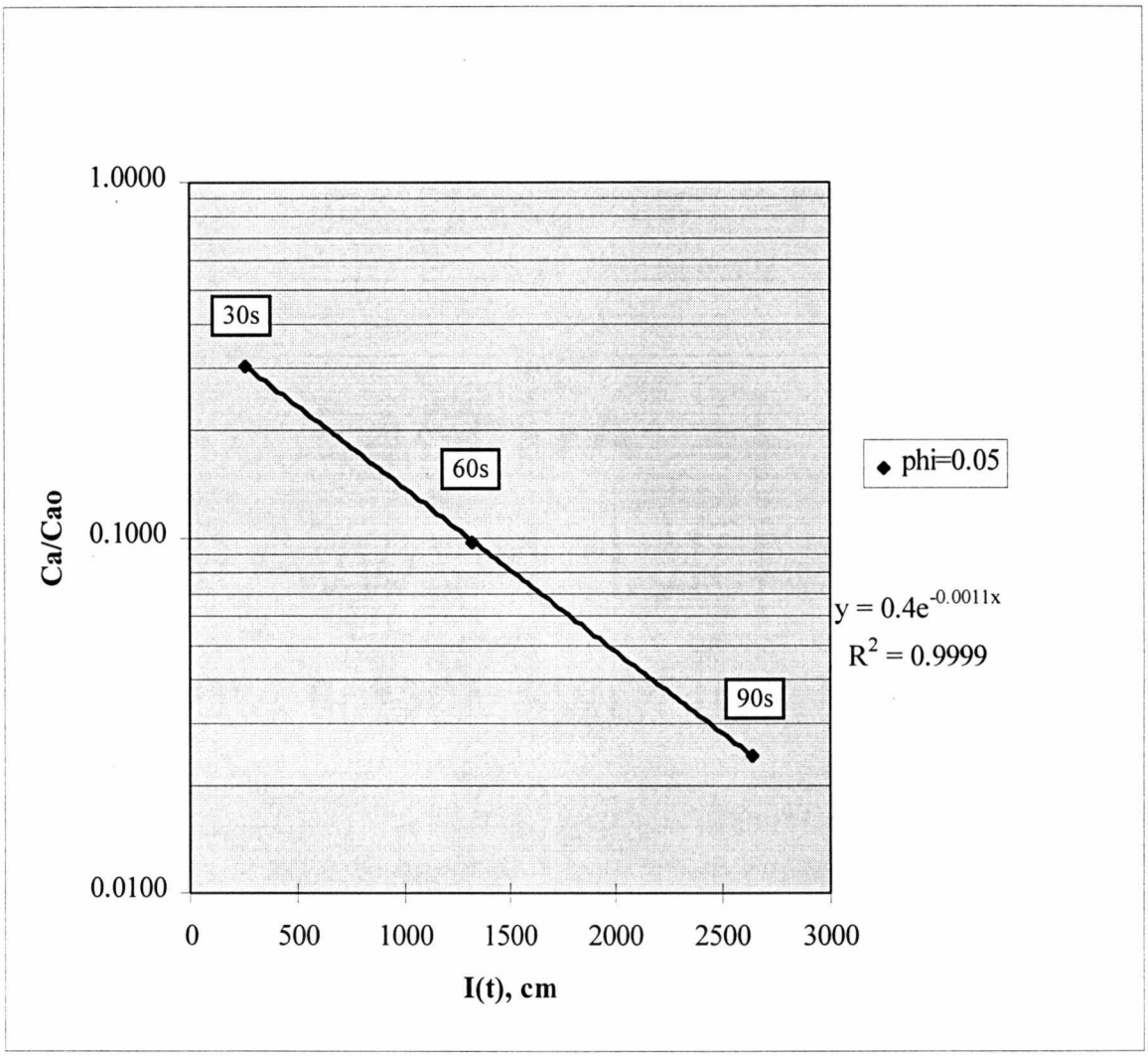

Figure 6.13: Plot of lnC_a/C_{ao} versus I(t) where $I(t) = \int_{20} \frac{1}{\alpha \cdot t^{-0.7} + d_{32}^*} dt$ for ϕ=0.05.

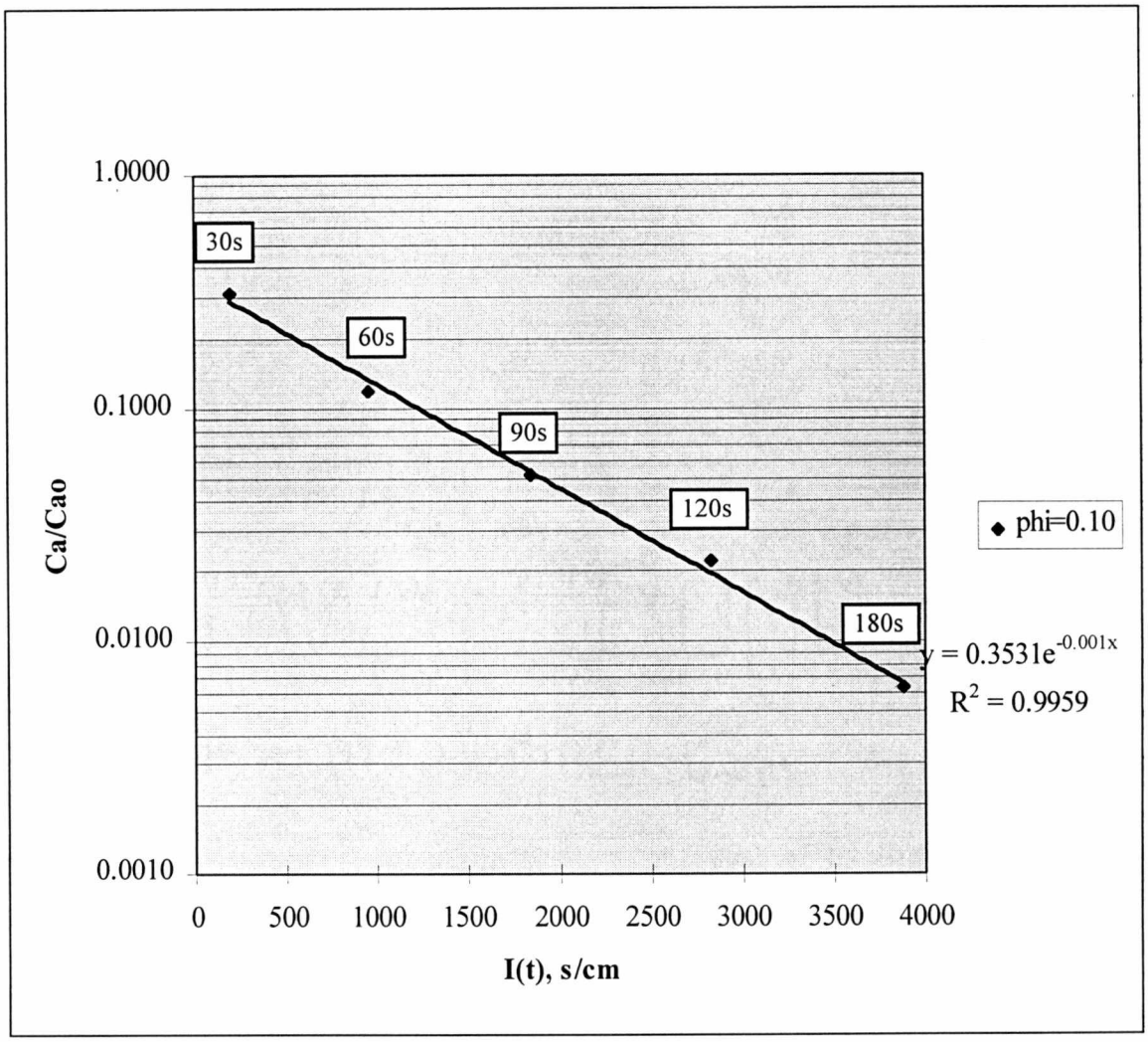

Figure 6.14: Plot of lnC_a/C_{ao} versus I(t) where $I(t) = \int_{20} \frac{1}{\alpha \cdot t^{-0.7} + d_{32}^*} dt$ for ϕ=0.1.

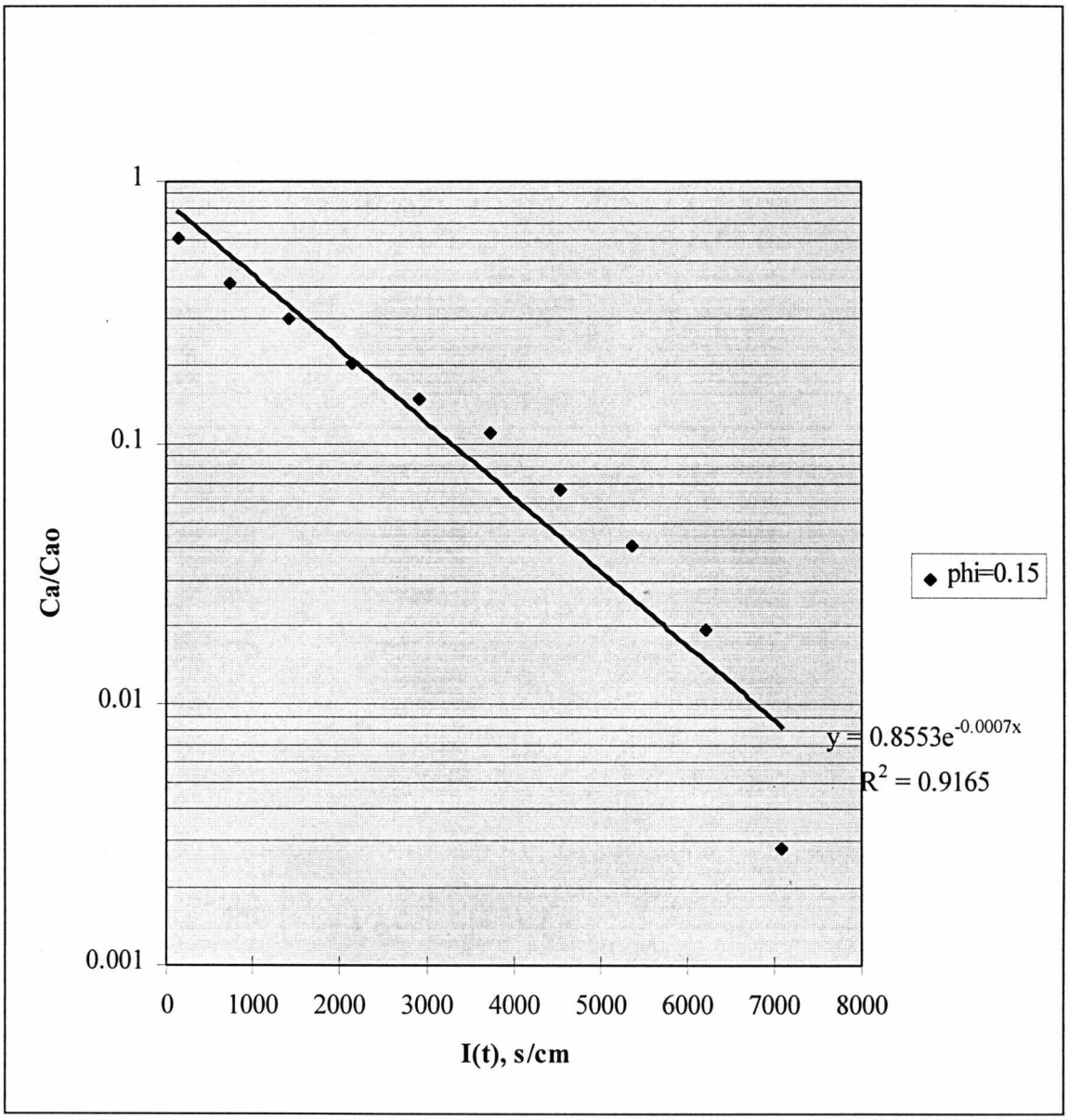

Figure 6.15: Plot of lnC_a/C_{ao} versus $I(t)$ where $I(t) = \int_{20} \frac{1}{\alpha \cdot t^{-0.7} + d_{32}^*} dt$ for ϕ=0.15.

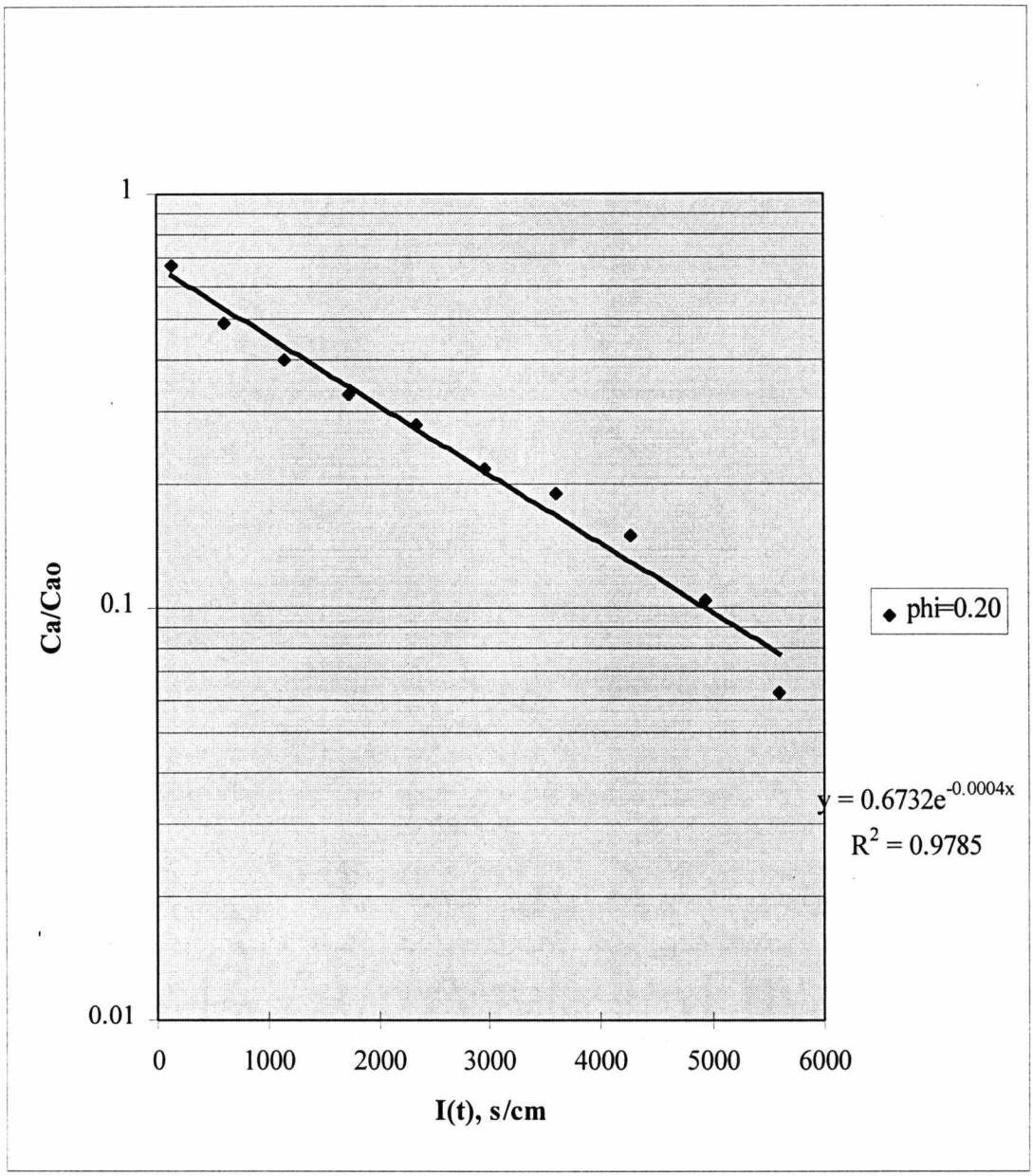

Figure 6.16: Plot of lnC_a/C_{ao} versus $I(t)$ where $I(t) = \int_{20}^{t} \frac{1}{\alpha \cdot t^{-0.7} + d_{32}^{*}} dt$ for ϕ=0.20.

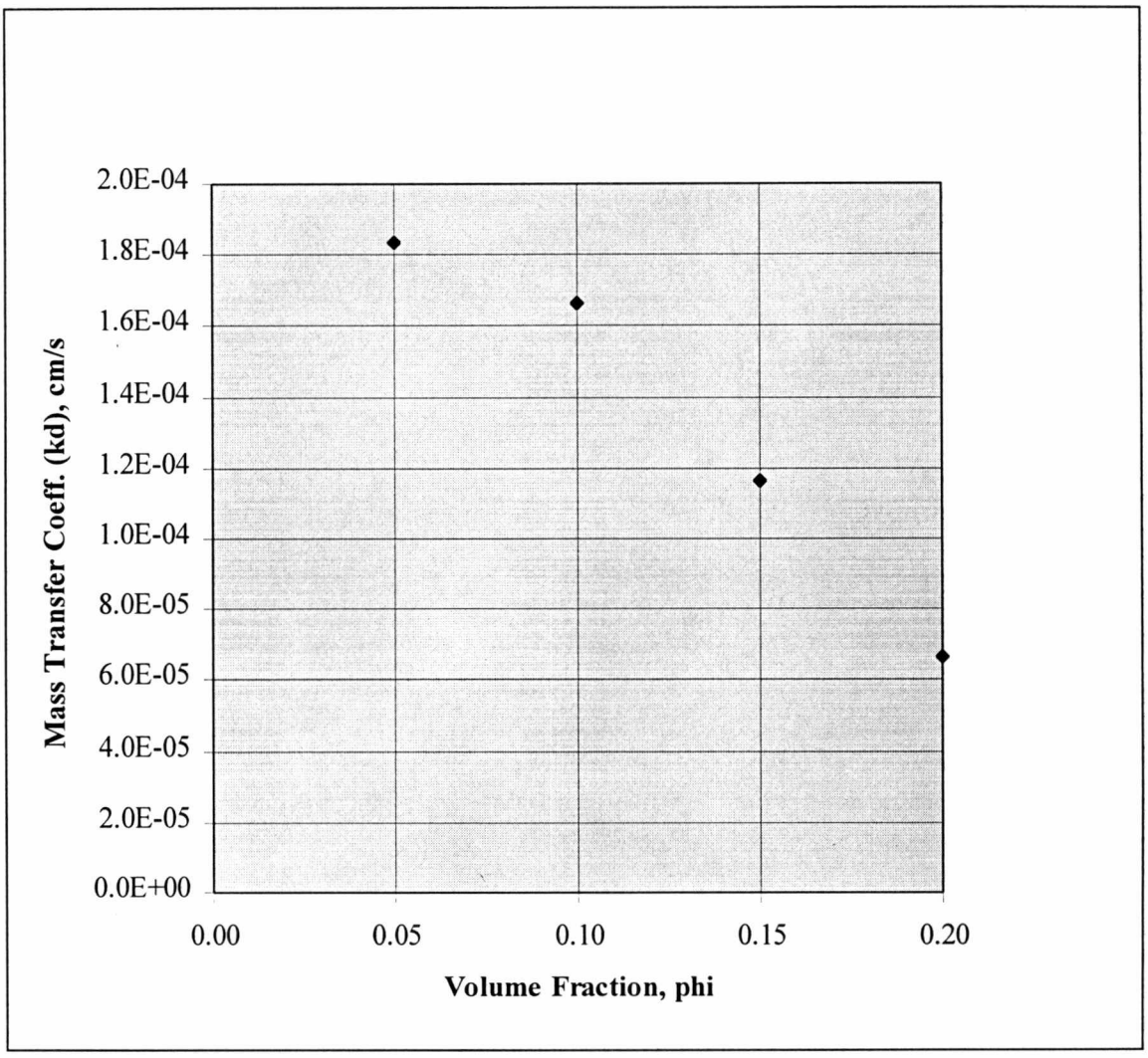

Figure 6.17: Effect of dispersed-phase volume fraction, ϕ, on dispersed-phase mass transfer coefficient calculated using equation 1.11: $\ln\frac{C_a}{C_{ao}} = -6k_d\int_0 \frac{1}{\alpha(t)^{-0.7} + d_{32}^*}dt$ which is derived from the Hong and Lee (1985) Sauter-mean Diameter relationship.

CHAPTER 7

COMPARISON OF MASS TRANSFER COEFFICIENT MODELS

Introduction

In Chapter 6 dispersed-phase mass transfer coefficients were estimated by (1) using empirical models - Higbie (1935), Skelland-HuXien (1990), and Equation 1.11 with experimentally measured physical properties and calculated transport properties; and (2) by using a solute mass balance- Equation 5.2, with experimentally measured solute concentration-time data and visually estimated droplet size data (equal to 0.02cm, 0.03cm and 0.04cm, respectively). Chapter 7 will compare the dispersed-phase coefficients predicted by models with the dispersed-phase mass transfer coefficients estimated experimentally.

Discussion

Penetration Theory

Table 6.2 shows that for small droplets (where dp=0.02cm) the Penetration Theory is generally half of the experimental dispersed-phase mass transfer coefficient regardless of exposure time. Regarding the Penetration Theory, Skelland and HuXien (1990) point out a subtlety on the affect of drop breakage; "transfer rates are repeatedly

enhanced and restored to a predominantly "penetration-type" mechanism, prevailing just after the creation of new surface, by recurrent drop breakages throughout the period t_f-t_o. This point is validated by $d_{32}=f(t)$ data in Table A6.17. Note that up to 5 fold reductions in d_{32} were found during this time period (for ϕ=0.1), corresponding to a quintupleting of the total surface. In summary, most of the transfer may occur under conditions not far removed from the Penetration Theory framework

Skelland and HuXien (1990) Expression

This empirical correlation for k_d builds on the Penetration Theory which states that k_d is proportional to $D^{0.5}$. Similarly, the Skelland and HuXien Model (1990) does not adequately predict the dispersed-phase mass transfer coefficient for the system studied herein. Dispersed-phase mass transfer coefficients generated from this empirical correlation are generally an order of magnitude lower than experimentally estimated dispersed-phase mass transfer coefficients. Figure 7.1 provides a frame of reference for comparing the Skelland and HuXien Model to Higbie's (1935) Penetration Theory.

Hong and Lee (1985) Sauter-mean Diameter Relationship

Equation 1.11 adequately predicts the dispersed-phase mass transfer coefficient for the type system study herein. Dispersed-phase mass transfer coefficients generated by this method fit within the accountable experimental error as shown in Figure 7.2. It follows from Appendix Table A6.17 that Sauter-mean diameters were essentially the

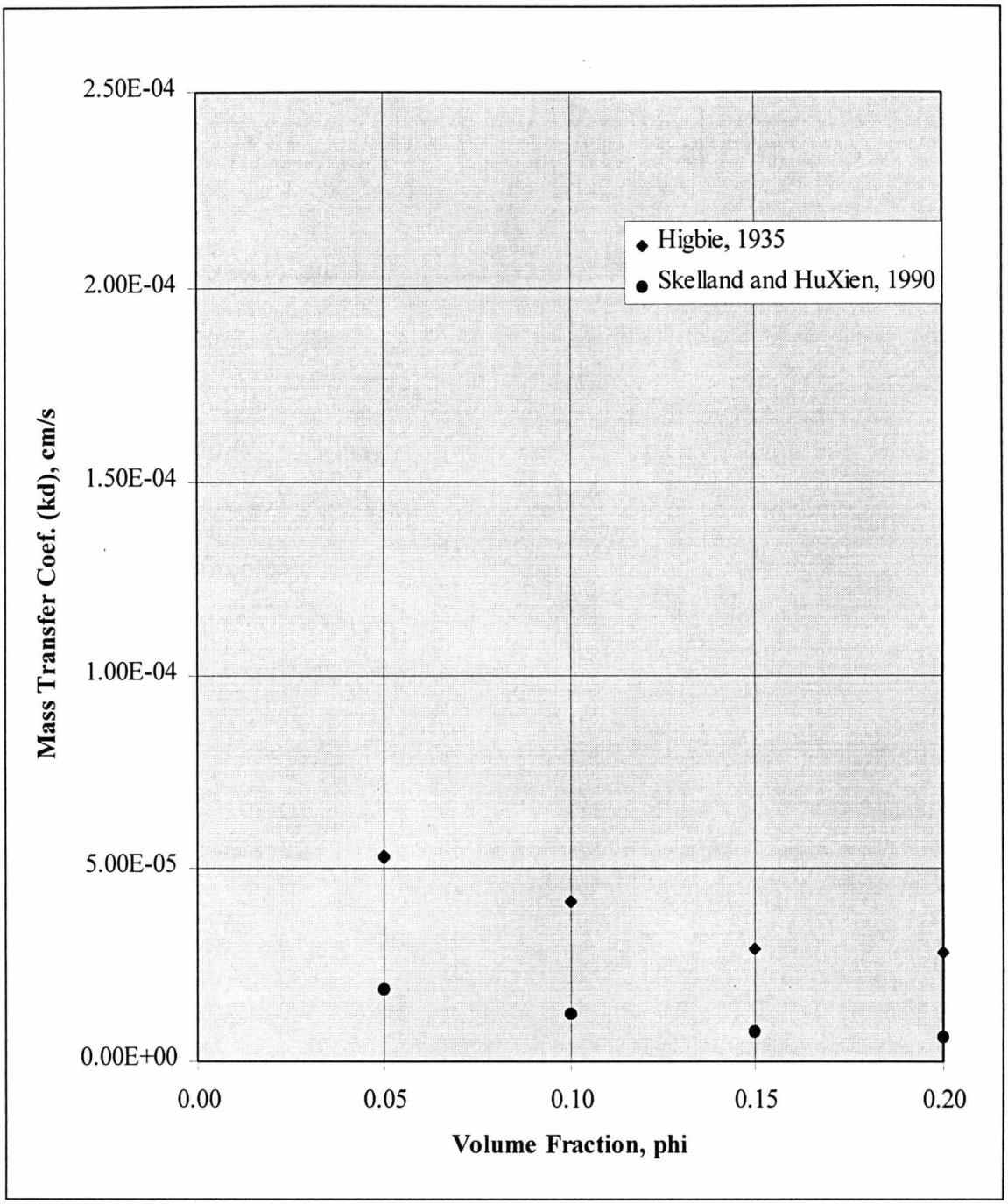

Figure 7.1: Comparison of model predicted dispersed-phase mass transfer coefficients. Both the Penetration Theory and the Skelland and HuXien Model underestimated the dispersed-phase mass transfer coefficient.

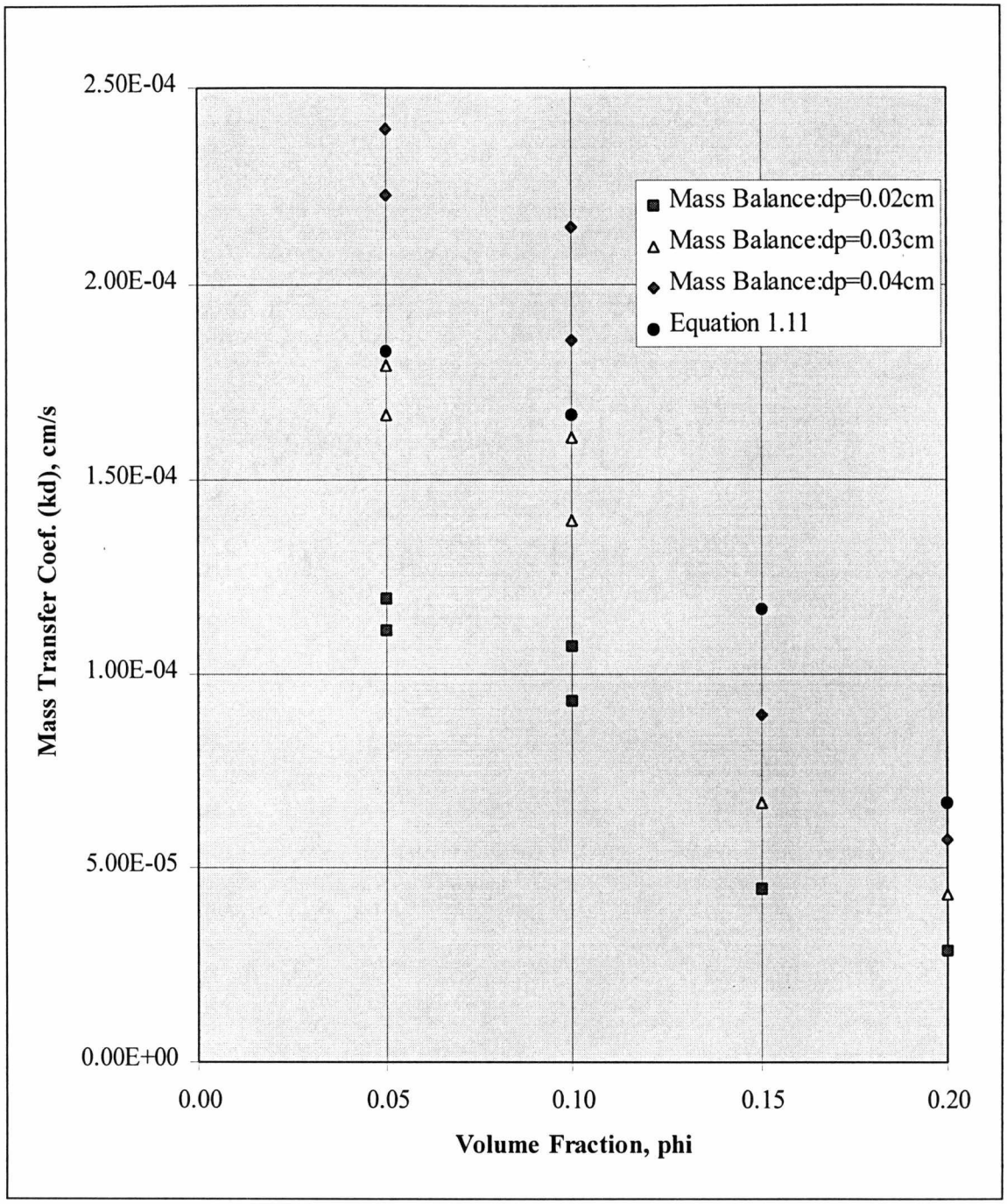

Figure 7.2: Comparison of dispersed-phase mass transfer coefficient predicted using the Sauter-mean diameter relationship, Equation 1.11 with experimentally measured dispersed-phase mass transfer coefficients at visually estimated drop sizes- 0.02cm, 0.03cm, and 0.04cm. Sauter-mean diameters were essentially the same for any given volume fraction but ranged from 0.04cm to 0.02cm over time.

same for any given dispersed-phase volume fraction (ϕ=0.05, 0.10, 0.15, 0.20) but ranged from 0.04cm to 0.02cm over time (t=30seconds through t=300seconds).

Conclusions

1. Both the Penetration Theory (Higbie, 1935) and the Skelland and HuXien Model (1990) underestimate the dispersed-phase mass transfer coefficient in this kind of system. Therefore these expressions will yield a conservative extractor design.
2. The difference between the measured value of k_d and that estimated from Penetration Theory could be accounted for by errors in the physical and transport property estimations especially diffusivity, D_{AB} which is difficult to estimate for the liquid-liquid system described herein.
3. Experimentally estimated drop sizes generally agree with the Hong and Lee (1985) Sauter-mean diameter model.
4. As expected, the continuous-phase mass transfer coefficient had very little influence on the overall mass transfer coefficient as predicted by the Skelland and Moeti (1990) expression.

LIST OF REFERENCES

LIST OF REFERENCES

Arlt, W., J. Sorensen, Liquid-Liquid Equilibrium Data Collection-Ternary Systems, DECHEMA,1980.

Bapat P.M., L.L.Tavlarides, G.W. Smith, "Monte Carlo Simulation of Mass Transfer in Liquid-Liquid Dispersions," Chem. Eng. Sci., 38, 1983, pp. 2003-2013.

Boyadzhiev L., Elenkov D., "On the mechanism of liquid-liquid mass transfer in a turbulent flow field," Chem. Eng. Sci., 21, 1966, pp. 955-959.

Boyd, E.T., "Solubility of Cellulose Acetate Butyrate Esters in Various Solvents," Eastman Technical Report, 1977.

Calderbank, P.H., Mass Transfer in Mixing, V.W. Uhl, J.B. Gray Editors, Academic Press: New York, 1967, vol. 2, Chapter 6.

Clift, R., J.R. Grace, M.E. Weber, Bubbles, Drops, and Particles, Academic Press: New York, 1978, pp. 38-41.

Davies, J.T., Turbulence Phenomena, Academic Press: New York, 1972, p.307.

Garner, F.H., A.R. Hale, "Solute Transfer to and from Liquid Drops," J. Appl. Chem., 5, 1955, pp. 653-663.

Harriott, P., "Mass Transfer to Particles: Part I. Suspended in Agitated Tanks," AIChE J., 8, 1962, pp. 93-101.

Higbie, R., Trans. A.I.Ch.E., vol. 31, 1935, p. 365.

Hines, A.L., R.N. Maddox, Mass Transfer Fundamentals and Applications, Prentice Hall: New Jersey, 1985, pp. 148-149, 156.

Hong, P.O.; J.M. Lee "Changes of the Average Drop Sizes During the Initial Period of Liquid-Liquid Dispersions in Agitated Vessels" Ind. Eng. Chem. Process Des. Dev., 24, 1985, pp. 868-872.

Holmes, J.T., C.R. Wilke, D.R. Olander, "Convective Mass Transfer in a Diaphragm Diffusion Cell," J. Phys. Chem., 67, 1963, pp. 1469-1472.

Howarth, W.J., "Mechanisms of Mass Transfer in an Agitated Vessel," Chem. Eng. Sci., 18, 1963, pp. 47-49.

Kanel, J.S., "Effects of some Interfacial Phenomena in Agitated Liquid-Liquid Dispersions," Ph.D. Dissertation, The Georgia Institute of Technology, Atlanta, GA, 1990, pp. 152-162.

Kanel, J.S., C.M. Farmer, C.W. Sink, Eastman Technical Report, 1991.

Kanel, J.S., J. Moncier, "Experimental Determination of the Quaternary Phase Diagram for Cellulose Acetate-Isopropyl Acetate-Acetic Acid-Water System," Eastman Technical Report, 1990.

Keey, R.B., J.B. Glen, "Area-Free Mass Transfer Coefficients for Liquid Extraction in a Continuously Worked Mixer," AIChE Journal, 15, 1969, pp. 942-947.

Laity, D.S., Treybal, R.E. Dynamics of Liquid Agitation in the Absence of an Air-Liquid Interface. AIChE Journal, 3, 1957, pp. 176-180.

Lusis, M.A., G.A. Ratcliff, "Diffusion in Binary Liquid Mixtures at Infinite Dilution," Can. Journal of Chem. Eng., 46, 1968, pp. 385-387.

Metzner, A.B., R.H. Feehs, H.L. Ramos, R.E. Otto, J.D. Tuthill, "Agiation of Viscous Newtonian and Non-Newtonian Fluids," AIChE Journal, 7(1), 1961, pp. 3-9.

Metzner, A.B.; R.E Otto, "Agitation of Non-Newtonian Fluids" AIChE Journal, 3(1), 1957, pp.3-10.

Metzner, A.B., J.S. Taylor, "Flow Patterns in Agitated Vessels," AIChE Journal, 6(1), 1960, pp. 109-114.

Mok, Y.I., R.E. Treybal, "Continuous Phase Mass Transfer Coefficients for Liquid Extraction in Agitated Vessels II," AIChE Journal, 17(4), 1971, pp. 916-920.

Murti, P.S., J. Sci. Industr. Res., 13B, 1954p. 395.

Nernst, W., Z. Phys. Chem., 2, 1888, p. 613.

Payne, D., Personal Communication, 1995.

Othner, White and Trueger, "Liquid-Liquid Extraction Data," Ind. Eng. Chem., 1941, pp.

33, 1243.

Rushton, J.H., S. Nagata, T.B. Rooney, "Measurement of Mass Transfer Coefficients in Liquid-Liquid Mixing," AIChE Journal, 10(3), 1964, pp. 298-302.

Schindler, H.D., R.E. Treybal, "Continuous Phase Mass Transfer Coefficients for Liquid Extraction in Agitated Vessels," AIChE Journal, 14(5), 1968, pp. 790-798.

Sink, C. W., Eastman Technical Report, 1990.

Skelland, A.H.P., Diffusional Mass Transfer, Reprint edition, R.E. Krieger Publishing Co. Inc.: Malabar FL , 1995, pp. 50-52, 56, 91.

Skelland, A.H.P.; J.S. Kanel, "Minimum Impeller Speeds for Complete Dispersion of Non-Newtonian Liquid-Liquid Systems in Baffled Vessels" I&EC Research, 29, 1990, pp. 1300-1306.

Skelland A.H.P., Hu Xien, "Dispersed Phase Mass Transfer in Agitated Liquid-Liquid Systems," I&EC Res., 1990, pp. 415-420.

Skelland A.H.P., Lee, J. M. "Drop Size and Continuous-Phase Mass Transfer in Agitated Vessels" AIChE Journal, 27(1), 1981, pp. 99-111.

Skelland A.H.P., L.T. Moeti, "Mechanism of Continuous-Phase Mass Transfer in Agitated Liquid-Liquid Systems", Ind. Eng. Chen. Res., 29, 1990, pp. 2258-2267.

Skelland, A.H.P.; G.G. Ramsay, "Minimum Agitator Speeds for Complete Liquid-Liquid Dispersion," I&EC Research, 26, 1987, pp. 77-81.

Thorton, J.D., T.J. Anderson, K.H. Javed, and S.K.Achwal, "Surface Phenomena and Mass Transfer Interactions in Liquid-Liquid Systems," AIChE Journal, 31(7), 1985, pp. 1069-1076.

Treybal, R.E., Liquid Extraction, McGraw Hill: New York, 3rd ed., 1980, p. 110.

Treybal, R.E., Liquid Extraction, McGraw Hill: New York, 2nd ed., 1963, pp. 7,8,1 5-21, 50-52.

Vermeulen, T., G.M. Williams, G.E. Langlois, G.E., "Interfacial Area in Liquid-Liquid and Gas-Liquid Agitation," Chem. Eng. Prog., 51(2), 1955, pp. 85F-94F.

Wilke, C.R., P. Chang, "Correlation of Diffusion Coefficients in Dilute Solutions," AIChE Journal, 1, 1955, pp. 264-270.

APPENDIX

APPENDIX 1

List of Symbols

a	=	interfacial area per unit volume of liquid mixture, cm^2/cm^3
A	=	total interfacial area available for mass transfer, cm^2
C_a	=	concentration of the solute in the dispersed phase at time t, g/ml
C_a^*	=	concentration of the solute at the interface between the two phases at time, t, g/ml
D_{AB}	=	diffusivity of Na_2SO_4 in the Dispersed Phase, cm^2/s
D^o_{AB}	=	diffusivity of Na_2SO_4 in the Continuous Phase, cm^2/s
d_I	=	impeller diameter, cm
d_V	=	vessel diameter, cm
d_{32}	=	Sauter-mean drop diameter, cm
d^*_{32}	=	steady-state Sauter-mean drop diameter, cm
g	=	acceleration due to gravity, cm/s^2
H	=	height of liquid in the vessel, cm
k_c	=	continuous-phase mass transfer coefficient, cm/s
k_d	=	dispersed-phase mass transfer coefficient, cm/s
k_{dpred}	=	predicted dispersed-phase individual mass transfer coefficient, cm/s
K	=	fluid consistency index, cP
K_d	=	overall dispersed-phase mass transfer coefficient, cm/s
K_T	=	constant value for given type of impeller (Bates et al., 1963), dimensionless
m	=	distribution ratio, $g_{organic}/g_{aqueous}$
n	=	flow behavior index, dimensionless

N = impeller speed, rpm, 1/s

N_{Wec} = impeller Weber number, $N^2 d_I^3 \rho_c / \sigma$, dimensionless

N_{Rec} = impeller Reynolds number, $N d_I^2 \rho_c / \mu_c$, dimensionless

N_{Frc} = impeller Froude number, $N^2 d_I^2 \rho_c / \Delta\rho Hg$, dimensionless

t = time, s

t_0 = time at which all dispersed phase has been added to the vessel, s

t_s = exposure time, s (used with Penetration Theory)

t_f = time at which 99% of solute has transferred, s

T = absolute temperature, Kelvin

V_{bA} = molar volume of Na_2SO_4, cm^3/gmole

V_{bB} = average molar volume of all components, cm^3/gmole

V_d = volume of the dispersed phase, cm^3

V_s = volume of a spherical dispersed droplet, cm^3

V_T = total volume, cm^3

Greek Letters

α = constant used in equation 5.5 to determine the Sauter-mean drop diameter, $cm/s^{0.7}$

β = 0.7, constant used in equation 5.5 to determine the Sauter-mean drop diameter.

γ = d_{32}^*, constant used in equation 5.5 to determine the Sauter-mean drop diameter, cm

ε = rate of energy dissipation per unit mass of fluid, m^2/s^3

ϕ = volume fraction of the dispersed phase, dimensionless

η = eddy length scale, m

μ = viscosity of dispersed phase, N s/m^2

μ_a = apparent viscosity, cP

ν = kinematic viscosity, m^2/s

ρ = density of dispersed phase, kg/m^3

ρ_c = density of continuous phase, kg/m^3

APPENDIX 2

Sample Calculations for Chapter 1

A.2.1 Validate Assumption of No Droplet Internal Circulation

Eddy Length Scale, η:

Skelland and Moeti, (1990)

$$\eta = \varepsilon^{-\frac{1}{4}} \upsilon^{\frac{3}{4}}$$

Rate Of Energy Dissipation Per Unit Mass Of Fluid, ε:

$$\varepsilon = \frac{4 K_T}{\pi} \frac{d_I^5 N^3}{d_v^3}$$

K_T = 2.5, for a 6-blade turbine (Bates et al., 1963)

d_I = 0.0508 m

N = 16.6667 rpm

d_v = 0.1302 m

therefore,

$$\varepsilon = \frac{4(2.5)}{3.1416} \frac{(0.0508m)^5 (16.6667rps)^3}{(0.1302m)^3}$$

$$\varepsilon = 2.2588 \frac{m^2}{s^3}$$

Kinematic Viscosity, ν:

$$\upsilon = \frac{\mu}{\rho}$$

μ = 3,556 cP = 3.556 N s/m^2

ρ = 1.01 g/cm^3 = 1,010 kg/m^3

therefore,

$$\upsilon = \frac{3.556 \frac{Ns}{m^2}}{1010 \frac{kg}{m^3}}$$

$$\upsilon = 0.003521 \frac{m^2}{s}$$

and,

$$\eta = \left(2.2588 \frac{m^2}{s^3}\right)^{-\frac{1}{4}} \left(0.003521 \frac{m^2}{s}\right)^{\frac{3}{4}}$$

$$\eta = 0.0118m$$

if N= 4 rpm then,

$$\eta = \left(0.003122 \frac{m^2}{s^3}\right)^{-\frac{1}{4}} \left(0.003521 \frac{m^2}{s}\right)^{\frac{3}{4}}$$

$$\eta = 0.06115m$$

A.2.2 Derivation of Equation 1.11

Calculate the total interfacial area, A, using the experimentally determined droplet diameter:

$$\mathbf{A = a * \Sigma droplets}$$

First, calculate the area of an individual spherical droplet,

$$a = 4\pi \cdot r^2.$$

Then determine the number of droplets,

$$\Sigma droplets = \frac{V_d}{V_s};$$

followed by the volume of a single droplet,

$$V_s = \tfrac{4}{3}\pi \cdot r^3.$$

Substitution of these relationships into the interfacial area expression gives,

$$A = 4\pi \cdot r^2 * \frac{V_d}{\frac{4}{3}\pi \cdot r^3}$$

simplification gives,

$$A = \frac{3V_d}{r}$$

and,

$$A = \frac{6V_d}{d_p}$$

If d_p=d_{32}, then substitution of

$$d_{32} = t^{-\beta}\alpha + d_{32}^*$$

gives,

$$\frac{A}{V_d} = \frac{6}{d_{32}^* + \alpha t^{-0.7}}.$$

Given the mass balance relationship,

$$V_d dC_a = k_d A(C_a^* - C_a)dt,$$

setting $C_a^*=0$ and substituting A/V_d, gives,

$$\frac{1}{C_a}dC_a = -6k_d \frac{1}{d_{32}^* + \alpha \cdot t^{-0.7}}dt$$

Integrating both sides of the equation from C_{ao} to C_a and from t_o to t:

$$\int_{C_{a0}}^{C_a} \frac{1}{C_a}dC_a = -6k_d \int_0 \frac{1}{d_{32}^* + \alpha \cdot t^{-0.7}}dt$$

For the left hand side of the equation

$$\int_{C_{a0}}^{C_a} \frac{1}{C_a}dC_a \Rightarrow \ln \frac{C_a}{C_{a0}}$$

The right hand side of the equation can be evaluated numerically.

Appendix 3

Sample calculations for Chapter 3

A.3.1. Molecular Diffusivity of Na_2SO_4 Salt in the Dispersed Phase

BASIS: 50% weight IPA in CA Dope

Using the Lusis and Ratcliff (1968) correlation for organic solvents,

$$\frac{D_{AB}\mu_B}{T} = 8.52X10^{-10}(V_B)^{-1/3}\left[1.40\left(\frac{V_B}{V_A}\right)^{1/3} + \left(\frac{V_B}{V_A}\right)\right],$$

with Physical Properties Data from Table 3.3:

T = 298.16K

μ_B = 12,200 cP = 12.2 P (g/cm-s)

STEP 1:

Calculate Molar Volume of organic phase:

V_{bB} = molar volume of experiment B = cm^3/gmole

V_{bA} = molar volume of solute A = cm^3/gmole

The solute (transferring unit) is Na_2SO_4:

Na	2(18)
S	1(25.6)
O_4	4(8.3)
V_{bA}=	96.8 cm^3/gmole

The dispersed organic solution has the composition by weight:

50% isopropyl acetate, 4.7% water, 36.9% acetic acid, and 8.5% Cellulose Acetate

	isopropyl acetate		water		acetic acid		Cellulose Acetate
MW:g/gmol	102		18		60		
							Neglected due to
	5(14.8)	C	0	C	2(14.8)	C	small mole%.
	10(3.7)	H	2(3.7)	H	4(3.7)	H	
	2(11.0)	O	1(7.4)	O	2(12.0)	O	**Composite V_{bB}**
Molar Volume:	133 cm^3/gmol		14.8 cm^3/gmol		68.4cm^3/gmol		**69.55 cm^3/gmol**
Weight%:	0.366		0.295		0.231		
Mole%:	0.15		0.69		0.16		

STEP 2:

Substituting V_{bB} and V_{bA} into

$$\frac{D_{AB}\mu_B}{T} = 8.52X10^{-10}(V_B)^{-1/3}\left[1.40\left(\frac{V_B}{V_A}\right)^{1/3} + \left(\frac{V_B}{V_A}\right)\right]$$

gives,

$$D_{AB} = 1.0147E-09\frac{cm^2}{s}$$

A.3.2. Diffusivity of Na_2SO_4 Salt in the Continuous Phase, D^oAB

Assuming strong electrolyte at infinite dilution compute diffusivity at 25°C (Skelland, p. 68).

$$D^o_{AB} = 8.931E-10T\frac{\lambda^o_+\lambda^o_-}{\lambda^o_+ + \lambda^o_-}\frac{|Z_-|+|Z_+|}{|Z_+Z_-|},$$

$\lambda^o_{+Na^+} = 50.1\frac{mho}{equivalent}$

$\lambda^o_{-SO_4^{-2}} = 80.0\frac{mho}{equivalent}$

$Z_+ = 1$

$Z_- = 2$

$T = 298.16K$

therefore,

$$D^o_{AB} = 8.931E-10(298.16)\frac{50.1\cdot 80.0}{50.1+80}\frac{|2|+|1|}{|1\cdot 2|}$$

$$D^o_{AB} = 1.23E-5\frac{cm^2}{s}$$

Appendix 4

Sample calculations for Chapter 4

A.4.1. Prediction of Minimum Agitator Speed Needed to Maintain Dispersion (Skelland and Kanel, 1990)

$$N_{\min} = C\left(\frac{d_v}{d_i}\right)^{\alpha} \frac{g^{0.42}\Delta\rho^{0.42}\mu_m^{0.08}\sigma^{0.04}\phi^{0.05}}{d_i^{0.71}\rho_m^{0.54}},$$

where

$$\rho_m = \phi\rho_d + (1-\phi)\rho_c$$

$$\mu_m = \frac{\mu_c}{1-\phi}\left(1+\frac{1.5\mu_d\phi}{\mu_d+\mu_c}\right)$$

Physical Property data average from 3 runs in 50%IPA Experiment Set in Table 3.3.

μ_c = 0.017 g/(cm sec)

μ_d = 45.0 g/(cm sec)

ρ_c = 1.026 g/cm^3

ρ_d = 0.953 g/cm^3

σ = 2 dyne/cm

Vessel geometry data was taken from Table 5.5

d_V = 13.02 cm

d_i = 5.08 cm

H = 21.17 cm (height of liquid in the vessel)

C= 0.95 Using H/2 with Table from Skelland and Kanel, (1990)

α= 1.38 Using H/2 with Table From Table in Skelland and Kanel, (1990)

ϕ= 0.10

Substitution of values gives,

$$\rho_m = 0.1(0.953) + (1-0.1)1.026 = 1.0187\frac{g}{cm^3}$$

and

$$\mu_m = \frac{0.017}{1-0.1}\left(1+\frac{1.5(45.0)0.1}{45.0+0.017}\right) = 0.0217\frac{g}{cm\cdot \sec}$$

and

$$N_{\min} = 0.95\left(\frac{13.02}{5.08}\right)^{1.38}\frac{980^{0.42}(1.026-0.953)^{0.42}.0217^{0.08}2^{0.04}0.1^{0.05}}{5.08^{0.71}1.0187^{0.54}}$$

Gives

N_{min}= 4.4 rps= 265rpm

By comparison, the experiment sets in Chapter 5 were run at 1000rpm.

Appendix 5

Sample calculations for Chapter 5

A.5.1. Sodium Sulfate Concentration Profile in the Continuous Phase for Experimental Runs 2-11.

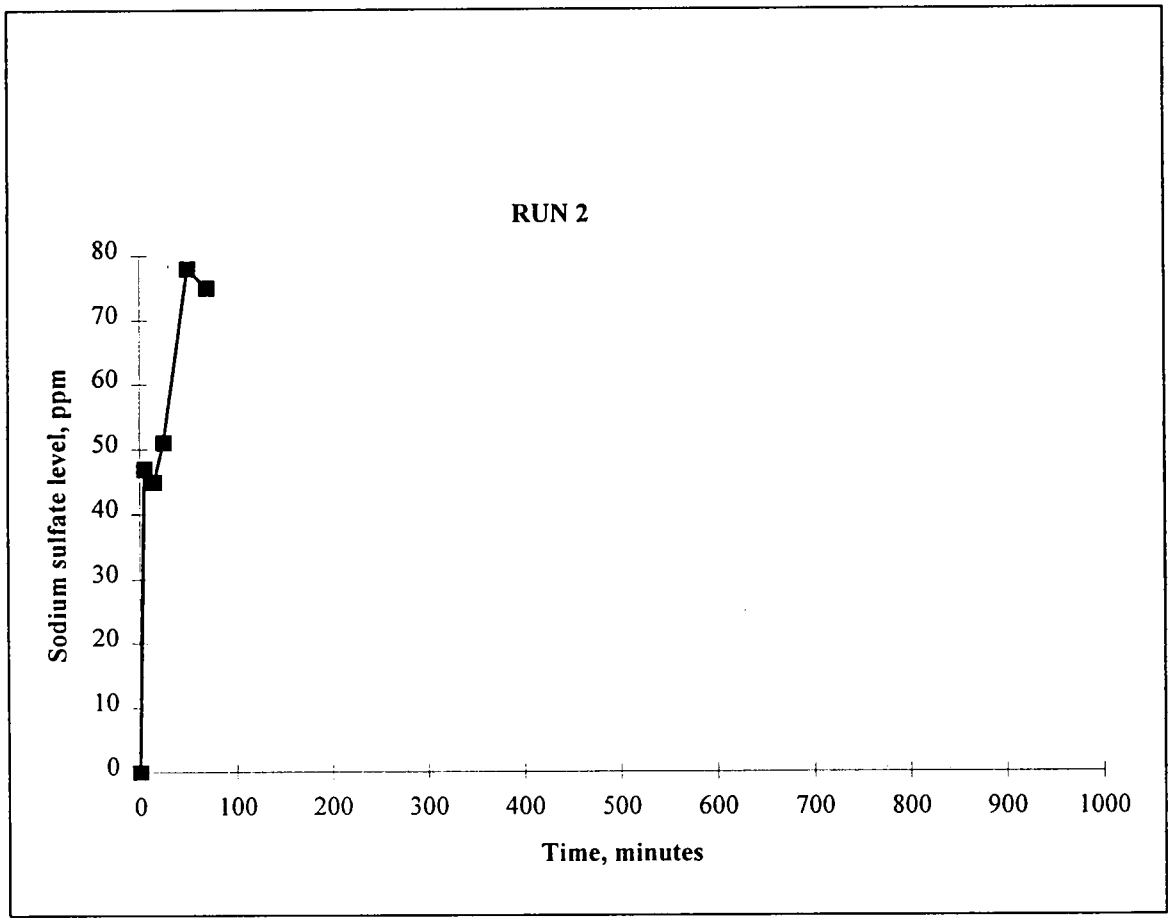

Figure A5.1: Time required for Sodium sulfate concentration in the continuous phase to reach equilibrium for Run 2.

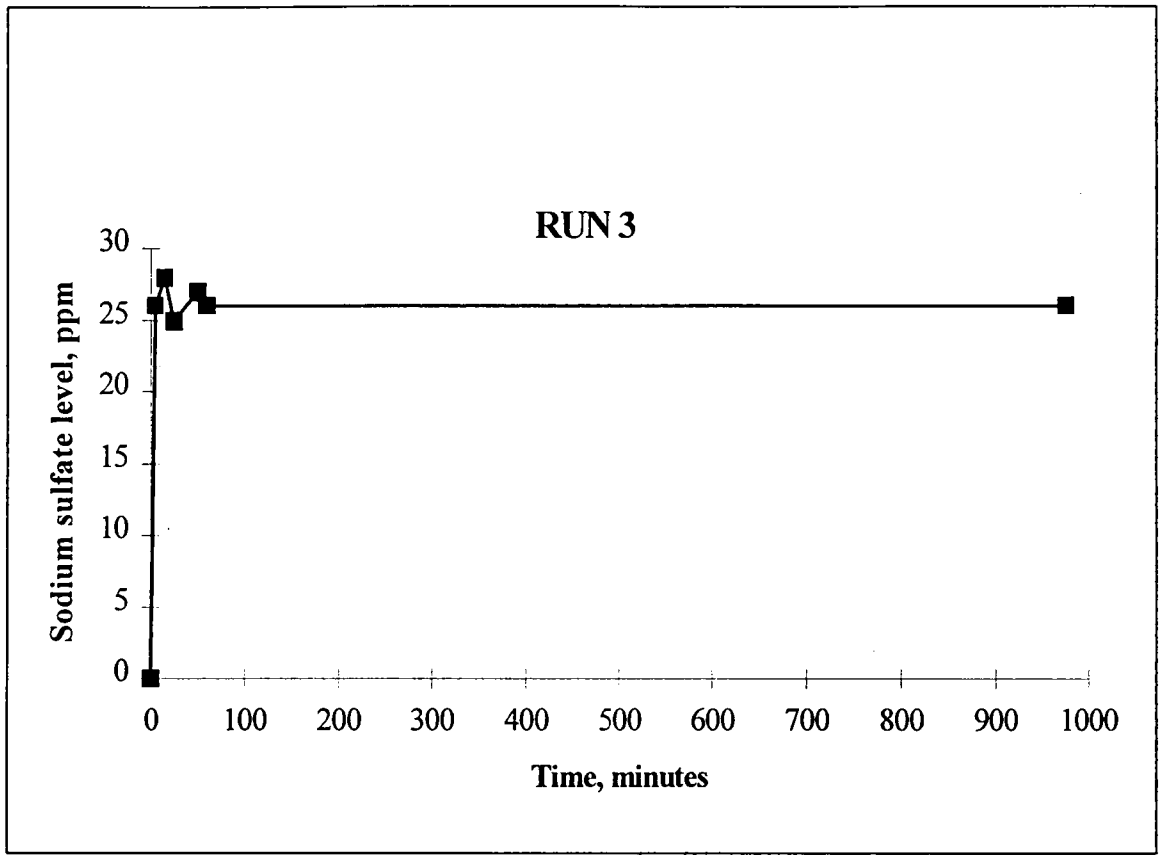

Figure A5.2: Time required for Sodium sulfate concentration in the continuous phase to reach equilibrium for Run 3.

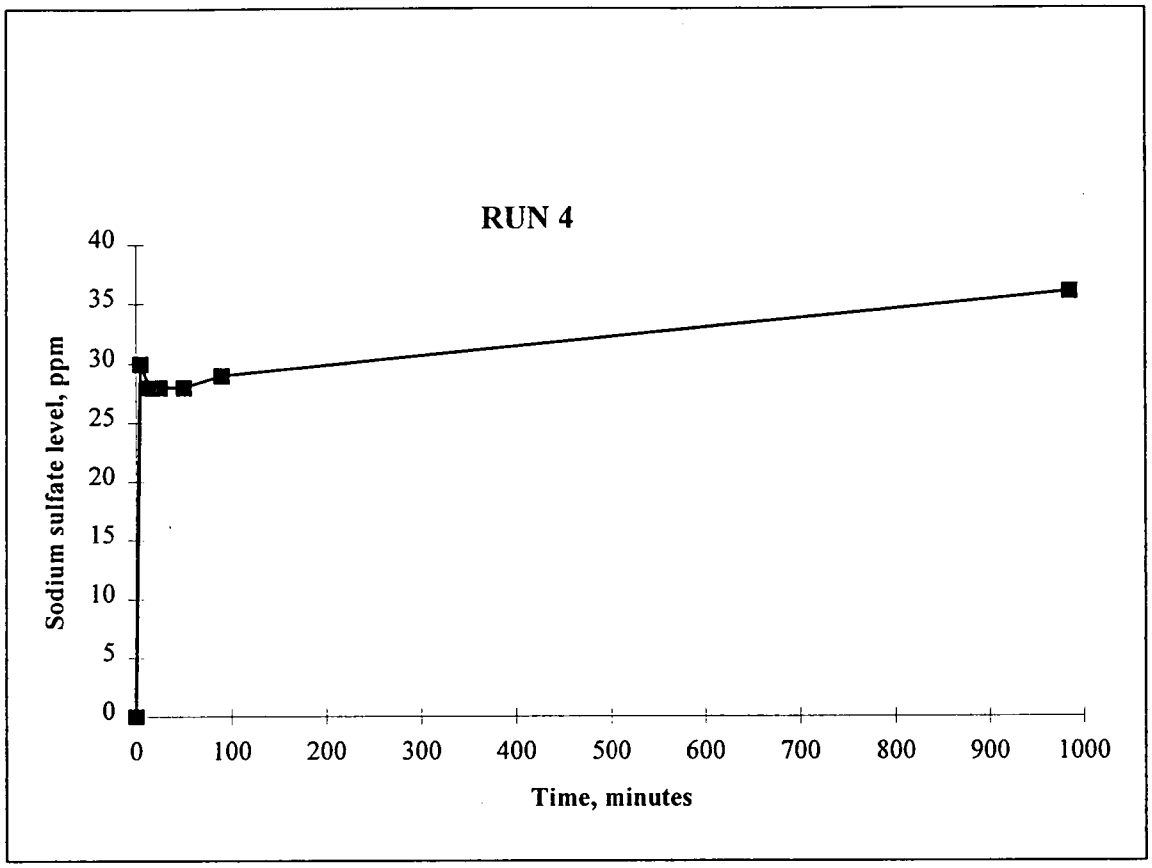

Figure A5.3: Time required for Sodium sulfate concentration in the continuous phase to reach equilibrium for Run 4.

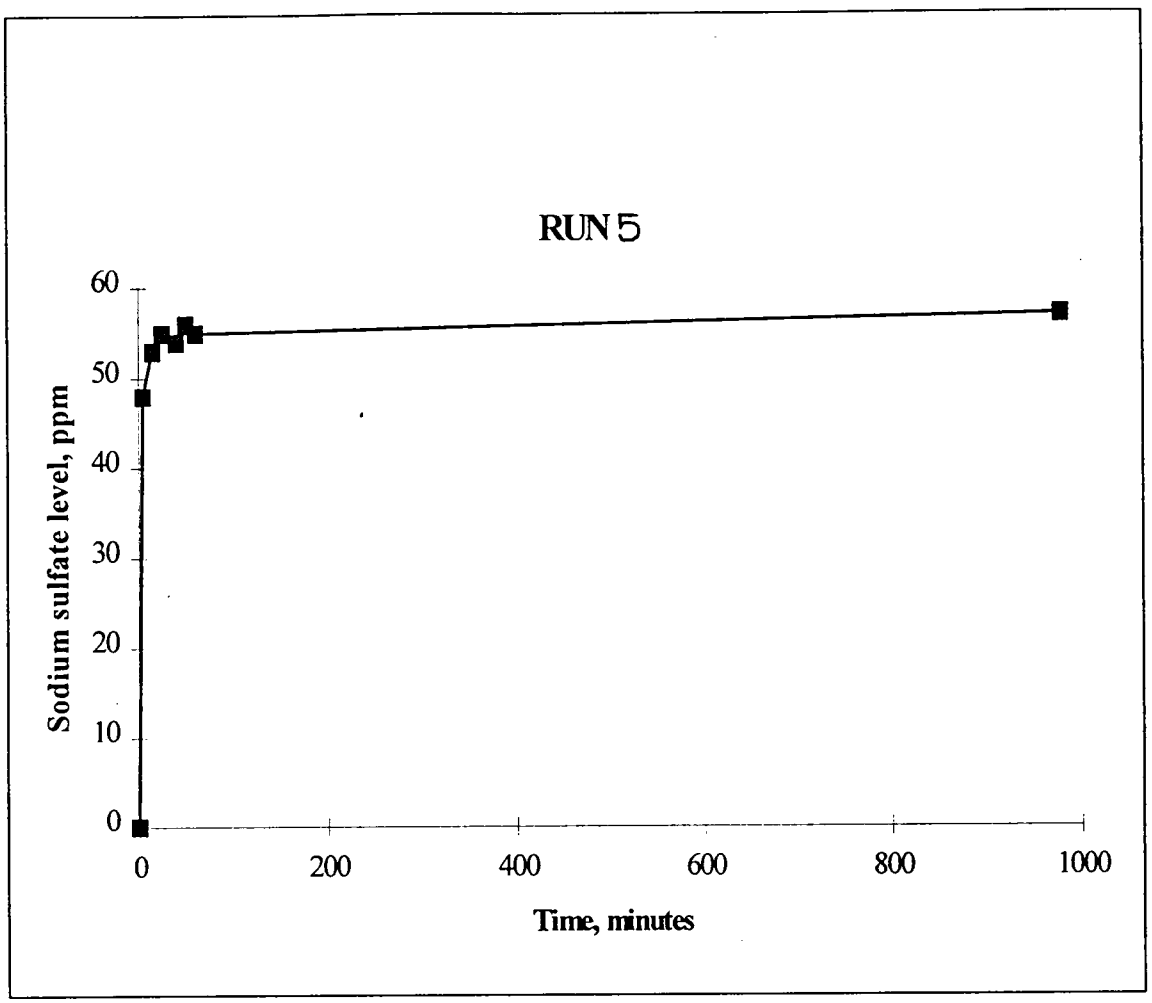

Figure A5.4: Time required for Sodium sulfate concentration in the continuous phase to reach equilibrium for Run 5.

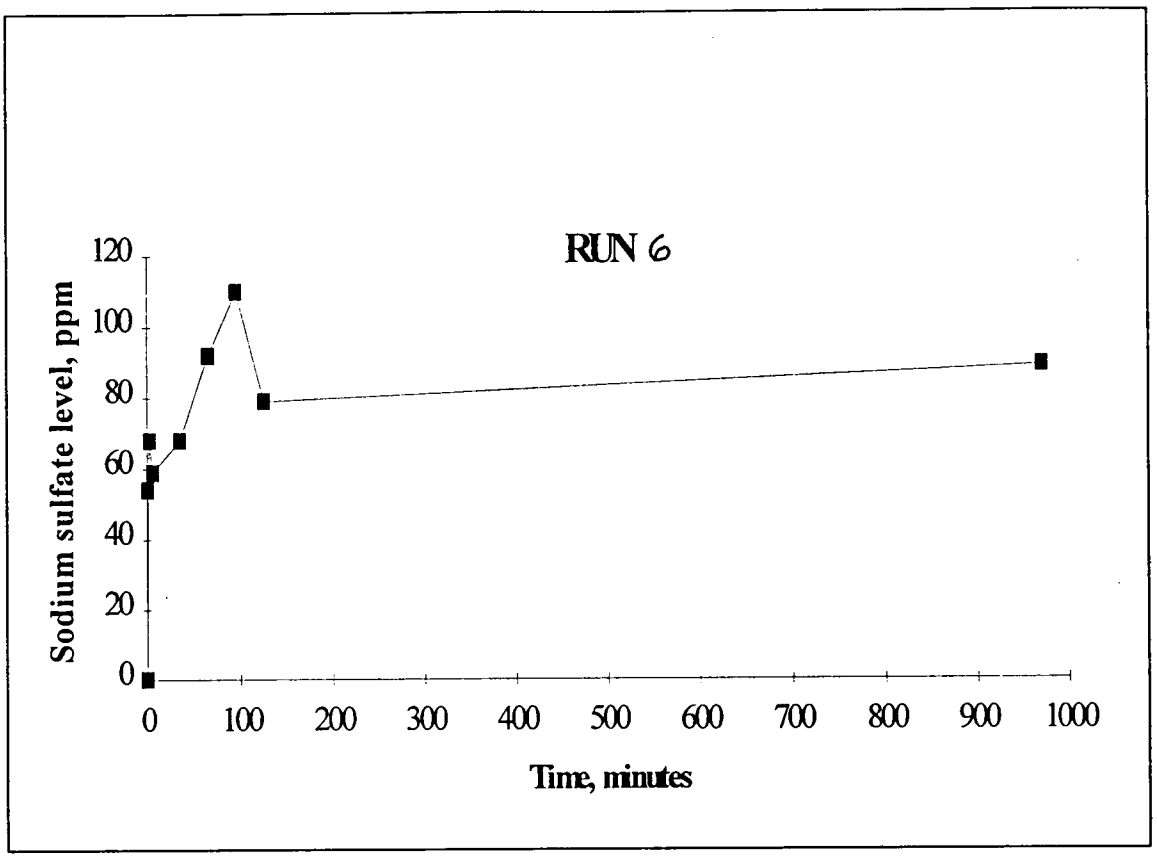

Figure A5.5: Time required for Sodium sulfate concentration in the continuous phase to reach equilibrium for Run 6.

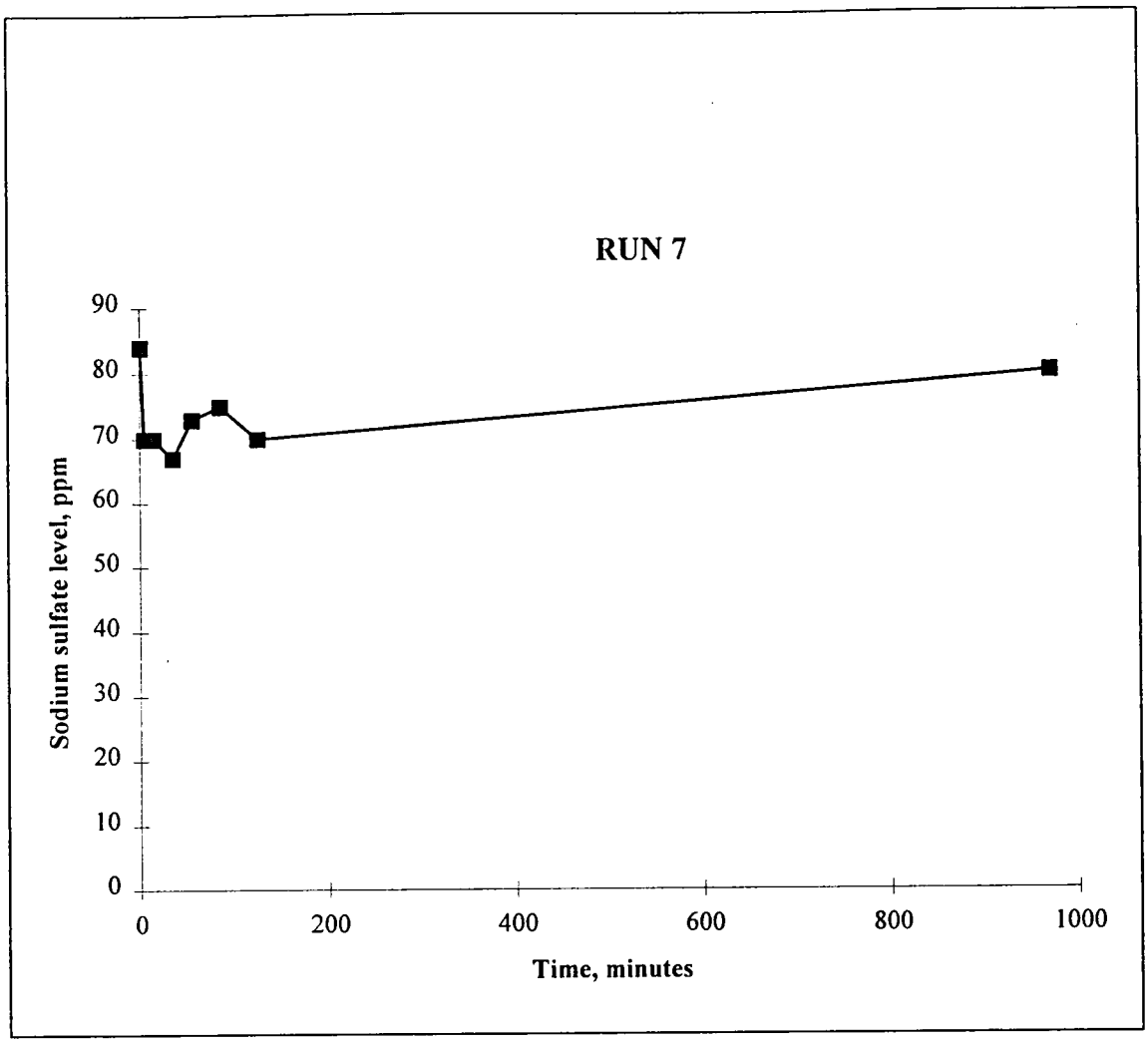

Figure A5.6: Time required for Sodium sulfate concentration in the continuous phase to reach equilibrium for Run 7.

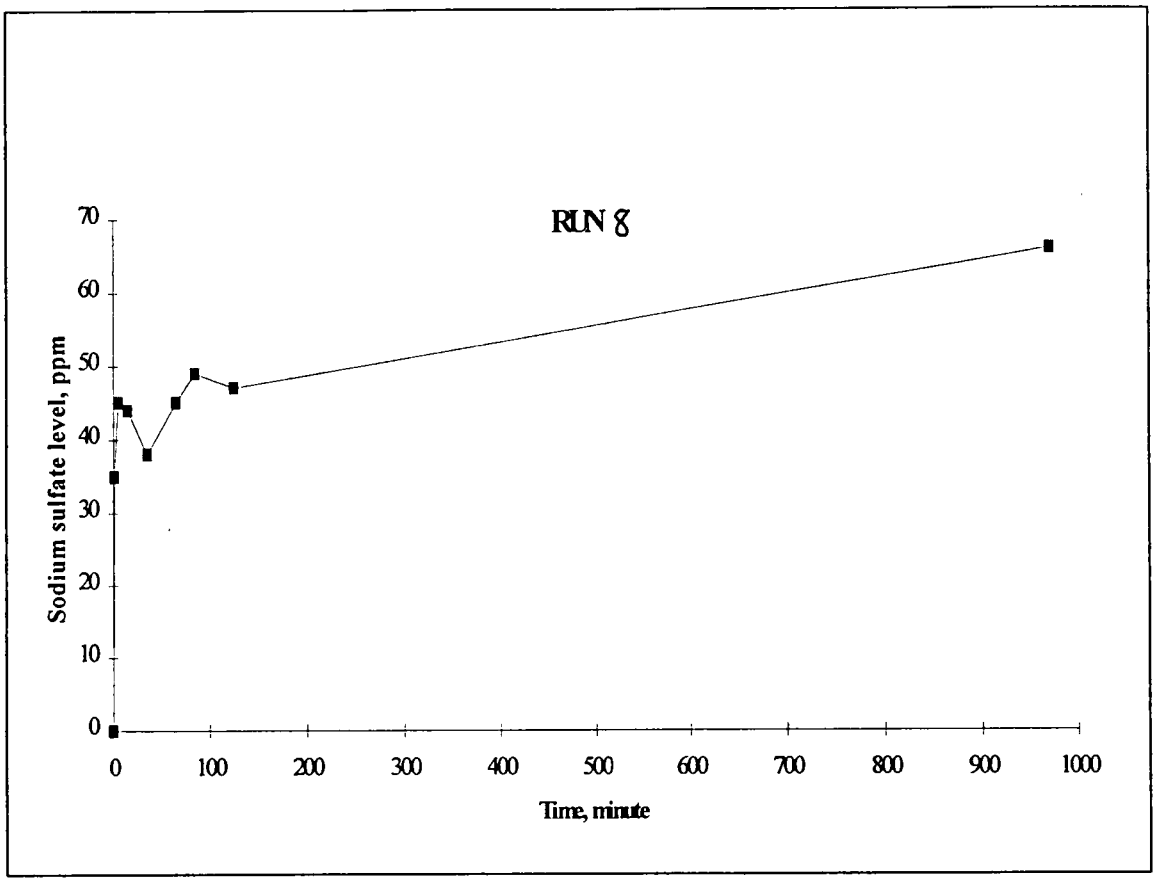

Figure A5.7: Time required for Sodium sulfate concentration in the continuous phase to reach equilibrium for Run 8.

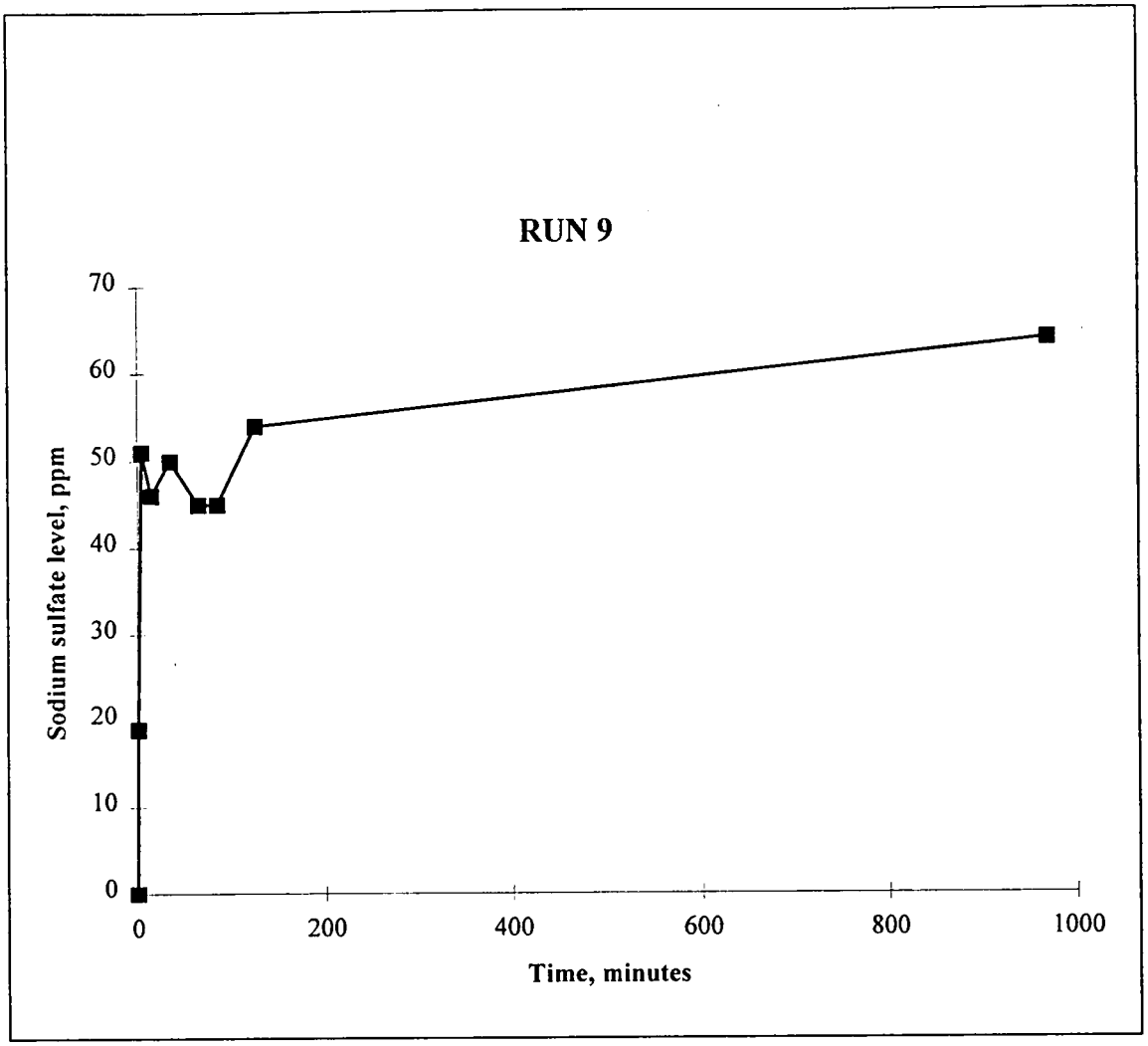

Figure A5.8: Time required for Sodium sulfate concentration in the continuous phase to reach equilibrium for Run 9.

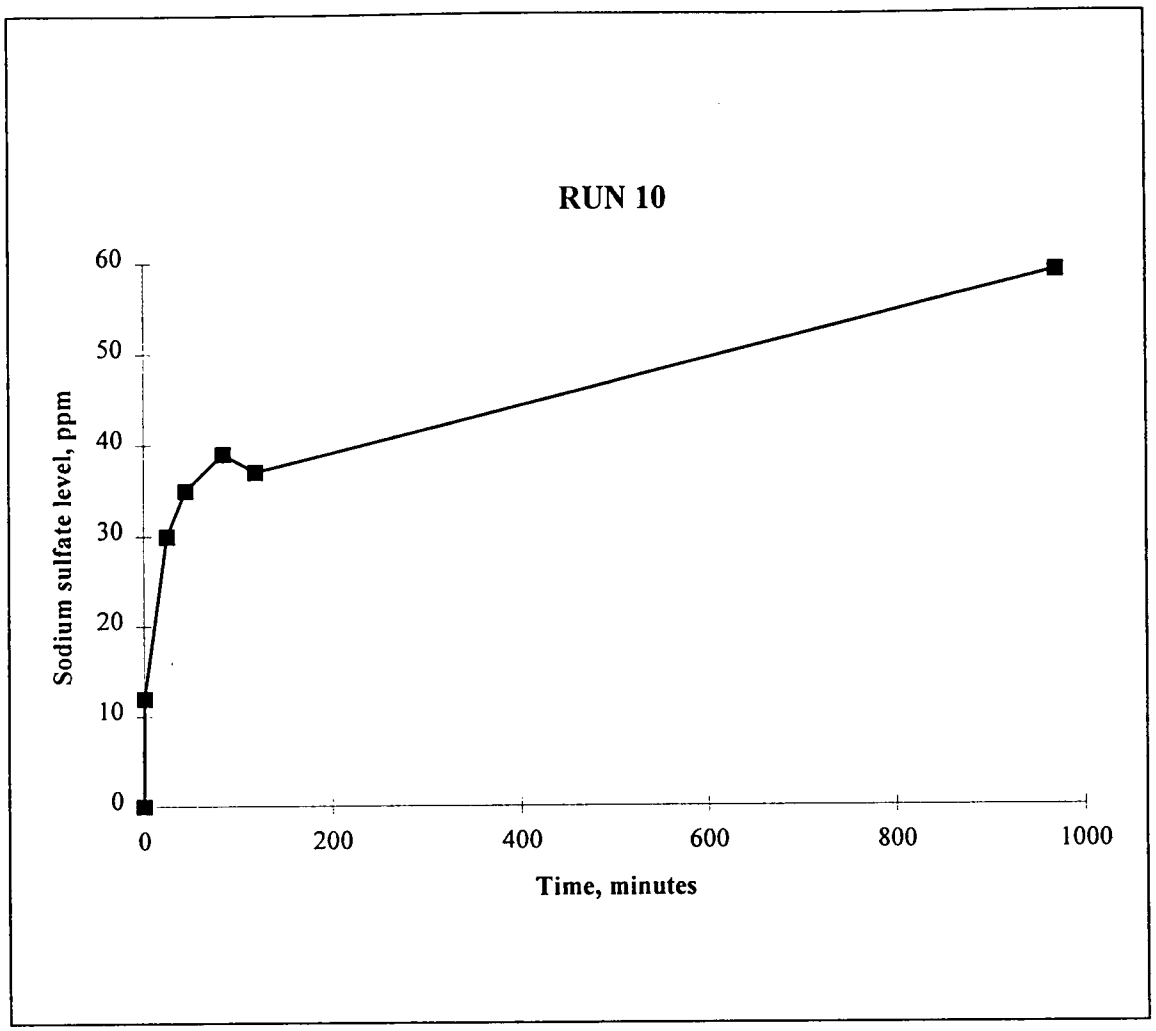

Figure A5.9: Time required for Sodium sulfate concentration in the continuous phase to reach equilibrium for Run 10.

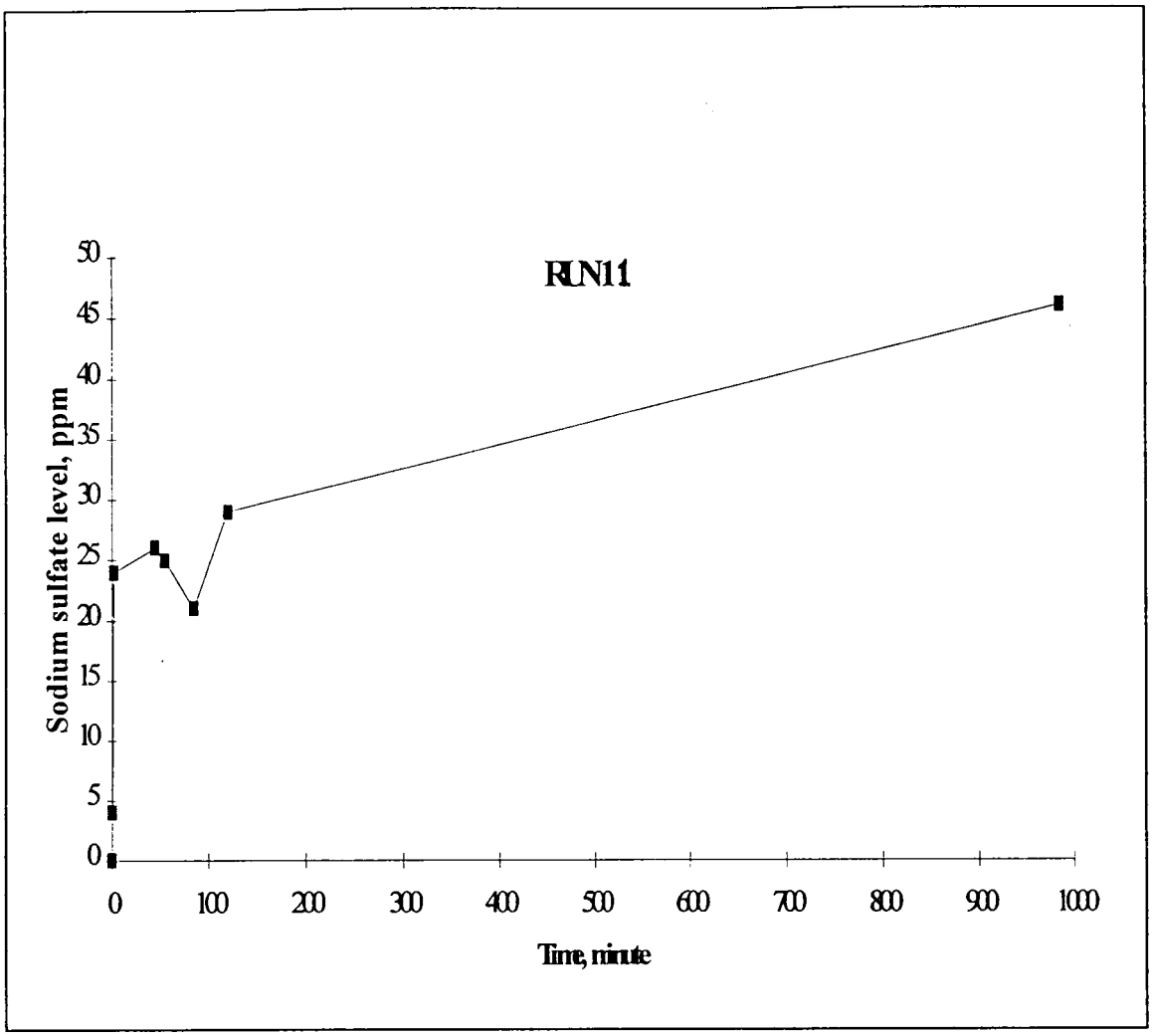

Figure A5.10: Time required for Sodium sulfate concentration in the continuous phase to reach equilibrium for Run 11.

A.5.2 Prediction of the Sauter-mean diameter

STEP 1:

As shown in table A6.16 Calculate the Impeller Reynolds, Weber and Froude Numbers for use in the Sauter-mean Diameter Expression, Table A5.2

Table A5.1: Approximating the Impeller Reynolds, Weber and Froude Numbers for use in the Sauter-mean Diameter Expression, Table A5.2

Expt. Run	Dispersed Density g/cc	Continuous Phase Viscosity g/cm-sec	Continuous Phase Density g/cc	Impeller Weber Number.	Impeller Reynolds Number	Impeller Froude Number
	Viscous Droplet					
1	0.9960	0.0164	1.036	20960	27061	9
2	0.9900	0.0164	1.036	20960	27163	8
3	1.0290	0.0166	1.036	20960	26815	54
	Fluid Droplet					
1	0.9480	0.0165	1.036	18864	26940	4
2	0.9570	0.0164	1.036	18864	27157	5
3	0.9530	0.0166	1.036	18864	26701	4

Note:
(1) Input Date Source: Physical Properties Table 3.3, Apparatus Table 5.5
(2) Impeller Speed 16.67 rpm (1000rpm)

STEP 2:
As shown in Table A5.2, calculate the Sauter-mean diameter using equations 5.5-5.7.

Table A5.2: Prediction of the Sauter-mean diameter using Hong and Lee (1985) Model in Equations 5.5-5.7. *

TIME, sec	Sauter Mean Diameter (d_{32}), cm	
	Viscous Droplet	Fluid Droplet
30	0.0039	0.0044
60	0.0029	0.0033
90	0.0025	0.0028
120	0.0022	0.0026
150	0.0021	0.0024
180	0.0020	0.0023
210	0.0019	0.0022
240	0.0018	0.0021
270	0.0018	0.0021
300	0.0018	0.0020

*Note:

$$d_{32} = \alpha t^{-0.7} + d_{32}^{*} \tag{5.5}$$

$$\alpha = 29.7 d_{32}^{*} \left(\frac{d_I}{d_i}\right)^{-2.015} \left(\frac{N_{Wec}}{N_{Rec}}\right)^{0.5508} N^{-0.7} \tag{5.6}$$

$$d_{32}^{*} = d_I 0.05(1 + 2.316\phi)\left(\frac{d_I}{d_i}\right)^{-0.75} N_{Frc}^{-0.13} N_{Wec}^{-0.6} \tag{5.7}$$

Averaging the first 5 data points gives $\mathbf{d_{32}}$ = **0.0094cm** for the **fluid droplet** and $\mathbf{d_{32}}$=**0.008cm** for the **viscous droplet** when ϕ=**0.1**.

A.5.3 Estimation of Experimental k_d : Fluid Droplet

$$\ln \frac{C_a}{C_{ao}} = -\frac{k_d A(t - t_o)}{V_d} \qquad (1.10)$$

STEP 1:

Initial time, t_o, is the time at which all of the dispersed phase as entered the vessel. It is calculated from the Pump Calibration Curve in Table 5.3. As shown in Table A5.3, calculate the sodium concentration in the dispersed-phase droplet over time.

Table A5.3: Sodium Mass Balance for Fluid Droplet

Time, min.	Continuous Phase ppmNa	gramsNa	Dispersed Phase grams Na	C_a, g/ml	$t-t_{o(35sec)}$	C_a/C_{ao}
0	0	0.0000	0.332525	8.313E-04	0	1.0000
1	54	0.1944	0.138125	3.453E-04	25	0.4180
3	68	0.2448	0.087725	2.193E-04	145	0.2654
6	59	0.2124	0.120125	3.003E-04	325	0.3635
36	68	0.2448	0.087725	2.193E-04	2125	0.2654
66	92	0.3312	0.001325	3.312E-06	3925	0.0040

STEP 2:

Plot C_a versus t as shown in Figure A6.11, followed by non-linear regression of the resulting curve. Calculate C_{ao} and t_0 using the resulting correlation.

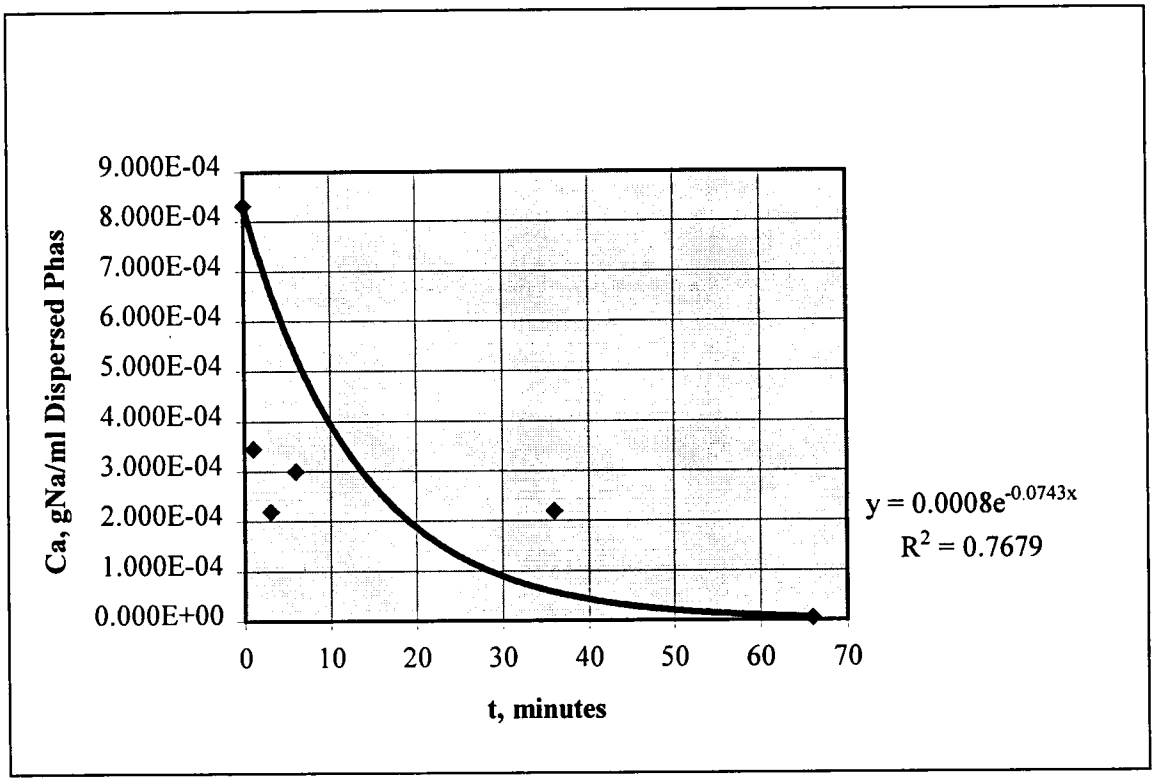

Figure A5.11: Non-linear regression of [Na-] versus Time to approximate [Na-] in the continuous-phase when C_a/C_{ao}=1 for fluid droplets.

STEP 3:

Using non-linear regression on ln C_a/C_{ao} *vs* t-t_0 data (as shown in Table A5.11) to estimate the slope gives,

$$-\frac{k_d A}{V_d} \cong -.0012$$

STEP 4:

Solving for k_d gives,

$$k_d \cong 0.0012 \frac{V_d}{A}$$

STEP 5:

From experimental results (see Chapter 5):

d_p=0.05cm from Table 5.3

STEP 6:

Calculate the total interfacial area, A, using the experimentally determined droplet diameter:

$$A = a \cdot \sum droplets$$

First, calculate the area of an individual spherical droplet,

$$a = 4\pi \cdot r^2.$$

Then determine the number of droplets,

$$\sum droplets = \frac{V_d}{V_s};$$

followed by the volume of a single droplet,

$$V_s = \tfrac{4}{3}\pi \cdot r^3.$$

Substitution of these relationships into the interfacial area expression gives,

$$A = 4\pi \cdot r^2 * \frac{V_d}{\frac{4}{3}\pi \cdot r^3}$$

simplification gives,

$$A = \frac{3V_d}{r}$$

$$k_d \cong slope * \frac{V_d}{\frac{3V_d}{r}}$$

STEP 7:

simplification gives,

$$k_d \cong 0.0012 \frac{d_p}{6}$$

$$k_d = -\frac{0.05}{6}(-0.0012)$$

$$k_d \cong 1.0E-05 \frac{cm}{\text{sec}}.$$

A.5.4 Estimation of Experimental k_d : Viscous Droplet

STEP 1:

Initial time, t_O, is the time at which all of the dispersed phase as entered the vessel. It is calculated from the Pump Calibration Curve in Table 5.3. As shown in Table A5.4, calculate the sodium concentration in the dispersed-phase droplet over time.

Table A5.4: Na Mass Balance for Viscous Droplet

	Continuous Phase		Dispersed Phase			
Time, min	ppmNa	gramsNa	grams Na	Ca, g/ml	$t-t_{o(35sec)}$	C_a/C_{ao}
0	0	0.0000	0.2313	5.78E-04	0.00	1.0000
1	19	0.0684	0.1629	4.07E-04	25	0.7714
5	51	0.1836	0.0477	1.19E-04	265	0.2260
15	46	0.1656	0.0657	1.64E-04	865	0.3112
35	50	0.1800	0.0513	1.28E-04	2065	0.2430
65	45	0.1620	0.0693	1.73E-04	3865	0.3282
125	54	0.1944	0.0369	9.23E-05	7465	0.1748
970	64	0.2304	0.0009	2.30E-06	58165	0.0044

STEP 2:

Plot C_a versus t as shown in Figure A6.12, followed by non-linear regression of the resulting curve. Calculate C_{ao} and t_0 using the resulting correlation.

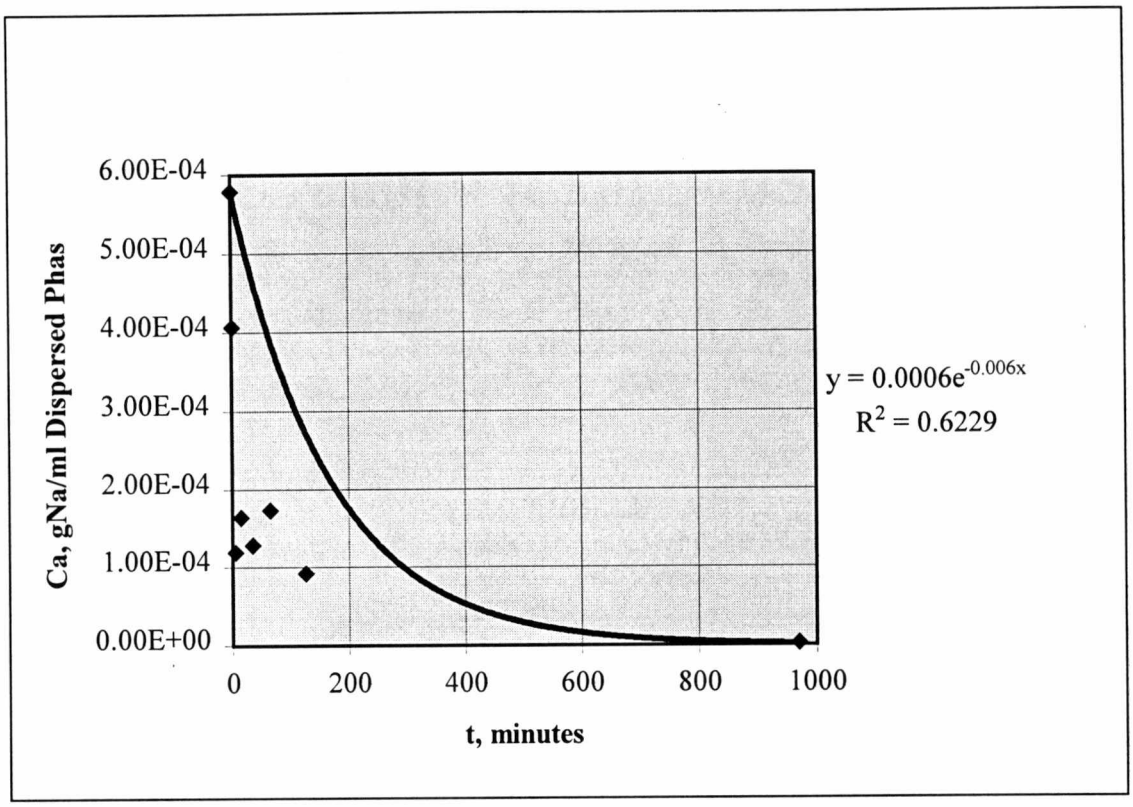

Figure A5.12: Non-linear regression of [Na-] versus Time to approximate [Na-] in the continuous-phase when $C_a/C_{ao}=1$ for viscous droplets.

STEP 3:

The mass transfer coefficient may be found as shown in the Fluid droplet Case Steps 3-7.

A.5.5. Prediction of k_d with the Skelland-HuXien Model.

STEP 1:

Calculate Mean Viscosity using data from Table 3.3 and phi=0.28 in equation 1.3. A summary of mean viscosities are captured in Table A5.5.

$$\mu_m = \frac{\mu_c}{1-\phi}\left[1+\frac{1.5\mu_d\phi}{\mu_d+\mu_c}\right] \tag{1.3}$$

Sample Calculation: Experiment Set 30% IPA

$$\mu_m = \frac{1.7643}{1-0.28}\left[1+\frac{1.5(203{,}668)0.28}{203{,}668+1.7643}\right]$$

$$\mu_m = 2.4504[1+0.42]$$

$$\mu_m = 3.4796cP$$

Sample Calculation: Experiment Set 40% IPA

$$\mu_m = \frac{1.6614}{1-0.28}\left[1+\frac{1.5(58{,}209)0.28}{58{,}209+1.6614}\right]$$

$$\mu_m = 2.3075[1+0.42]$$

$$\mu_m = 3.7267cP$$

Table A5.5: Calculation of Mean Viscosity

		Viscosity, P: g/cm-sec		
Experiment Set	Run No.	Continuos, μ_c	Dispersed, μ_d	Mean, μ_m
30%IPA				
	1	1.7643	203,668	0.035
	2	1.7253	169,885	0.034
	3	1.6178	262,323	0.032
40%IPA				
	1	1.6614	58,209	0.033
	2	1.6401	40,587	0.032
	3	1.6463	22,853	0.032
50%IPA				
	1	1.6587	6,286	0.033
	2	1.6405	3,555	0.032
	3	1.6685	3,661	0.033

Sample Calculation: Experiment Set 30% IPA

$$\mu_m = \frac{1.6537}{1-0.28}\left[1+\frac{1.5(6{,}286)0.28}{6{,}286+1.6537}\right]$$

$$\mu_m = 2.2968[1+0.42]$$

$$\mu_m = 3.2615cP$$

STEP 2:

Calculate Mean Density using data from Table 3.3 and phi=0.28 in equation 5.2,

$$\rho_m = \phi\rho_d + (1-\phi)\rho_c \tag{5.2}$$

Sample Calculation: Experiment Set 30% IPA

$$\rho_m = 0.28(1.062) + (1-0.28)1.03$$

$$\rho_m = 1.04\,g/cc$$

STEP 3: Calculate k_d using data from Table 3.3 and phi=0.28 in equation 5.1.

$$\frac{k_d}{\left[D/t_{95\%}\right]^{1/2}} = 5.0(10^{-6})\phi^{-0.0204}\left(\frac{d_I^2 N\rho_m}{\mu_m}\right)^{1.140}\left(\frac{\rho_c}{\Delta\rho}\right)^{0.518} \tag{5.1}$$

Sample Calculation: Experiment Set 30% IPA

$$\frac{k_d}{\sqrt{\frac{5.88e-9\frac{cm^2}{s}}{180s}}} = 5.0(10^{-6})(0.28)^{-0.0204}\left(\frac{(5.08cm)^2 16.67/s(1.04\frac{g}{cm^3})}{0.035\frac{g}{cm-s}}\right)^{1.140}\left(\frac{1.03\frac{g}{cm^3}}{(0.032)\frac{g}{cm^3}}\right)^{0.518}$$

$$\boxed{k_d = 5.89e-07\frac{cm}{s}}$$

Appendix 6

Sample Calculations for Chapter 6

A.6.1. Develop correlation between sodium concentration and conductivity in the continuous phase.

STEP 1:

Record sodium dilution data as shown in Table A6.1.

Table A6.1: Dilution Chart for Calibration of Conductivity Meter Starting with 1 gram of 1000ppm Sodium Standard. BASIS: 0.001 g Na

	Sodium Standard Solution	DI Water Added	Conductivity, μ Siemans	
ppmNa	Total grams	ml	RUN 1	RUN 2
100	1.0	9.0	1373	1470
90	10.0	1.1	1427	1376
80	11.1	1.4	1407	1402
70	12.5	1.8	1366	1360
60	14.3	2.4	1329	1272
50	16.7	3.3	1288	1270
40	20.0	5.0	1096	1240
30	25.0	175.0	1195	1210
1	200.0		1092	
0	10	10	1090	1090

STEP 2:

Plot [Na-] versus conductivity data followed by regression of the resulting curve as shown in Figure A6.1.

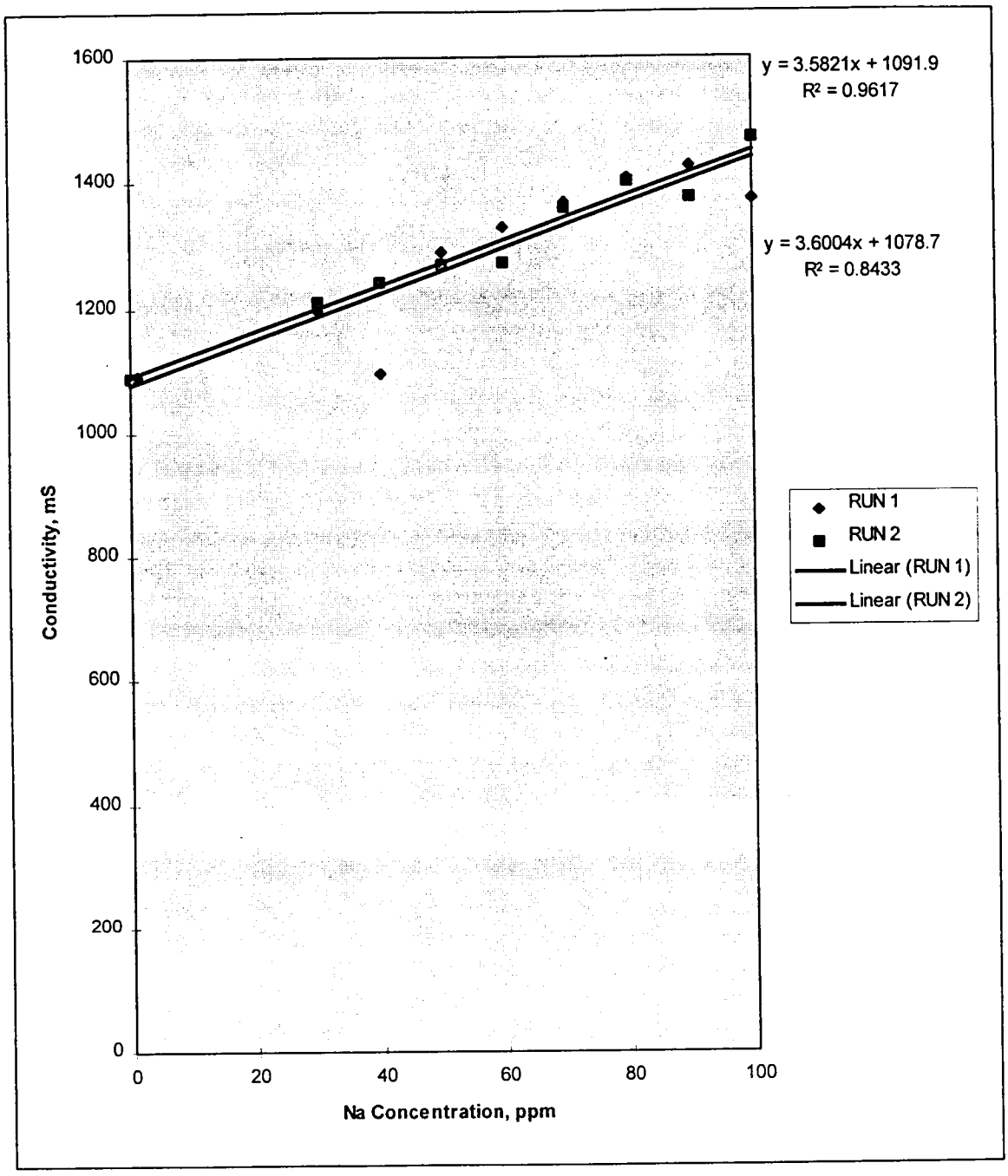

Figure A6.1 Calibration Curve for Conductivity Meter

STEP 3:

Use the regression correlation in Figure A6.1 to estimate the concentration of sodium in the continuous phase as shown in Table A6.2.

Table A6.2: Concentration by weight of sodium in the continuous phase over time as predicted by linear regression of conductivity versus ppmNa from calibration curve in Figure A6.1.

	ppmNa=(mS-1091.9)/3.5821					
TIME, sec	phi=0.05	phi=0.05	phi=0.10	phi=0.10	phi=0.15	phi=0.20
0	0.0000	0.0000	0.0000	0.0000	0.0000	0.0000
15	17.2233	14.1595	74.1984	77.8791	36.4608	19.6065
30	22.5907	22.9734	78.1616	80.5919	54.8451	44.2182
45	25.8938	26.3311	79.2625	80.5919	84.2598	53.1680
60	29.6096	27.5902	79.4827	81.4962	103.2569	66.5926
75	31.2612	28.4297	81.0240	81.4962	110.6106	95.6792
90	31.6740	29.2691	81.6845	81.9484	116.7387	111.3412
105	32.0869	30.5282	81.6845	82.4005	122.2539	106.8663
120	33.3255	30.9479	81.4644	81.0441	123.4795	142.6652
135	34.1513	31.3677	81.0240	82.4005	127.1564	160.5647
150	34.1513	30.9479	80.3634	81.4962	125.9308	176.2267
165	34.5642	31.3677	79.7029	81.4962	127.1564	180.7016
180	34.1513	31.7874	79.2625	81.0441	127.1564	182.9390
195	34.1513	31.7874	79.0424	81.9484	122.2539	196.3636
210	34.5642	31.3677	78.3818	81.9484	126.2155	198.6011
225	34.1513	30.9479	78.1616	81.9484	119.8027	214.2631
240	34.5642	30.5282	77.5011	82.8527	123.7643	220.9754
255	33.7384			82.4005	124.6580	216.5005
270	32.9127				125.8874	232.1625
285					126.1560	238.8748
300					127.9450	234.4000
315					123.4000	236.6374
330					127.0697	232.1625
345					122.4953	229.9251
360					128.5250	225.4502
375						232.1625
390						234.4000
405						229.9251
420						232.1625
1500	35.76115	30.7362	83.2193	83.7777	132.6717	227.6877

STEP 4:

Plot the [Na-] versus time data from Table A6.2 as shown in Figure A6.2.

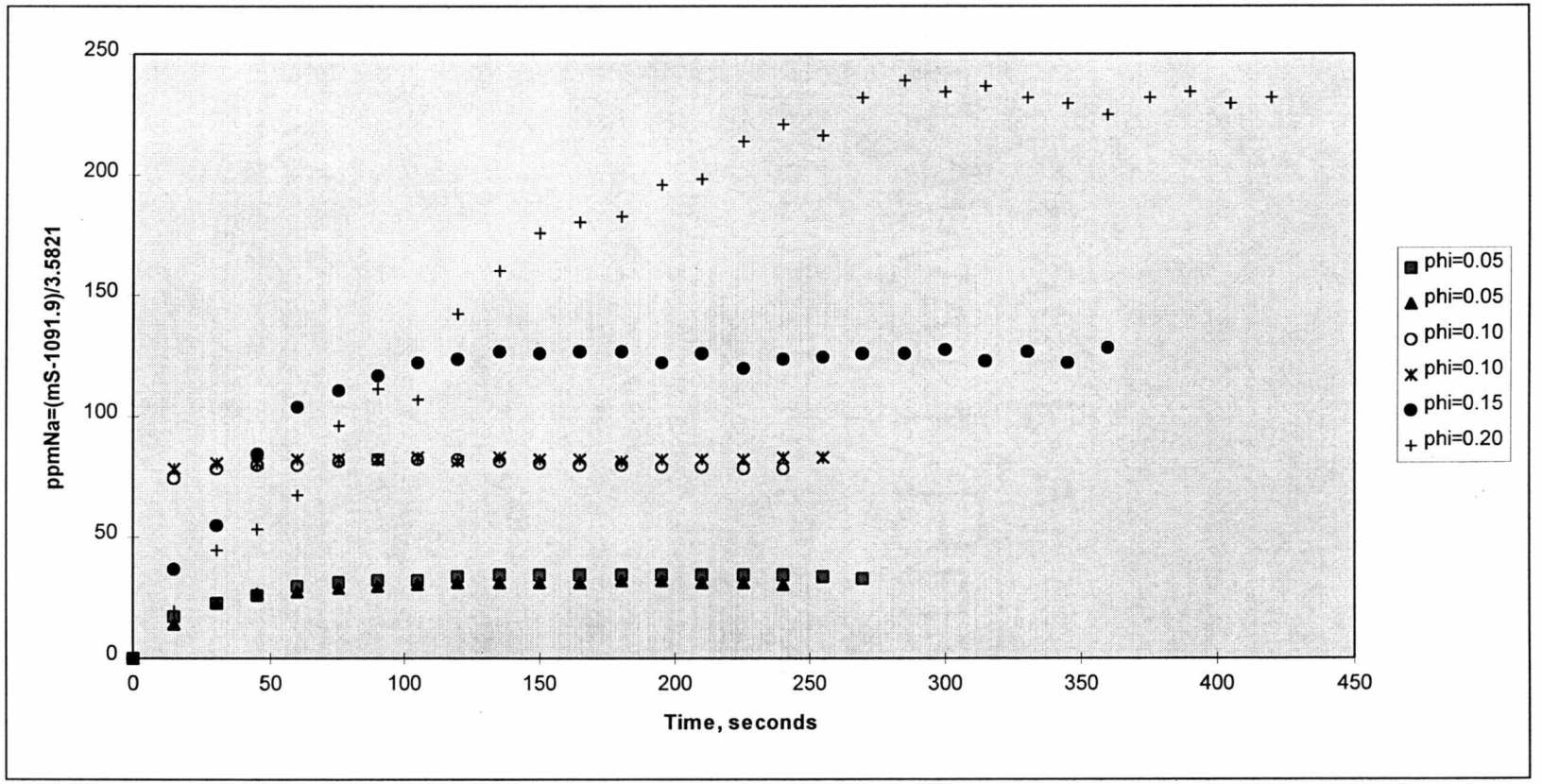

Figure A6.2: Plot of Concentration by weight of sodium in the continuous phase over time as predicted by linear regression of conductivity versus ppmNa from calibration curve in Figure A6.1.

A.6.2. Estimate C_{ao} and t_o at the point of Complete Dispersion: Experimental Run 1 where Volume Fraction, $\phi = V_d/V_T = 0.10$

STEP 1:

Record Sodium Sulfate Concentration as Measured Analytically in the Continuous Phase over time as shown in Table A6.3.

Table A6.3 Sodium Sulfate Concentration as Measured Analytically in the Continuous Phase over time for Experimental Run 1 where Volume Fraction, $\phi=V_d/V_T=0.10$.

Time		Sodium Sulfate Transferred		Dispersed Phase, gNa/ml		
seconds	ppmNa	From Disp.	To Cont.	C_a	$t-(t_o=0)$	C_a/C_{ao}
0	0.0	0.1500	0.0000	0.000750	0	1.0000
30	**52.4**	**0.0558**	**0.0942**	**0.000279**	**30**	**0.3717**
60	69.4	0.0251	0.1249	0.000125	60	0.1672
90	75.8	0.0136	0.1364	0.000068	90	0.0904
120	81.1	0.0040	0.1460	0.000020	120	0.0268
180	82.7	0.0011	0.1489	0.000006	180	0.0076
210	83.0	0.0006	0.1494	0.000003	210	0.0040
240	83.2	0.0002	0.1498	0.000001	240	0.0013
270	83.3	0.0001	0.1499	0.000000	270	0.0004
300	83.3	0.0000	0.1500	0.000000	300	0.0000

STEP 2:

Plot Ca versus time data from Table A6.3 followed by regression of the resulting curve as shown in Figure A6.3.

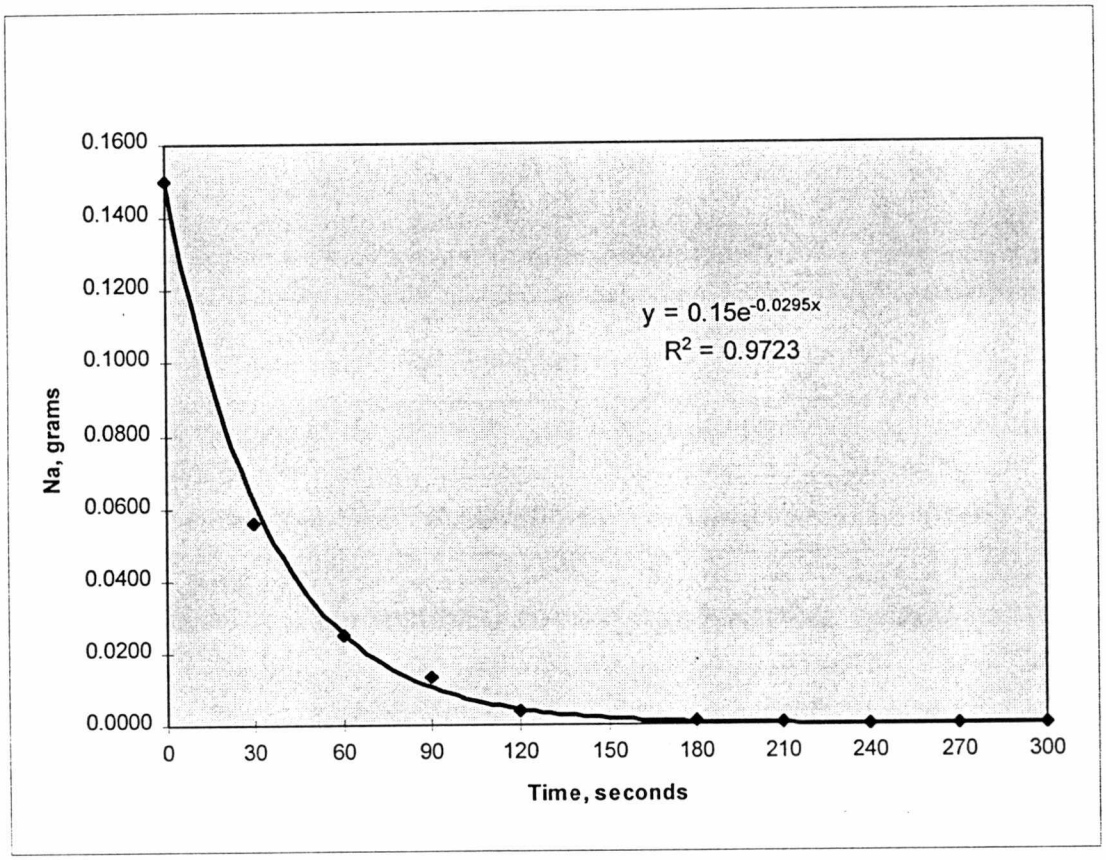

Figure A6.3: Mass Transfer Profile of Sodium Sulfate in the Dispersed Phase over time for Experimental Run 1 where Volume Fraction, $\phi = V_d/V_T = 0.10$.

STEP 3:
Plot $ln\ C_a/C_{ao}$ versus $t\text{-}t_0$ from Table A6.3, followed regression of the resulting curve as shown in Figure A6.4.

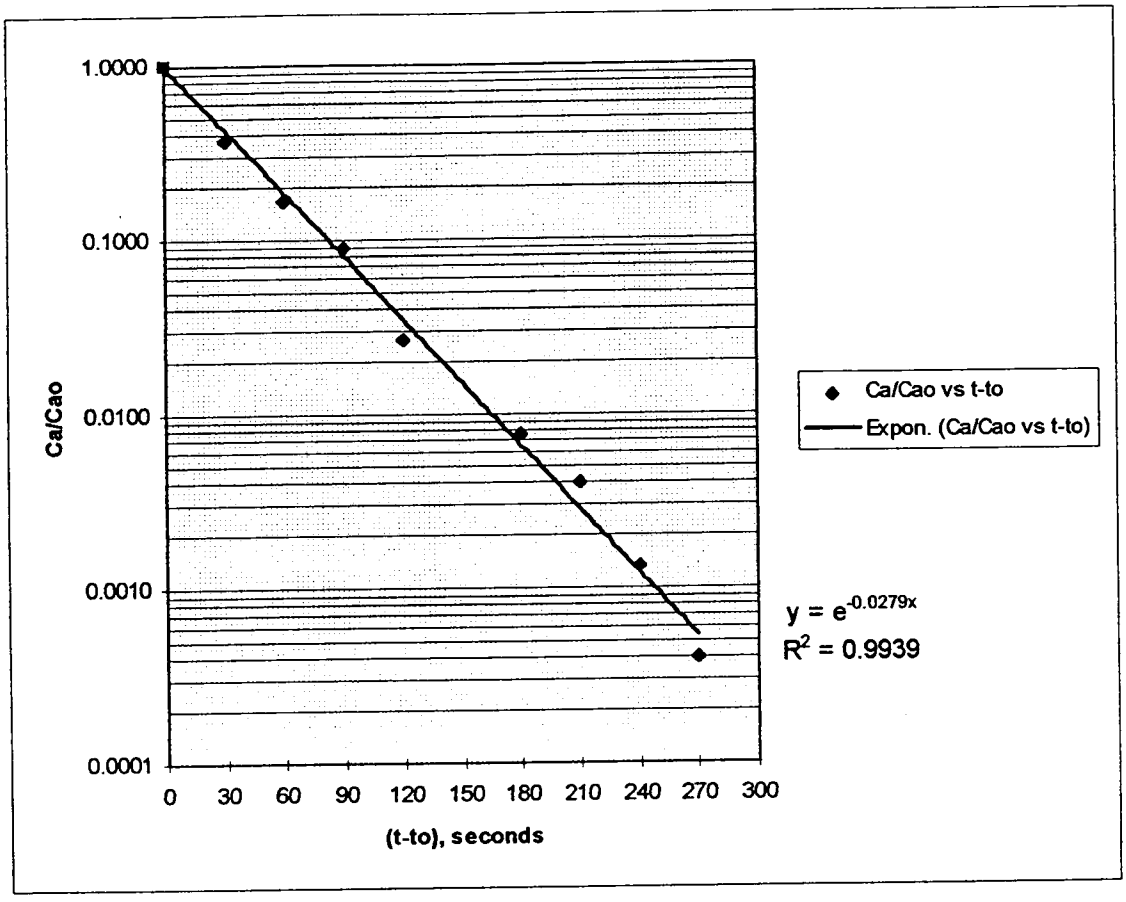

Figure A6.4: Experimental Run 1 where Volume Fraction, $\phi = V_d/V_T = 0.10$. Plot of $ln(C_a/C_{ao})$ versus $t\text{-}t_0$ where t_0=0seconds and $C_{ao}=C_a(t$=0seconds). This regression will be used to estimate C_{ao} and t_o at the point at which C_a/C_{ao}=1.

STEP 4:

Estimate C_{ao} and t_o at the point where C_a/C_{ao}=1. Given C_a/C_{ao} at t = 30sec From Table A6.3 and the slope from Plot in Figure A6.4, the Concentration and Time at the point of complete dispersion may be estimated.

Solve for t_o:

C_a/C_{ao}=exp[slope(t-t_o)]

ln C_a/C_{ao}= slope(t-t_o)

ln 0.28= -0.0279 (30-t_o)

t_o= **5.5 sec**

Solve for C_{ao}:

0.00021/C_{ao}=exp[-0.0279*(30-t_o)]

C_{ao}= **5.53E-04 g/ml**

STEP 5:

Calculate t-t_o and C_a/C_{ao} using estimated values for t_o and C_{a_o} as shown in Table A6.4.

Table A6.4: Recalculate t-t_o and C_a/C_{ao} using new values for t_o and C_{ao} with Data in Table A6.3

t-t_o	C_a/C_{ao}
0	1.0000
25	0.5045
55	0.2269
85	0.1227
115	0.0364
175	0.0103
205	0.0054
235	0.0018
265	0.0005
295	0.0001

A.6.3. Estimate C_{ao} and t_o at the point of Complete Dispersion: Experimental Run 2 where Volume Fraction, $\phi = V_d/V_T = 0.10$

STEP 1:

Record Sodium Sulfate Concentration as Measured Analytically in the Continuous Phase over time as shown in Table A6.5.

Table A6.5 Sodium Sulfate Concentration as Measured Experimentally in the Continuous Phase over time for Experimental Run 2 where Volume Fraction, $\phi = V_d/V_T = 0.10$.

Time		Sodium Sulfate Transferred		Dispersed Phase, gNa/ml		
seconds	ppmNa	From Disp.	To Cont.	C_a	$t-(t_o=0)$	C_a/C_{ao}
0	0.00	0.1500	0.0000	0.000750	0	1.0000
30	**57.38**	**0.0467**	**0.1033**	**0.000234**	**30**	**0.3114**
60	73.43	0.0178	0.1322	0.000089	60	0.1188
90	79.00	0.0078	0.1422	0.000039	90	0.0520
120	81.50	0.0033	0.1467	0.000017	120	0.0220
150	82.80	0.0010	0.1490	0.000005	150	0.0064
180	83.07	0.0005	0.1495	0.000002	180	0.0032
210	83.24	0.0002	0.1498	0.000001	210	0.0011
240	83.29	0.0001	0.1499	0.000000	240	0.0005
270	83.30	0.0001	0.1499	0.000000	270	0.0004
300	83.30	0.0001	0.1499	0.000000	300	0.0004

STEP 2:

Plot Ca versus time data from Table A6.5 followed by regression of the resulting curve as shown in Figure A6.5.

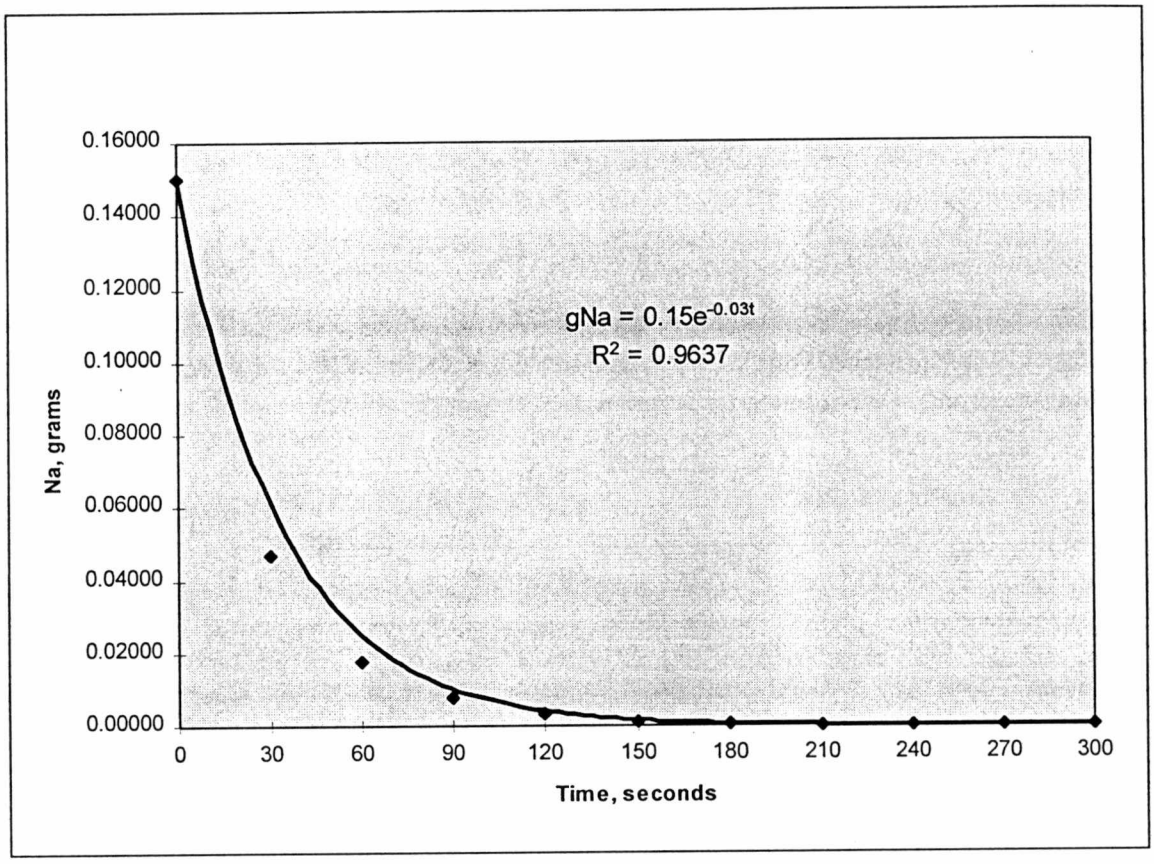

Figure A6.5: Mass Transfer Profile of Sodium Sulfate in the Dispersed Phase over time for Experimental Run 2 where Volume Fraction, $\phi = V_d/V_T = 0.10$.

STEP 3:

Plot $ln\ C_a/C_{ao}$ versus $t\text{-}t_0$ from Table A6.5, followed regression of the resulting curve as shown in Figure A6.6.

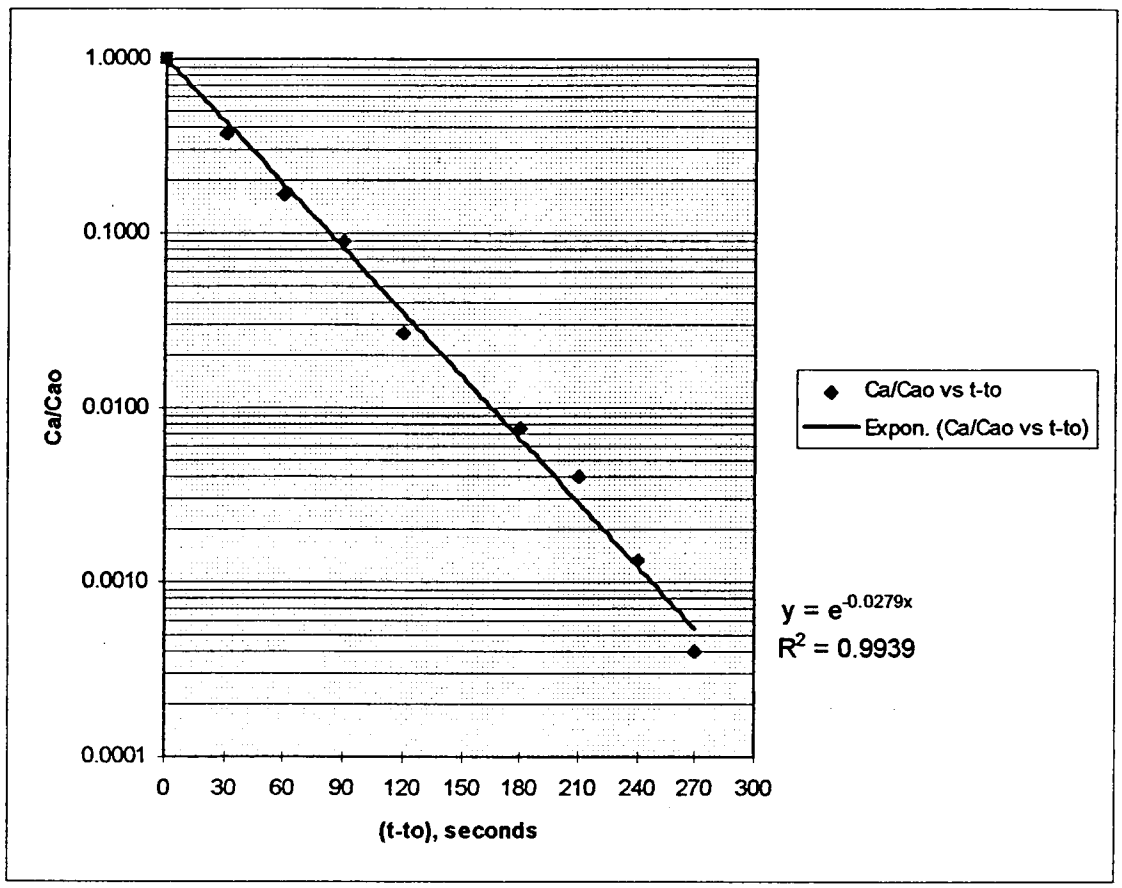

Figure A6.6: Experimental Run 2 where Volume Fraction, $\phi = V_d/V_T = 0.10$. Plot of $ln(C_a/C_{ao})$ versus $t\text{-}t_0$ where t_0=0seconds and $C_{ao}=C_a(t$=0seconds). This regression will be used to estimate C_{ao} and t_o at the point at which C_a/C_{ao}=1.

STEP 4:

Estimate C_{ao} and t_O at the point where C_a/C_{ao}=1. Given C_a/C_{ao} at t = 30sec From Table A6.5 and the slope from Plot in Figure A6.6, the Concentration and Time at the point of complete dispersion may be estimated.

Solve for t_o:

C_a/C_{ao}=exp[slope(t-t_O)]

ln C_a/C_{ao}= slope(t-t_O)

ln 0.311= -0.0322 (30-t_O)

t_o= 6.2 sec

Solve for C_{ao}:

0.000234/C_{ao}=exp[-0.0322*(30-t_O)]

C_{ao}= 5.02E-04 g/ml

STEP 5:

Calculate t-t_O and C_a/C_{ao} using estimated values for t_O and C_{a_o} as shown in Table A6.6.

Table A6.6: Recalculate t-t_O and C_a/C_{ao} using new values for t_O and C_{ao} with Data in Table A6.5.

t-t_O	C_a/C_{ao}
0	1.0000
24	0.4651
54	0.1774
84	0.0777
114	0.0329
144	0.0096
174	0.0047
204	0.0017
234	0.0008
264	0.0006

A.6.4. Estimate C_{ao} and t_o at the point of Complete Dispersion: Experimental Run 3 where Volume Fraction, $\phi = V_d/V_T = 0.05$

STEP 1:

Record Sodium Sulfate Concentration as Measured Analytically in the Continuous Phase over time as shown in Table A6.7.

Table A6.7 Sodium Sulfate Concentration as Measured Experimentally in the Continuous Phase over time for Experimental Run 3 where Volume Fraction, $\phi = V_d/V_T = 0.05$.

Time		Sodium Sulfate Transferred		Dispersed Phase, gNa/ml		
seconds	ppmNa	From Disp.	To Cont.	C_a	t-(t_o=0)	C_a/C_{ao}
0	0.00	0.0750	0.00000	0.00075	0	1.0000
30	**26.13**	**0.0254**	**0.04965**	**0.00025**	**30**	**0.3380**
60	34.68	0.0091	0.06589	0.00009	60	0.1214
90	37.24	0.0042	0.07076	0.00004	90	0.0566
120	38.95	0.0010	0.07401	0.00001	120	0.0133
150	39.25	0.0004	0.07458	0.00000	150	0.0057
180	39.35	0.0002	0.07477	0.00000	180	0.0031
210	39.44	0.0001	0.07494	0.00000	210	0.0008
240	39.46	0.0000	0.07497	0.00000	240	0.0004
270	39.46	0.0000	0.07498	0.00000	270	0.0003
300	39.47	0.0000	0.07498	0.00000	300	0.0003

STEP 2:

Plot Ca versus time data from Table A6.7 followed by regression of the resulting curve as shown in Figure A6.7.

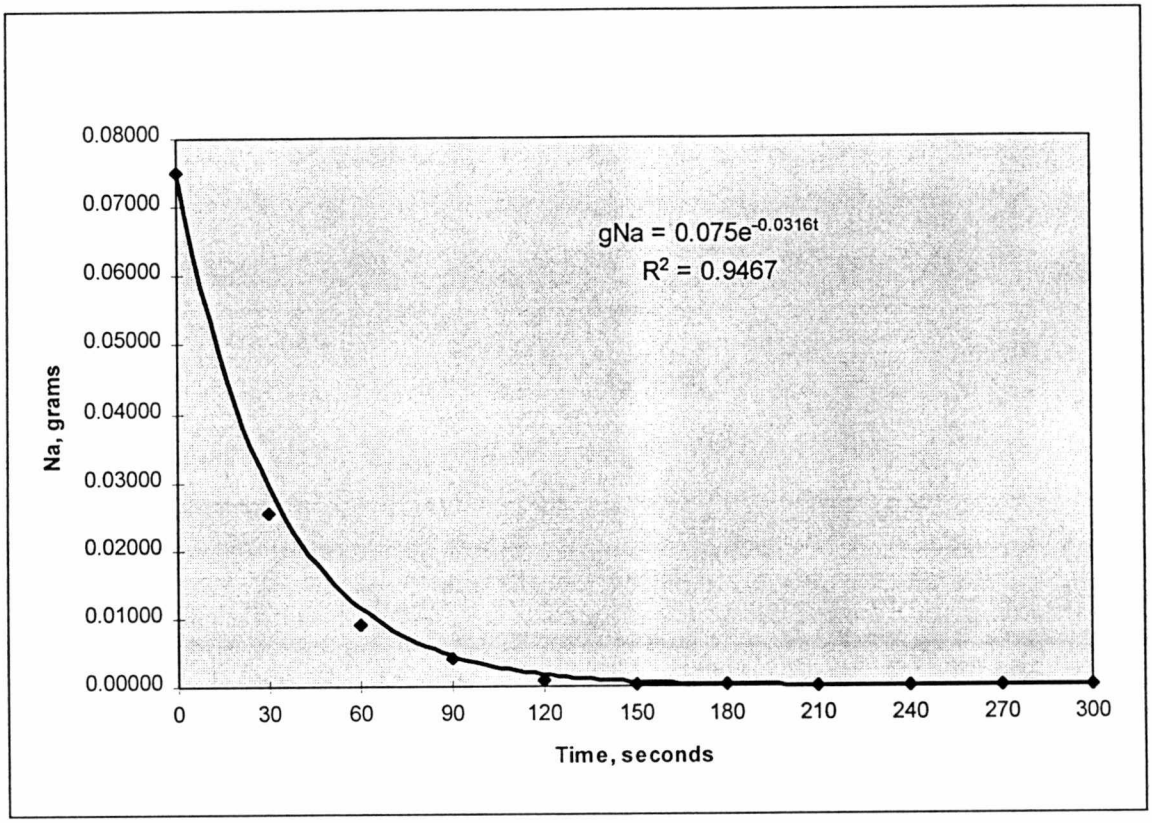

Figure A6.7: Mass Transfer Profile of Sodium Sulfate in the Dispersed Phase over time for Experimental Run 3 where Volume Fraction, $\phi = V_d/V_T = 0.05$.

STEP 3:

Plot $ln\ C_a/C_{ao}$ versus $t\text{-}t_0$ from Table A6.7, followed regression of resulting curve as shown in Figure A6.8.

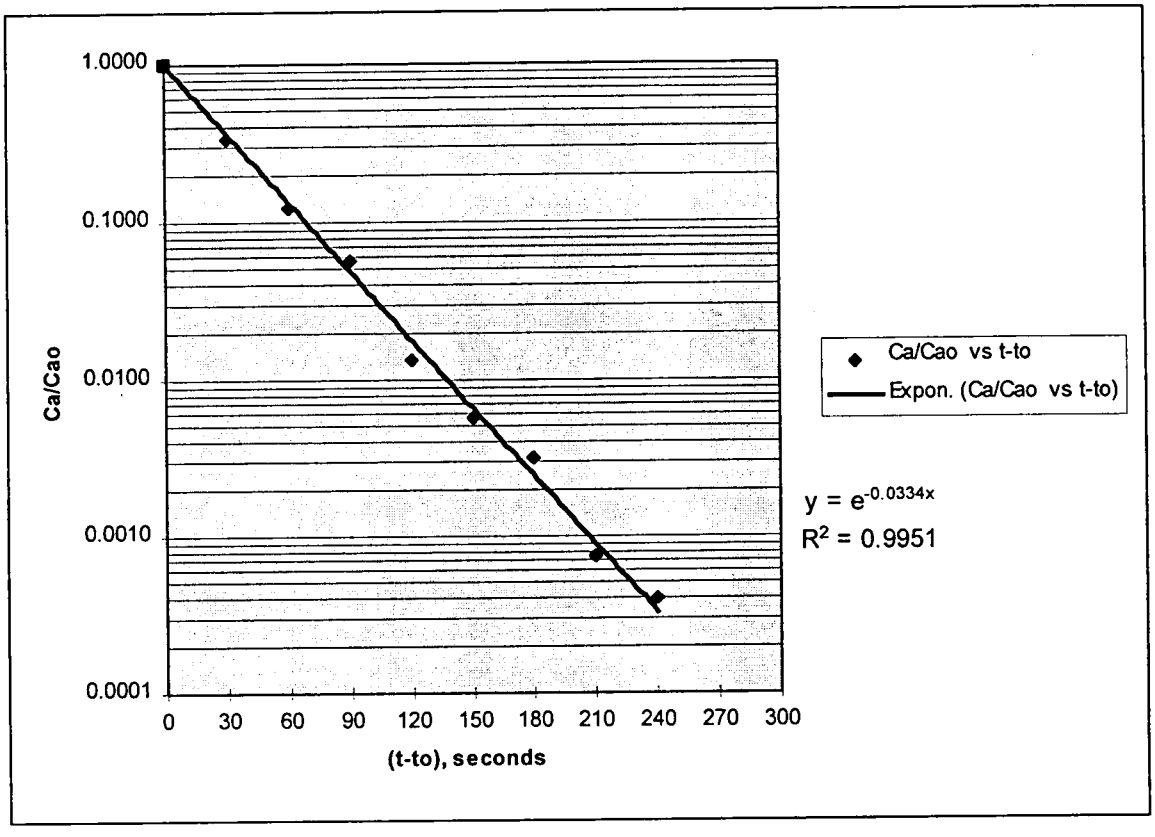

Figure A6.8: Experimental Run 3 where Volume Fraction, $\phi = V_d/V_T = 0.05$. Plot of $ln(C_a/C_{ao})$ versus $t\text{-}t_0$ where t_0=0seconds and $C_{ao}=C_a(t$=0seconds). This regression will be used to estimate C_{ao} and t_o at the point at which C_a/C_{ao}=1.

STEP 4:

Estimate C_{ao} and t_O at the point where C_a/C_{ao}=1. Given C_a/C_{ao} at t = 30sec From Table A6.7 and the slope from Plot in Figure A6.8, the Concentration and Time at the point of complete dispersion may be estimated.

Solve for t_o:

C_a/C_{ao}=exp[slope(t-t_O)]

ln C_a/C_{ao}= slope(t-t_O)

ln 0.338= -0.0334 (30-t_O)

t_o= 2.5 sec

Solve for C_{ao}:

0.00025/C_{ao}=exp[-0.0334*(30-t_O)]

C_{ao}= 4.49E-04 g/ml

STEP 5:

Calculate t-t_O and C_a/C_{ao} using estimated values for t_O and C_{a_o} as shown in Table A6.8.

Table A6.8: Recalculate t-t_o and C_a/C_{ao} using new values for t_o and C_{ao} with Data in Table A6.7

t-t_O	C_a/C_{ao}
0	1.0000
28	0.1433
58	0.0668
88	0.0156
118	0.0067
148	0.0037
178	0.0009
208	0.0005
238	0.0003
268	0.0003

A.6.5. Estimate C_{ao} and t_o at the point of Complete Dispersion: Experimental Run 4 where Volume Fraction, $\phi = V_d/V_T = 0.20$

STEP 1:

Record Sodium Sulfate Concentration as Measured Analytically in the Continuous Phase over time as shown in Table A6.9.

Table A6.9 Sodium Sulfate Concentration as Measured Experimentally in the Continuous Phase over time for Experimental Run 4 where Volume Fraction, $\phi = V_d/V_T = 0.20$.

Time		Sodium Sulfate Transferred		Dispersed Phase, gNa/ml		
seconds	ppmNa	From Disp.	To Cont.	C_a	$t-(t_o=0)$	C_a/C_{ao}
0	0.00	0.3000	0.0000	0.00075	0	1.0000
30	**60.75**	**0.2028**	**0.0972**	**0.00051**	**30**	**0.6760**
60	95.26	0.1476	0.1524	0.00037	60	0.4919
90	112.54	0.1199	0.1801	0.00030	90	0.3998
120	125.76	0.0988	0.2012	0.00025	120	0.3293
150	135.42	0.0833	0.2167	0.00021	150	0.2778
180	146.50	0.0656	0.2344	0.00016	180	0.2187
210	151.92	0.0569	0.2431	0.00014	210	0.1898
240	159.37	0.0450	0.2550	0.00011	240	0.1500
270	167.89	0.0314	0.2686	0.00008	270	0.1046
300	175.75	0.0188	0.2812	0.00005	300	0.0627

STEP 2:

Plot Ca versus time data from Table A6.9 followed by regression of the resulting curve as shown in Figure A6.9.

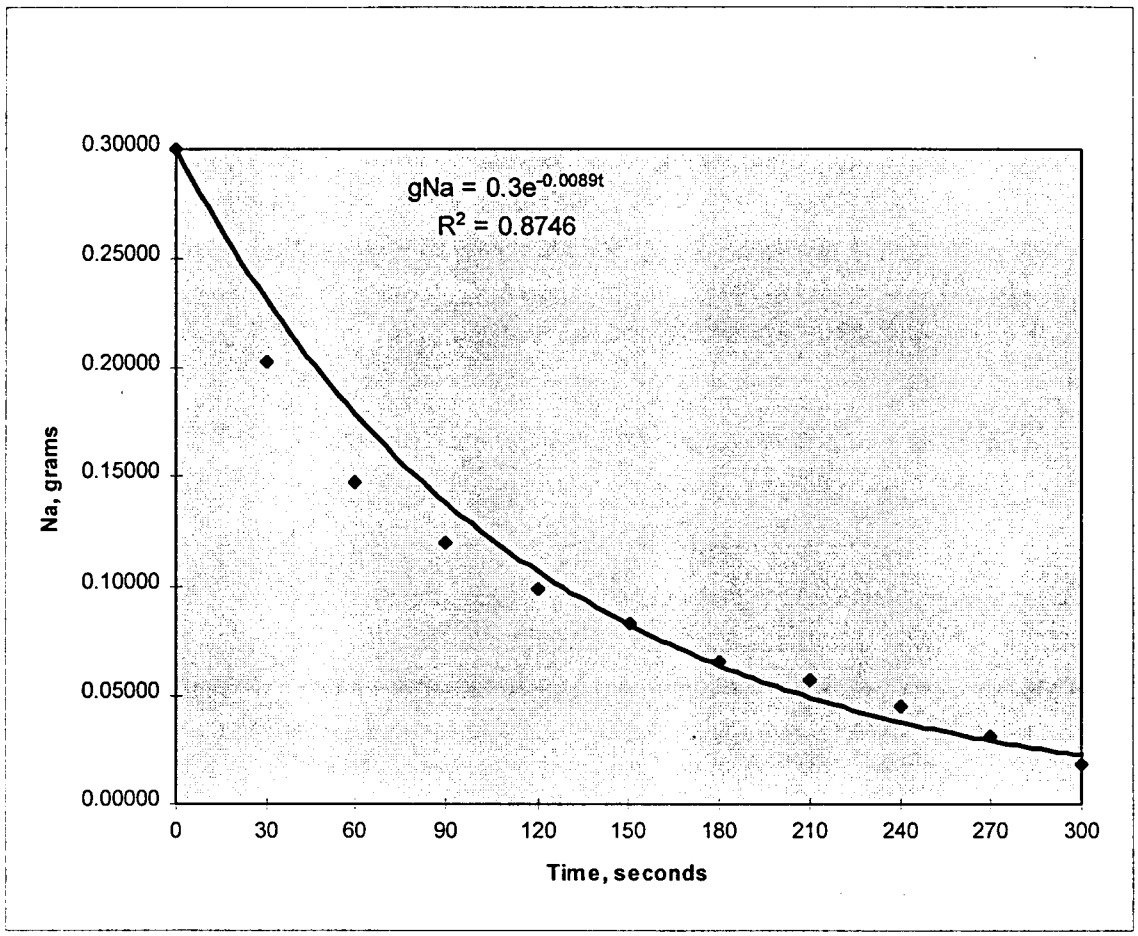

Figure A6.9: Mass Transfer Profile of Sodium Sulfate in the Dispersed Phase over time for Experimental Run 4 where Volume Fraction, $\phi = V_d/V_T = 0.20$.

STEP 3:

Plot $ln\ C_a/C_{ao}$ versus $t\text{-}t_0$ from Table A6.9, followed regression of the resulting curve as shown in Figure A6.10.

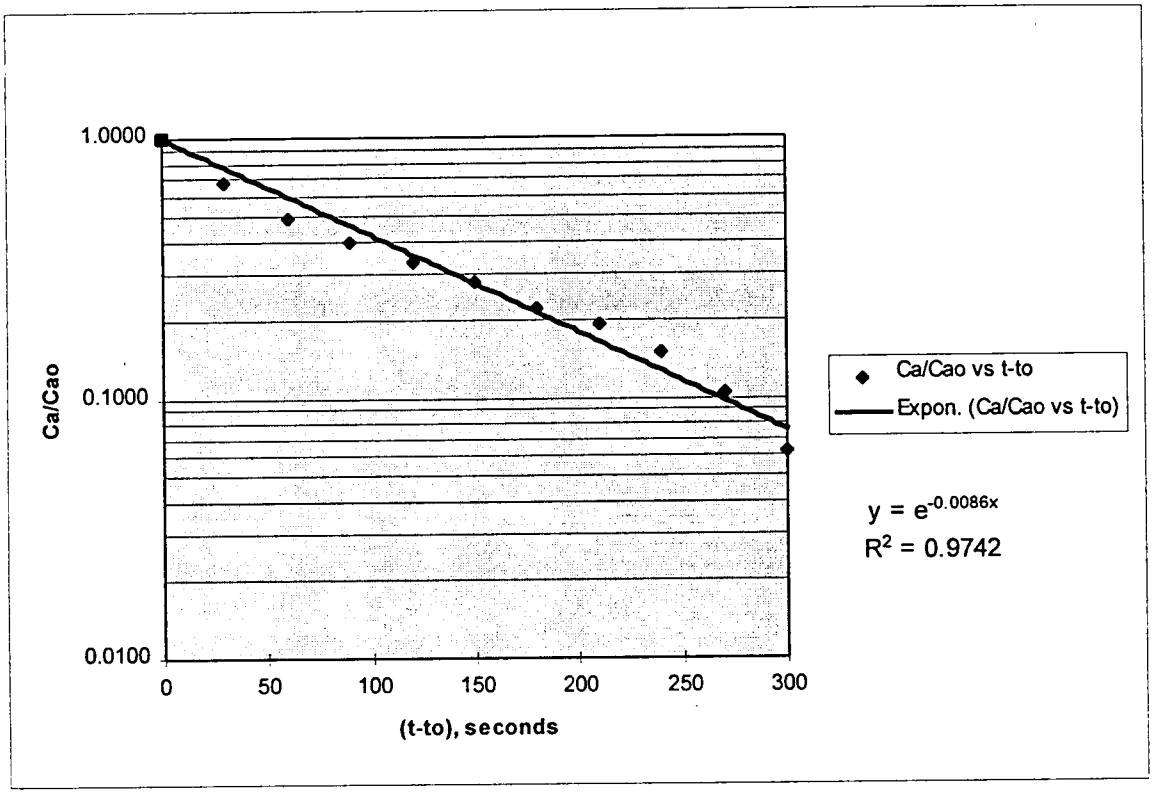

Figure A6.10: Experimental Run 4 where Volume Fraction, $\phi = V_d/V_T = 0.20$. Plot of $ln(C_a/C_{ao})$ versus $t\text{-}t_0$ where t_0=0seconds and $C_{ao}=C_a(t$=0seconds). This regression will be used to estimate C_{ao} and t_o at the point at which C_a/C_{ao}=1.

STEP 4:

Estimate C_{ao} and t_o at the point where C_a/C_{ao}=1. Given C_a/C_{ao} at t = 30sec From Table A6.9 and the slope from Plot in Figure A6.10, the Concentration and Time at the point of complete dispersion may be estimated.

Solve for to:

C_a/C_{ao}=exp[slope(t-t_o)]

ln Ca/C_{ao}= slope(t-t_o)

ln 0.6760 = -0.0086 (30-to)

t_o= 15.5 sec

Solve for C_{ao}:

0.00051 /Cao=exp[-0.0086*(30-t_o)]

Cao= 4.48E-04 g/ml

STEP 5:

Calculate t-t_O and C_a/C_{ao} using estimated values for t_O and C_{a_o} as shown in Table A6.10.

Table A6.10 Recalculate t-t_o and C_a/C_{ao} using new values for t_o and C_{ao} with data in Table A6.9.

t-t_o	C_a/C_{ao}
0	1.0000
14	0.8242
44	0.6698
74	0.5516
104	0.4653
134	0.3663
164	0.3179
194	0.2513
224	0.1752
254	0.1050

A.6.6. Estimate C_{ao} and t_o at the point of Complete Dispersion: Experimental Run 5 where Volume Fraction, $\phi = V_d/V_T = 0.15$

STEP 1:

Record Sodium Sulfate Concentration as Measured Analytically in the Continuous Phase over time as shown in Table A6.11.

Table A6.11 Sodium Sulfate Concentration as Measured Experimentally in the Continuous Phase over time for Experimental Run 5 where Volume Fraction, $\phi = V_d/V_T = 0.15$.

Time		Sodium Sulfate Transferred		Dispersed Phase, gNa/ml		
seconds	ppmNa	From Disp.	To Cont.	C_a	$t-(t_o=0)$	C_a/C_{ao}
0	0.00	0.2250	0.0000	0.00075	0	1.0000
30	**52.00**	**0.1366**	**0.0884**	**0.00046**	**30**	**0.6071**
60	78.07	0.0923	0.1327	0.00031	60	0.4101
90	92.36	0.0680	0.1570	0.00023	90	0.3022
120	105.58	0.0455	0.1795	0.00015	120	0.2023
150	112.65	0.0335	0.1915	0.00011	150	0.1489
180	117.85	0.0247	0.2003	0.00008	180	0.1096
210	123.46	0.0151	0.2099	0.00005	210	0.0672
240	126.94	0.0092	0.2158	0.00003	240	0.0409
270	129.76	0.0044	0.2206	0.00001	270	0.0196
300	131.98	0.0006	0.2244	0.00000	300	0.0028

STEP 2:

Plot Ca versus time data from Table A6.11 followed by regression of the resulting curve as shown in Figure A6.11.

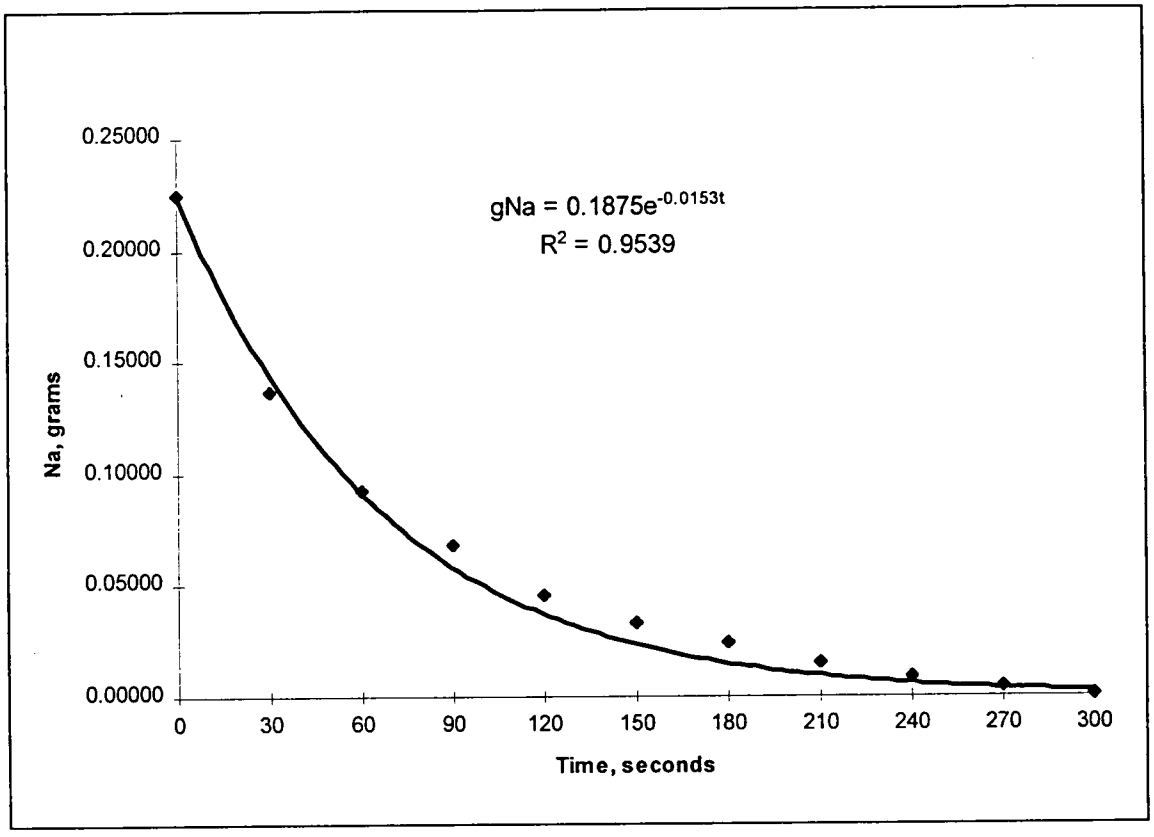

Figure A6.11: Mass Transfer Profile of Sodium Sulfate in the Dispersed Phase over time for Experimental Run 5 where Volume Fraction, $\phi = V_d/V_T = 0.15$.

STEP 3:

Plot $ln\ C_a/C_{ao}$ versus $t\text{-}t_0$ from Table A6.11, followed regression of the resulting curve as shown in Figure A6.12.

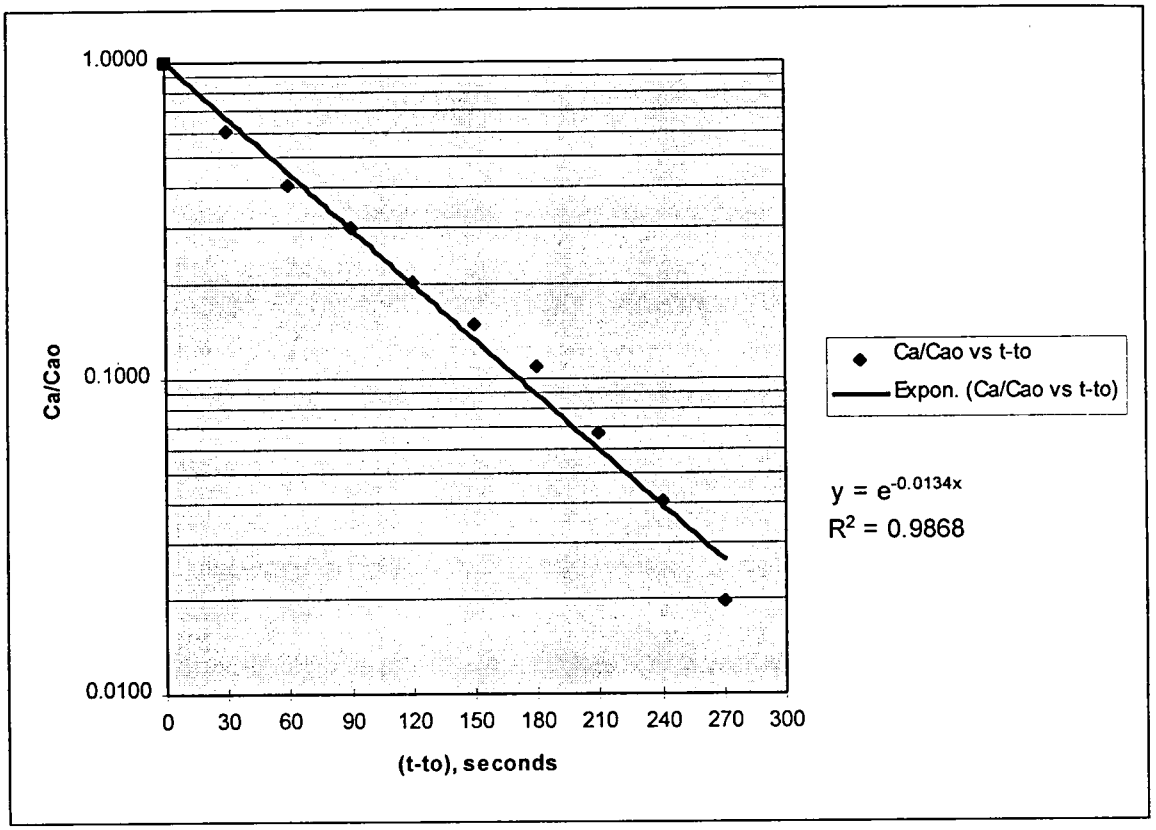

Figure A6.12: Experimental Run 5 where Volume Fraction, $\phi = V_d/V_T = 0.15$. Plot of $ln(C_a/C_{ao})$ versus $t\text{-}t_0$ where t_0=0seconds and $C_{ao}=C_a(t$=0seconds). This regression will be used to estimate C_{ao} and t_o at the point at which C_a/C_{ao}=1.

STEP 4:

Estimate C_{ao} and t_o at the point where C_a/C_{ao}=1. Given C_a/C_{ao} at t = 30sec From Table A6.11 and the slope from Plot in Figure A6.12, the Concentration and Time at the point of complete dispersion may be estimated.

Solve for to:

Ca/Cao=exp[slope(t-to)]

ln Ca/Cao= slope(t-to)

ln 0.6071 = -0.0134 (30-to)

to= 7.2 sec

Solve for Cao:

0.00046 /Cao=exp[-0.0134*(30-to)]

Cao= 6.18E-04 g/ml

STEP 5:

Calculate t-t_o and C_a/C_{ao} using estimated values for t_o and C_{a_o} as shown in Table A6.12.

Table A6.12 Recalculate t-t_o and C_a/C_{ao} using new values for t_o and C_{ao} with data in Table A6.11.

t-to	Ca/Cao
0	1.0000
23	0.7372
53	0.3669
83	0.2456
113	0.1808
143	0.1330
173	0.0816
203	0.0497
233	0.0238
263	0.0034

A.6.7. Estimate C_{ao} and t_o at the point of Complete Dispersion: Experimental Run 6 where Volume Fraction, $\phi = V_d/V_T = 0.05$

STEP 1:

Record Sodium Sulfate Concentration as Measured Analytically in the Continuous Phase over time as shown in Table A6.13.

Table A6.13 Sodium Sulfate Concentration as Measured Experimentally in the Continuous Phase over time for Experimental Run 6 where Volume Fraction, $\phi = V_d/V_T = 0.05$.

Time		Sodium Sulfate Transferred		Dispersed Phase, gNa/ml		
seconds	ppmNa	From Disp.	To Cont.	C_a	$t-(t_o=0)$	C_a/C_{ao}
0	0.00	0.0750	0.0000	0.00075	0	1.0000
30	**27.43**	**0.0229**	**0.0521**	**0.00023**	**30**	**0.3051**
60	35.64	0.0073	0.0677	0.00007	60	0.0971
90	38.51	0.0018	0.0732	0.00002	90	0.0244
120	39.26	0.0004	0.0746	0.00000	120	0.0054
150	39.42	0.0001	0.0749	0.00000	150	0.0013
180	39.45	0.0000	0.0750	0.00000	180	0.0005
210	39.46	0.0000	0.0750	0.00000	210	0.0004
240	39.47	0.0000	0.0750	0.00000	240	0.0001
270	39.47	0.0000	0.0750	0.00000	270	0.0001
300	39.47	0.0000	0.0750	0.00000	300	0.0000

STEP 2:

Plot *Ca* versus time data from Table A6.13 followed by regression of the resulting curve as shown in Figure A6.13.

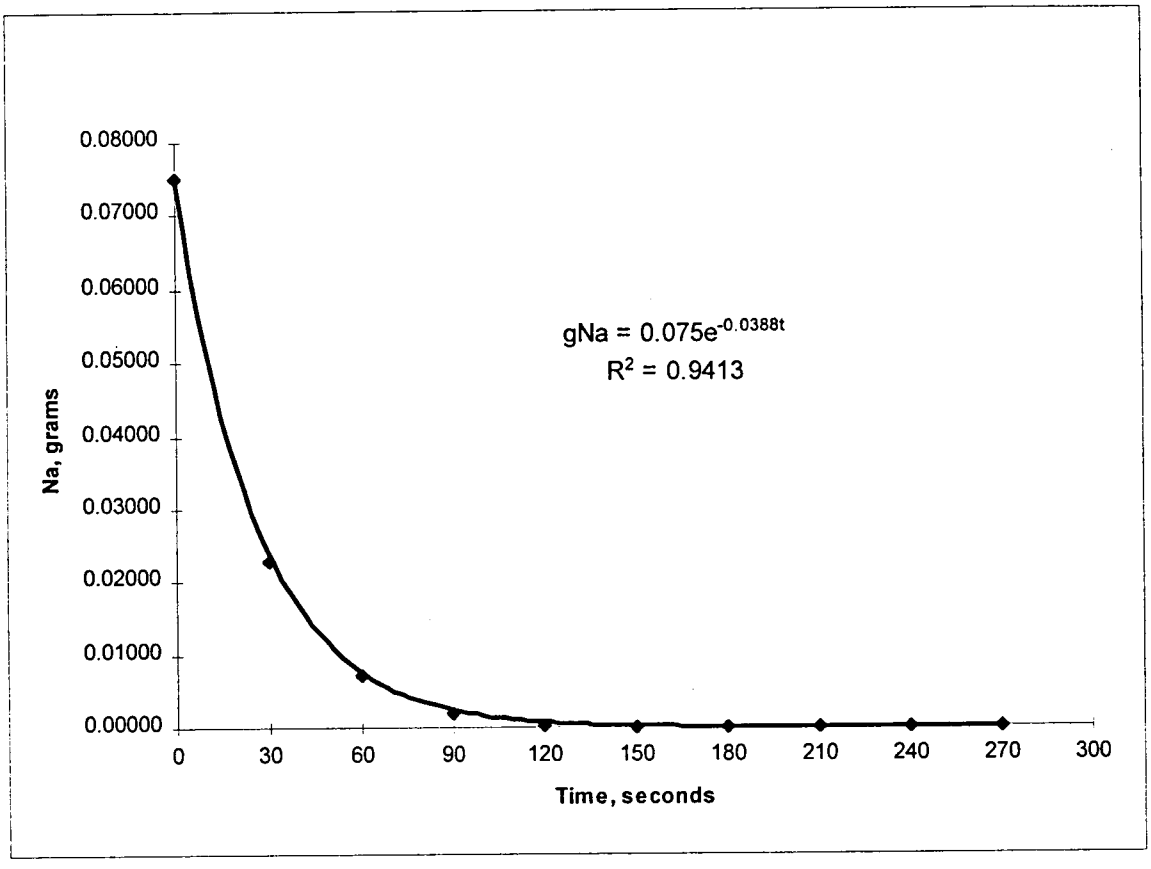

Figure A6.13: Mass Transfer Profile of Sodium Sulfate in the Dispersed Phase over time for Experimental Run 6 where Volume Fraction, $\phi = V_d/V_T = 0.05$.

STEP 3:

Plot $ln\ C_a/C_{ao}$ versus $t\text{-}t_0$ from Table A6.13, followed regression of the resulting curve as shown in Figure A6.14.

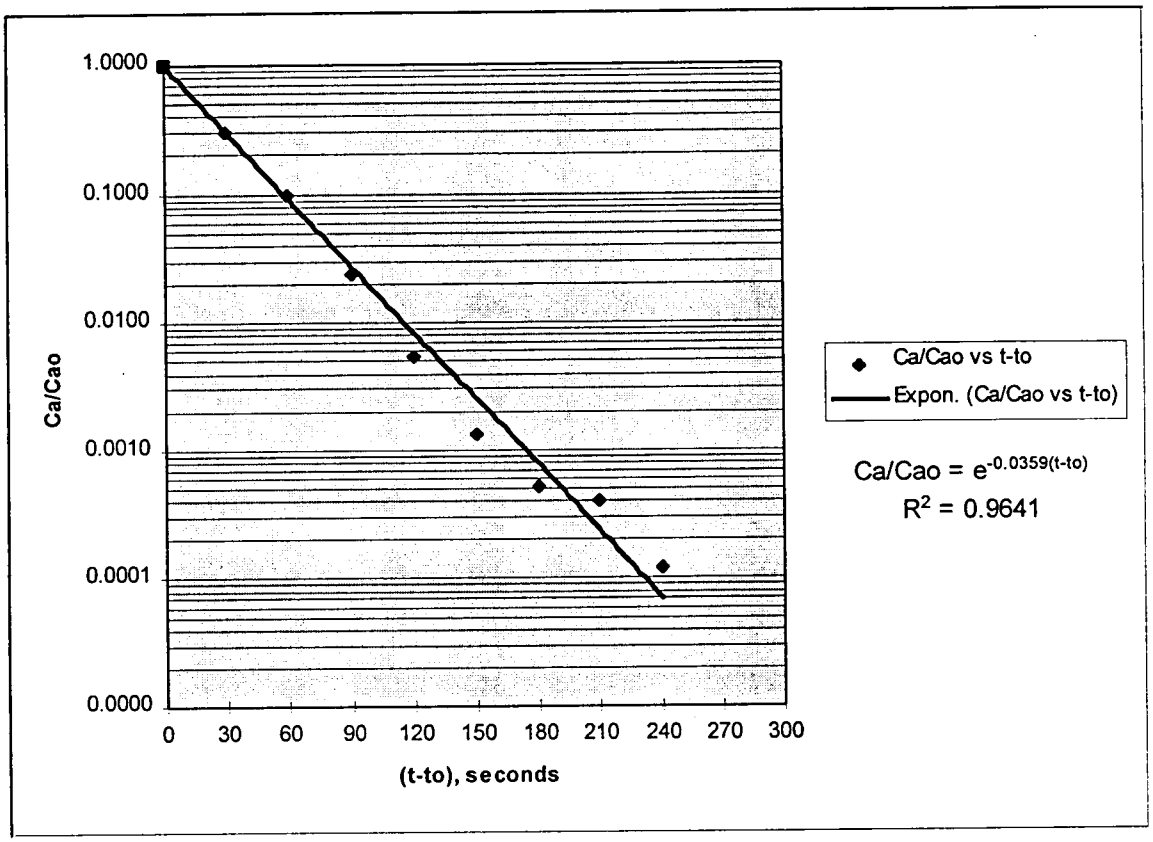

Figure A6.14: Experimental Run 6 where Volume Fraction, $\phi = V_d/V_T = 0.05$. Plot of $ln(C_a/C_{ao})$ versus $t\text{-}t_0$ where t_0=0seconds and $C_{ao}=C_a(t$=0seconds). This regression will be used to estimate C_{ao} and t_o at the point at which C_a/C_{ao}=1.

STEP 4:

Estimate C_{ao} and t_o at the point where C_a/C_{ao}=1. Given C_a/C_{ao} at t = 30sec From Table A6.13 and the slope from Plot in Figure A6.14, the Concentration and Time at the point of complete dispersion may be estimated.

Solve for to:

Ca/Cao=exp[slope(t-to)]

ln Ca/Cao= slope(t-to)

ln 0.3051 = -0.0359 (30-to)

to= 3.1 sec

Solve for *Cao*:

0.00023 /C_{ao}=exp[-0.0359*(30-t_o)]

***Cao*= 6.02E-04 g/ml**

STEP 5:

Calculate t-t_o and C_a/C_{ao} using estimated values for t_o and C_{a_o} as shown in Table A6.14.

Table A6.14 Calculate t-t_o and C_a/C_{ao} using estimated values for t_o and C_{ao} with data in Table A6.13.

t-to	Ca/Cao
0	1.0000
27	0.3803
57	0.1210
87	0.0304
117	0.0067
147	0.0016
177	0.0006
207	0.0005
237	0.0002
267	0.0001

Table A6.15: Non-linear Regression of raw data to estimate the instantaneous concentration at the point of dispersion.

RUN	Dispersion V_d, ml	$\phi = \frac{V_d}{V_T}$	$slope = \frac{\ln(\frac{C_a}{C_{ao}})}{t - t_o}$	Addition Period t_o, sec	Initial Droplet Concentration C_{ao}, g/ml
1	200	0.100	-0.0279	5.5	5.53E-04
2	200	0.100	-0.0322	6.2	5.02E-04
3	100	0.050	-0.0334	2.5	4.49E-04
4	400	0.200	-0.0086	15.5	4.48E-04
5	300	0.150	-0.0134	7.2	6.18E-04
6	100	0.050	-0.0359	3.1	6.02E-04

Note: The subscript "o" implies initial conditions; rather, the point at which all dispersed-phase has entered the vessel. This method neglects the time needed to completely disperse the discontinuous phase.

A.6.8. Calculation of Experimental k_d

Table A6.16: Approximating the Impeller Reynolds, Weber and Froude Numbers for use in the Sauter-mean Diameter Expression, Table A6.17.

Dispersed	Continuous Phase		Impeller		
Density g/cc	Viscosity g/cm-sec	Density g/cc	Weber Number.	Reynolds Number	Froude Number
0.9480	0.01654	1.036	1178.50	6.73E+03	0.29426

Note:
(1) Input Date Source: Physical Properties Table 3.3, Apparatus Table 5.5
(2) Impeller Speed 4.167 rps (250rpm)

A.6.9. Calculation of Sauter-mean Diameter

$$\alpha = 29.7 d_{32}^{*} \left(\frac{d_1}{d_v}\right)^{-2.015} \left(\frac{N_{Wec}}{N_{Rec}}\right)^{0.5508} N^{-0.7}$$

phi=0.05	phi=0.10	phi=0.15	phi=0.20
0.269373	0.297329	0.325285	0.353241

$$d_{32}^{*} = d_1 \, 0.05(1+2.316\phi)\left(\frac{d_1}{d_v}\right)^{-0.75} N_{Frc}^{\ -0.13} N_{Wec}^{\ -0.6}$$

phi=0.05	phi=0.10	phi=0.15	phi=0.20
0.009509	0.019018	0.028527	0.038036

Where units are α=cm·s$^{0.7}$ and $\mathbf{d_{32}^{*}}$**=cm.**

Table A6.17: Prediction of the Sauter-mean diameter using Hong and Lee (1985) Model*

	Sauter Mean Diameter (d_{32}), cm			
TIME, sec	phi=0.05	phi=0.10	phi=0.15	phi=0.20
1	0.3073	0.3083	0.3094	0.3104
5	0.1062	0.1072	0.1082	0.1092
15	0.0544	0.0554	0.0564	0.0574
30	**0.0372**	**0.0382**	**0.0392**	**0.0402**
60	**0.0266**	**0.0276**	**0.0286**	**0.0296**
90	**0.0224**	**0.0234**	**0.0244**	**0.0254**
120	0.0201	**0.0211**	**0.0221**	**0.0231**
150	0.0186	**0.0196**	**0.0206**	**0.0216**
180	0.0175	0.0185	**0.0195**	**0.0205**
210	0.0167	0.0177	**0.0187**	**0.0197**
240	0.0161	0.0171	**0.0181**	**0.0191**
270	0.0156	0.0166	**0.0176**	**0.0186**
300	0.0152	0.0162	**0.0172**	**0.0182**
	Average d_{32}(30s to 90s)	Average d_{32}(30s to 150s)	Average d_{32}(30s to300s)	Average d_{32}(30s to 320s)
	0.0287	0.0260	0.0226	0.0236

*Note:

$d_{32} = \alpha \cdot t^{-0.7} + d_{32}^{*}$ Hong and Lee (1985)

Table A6.18: Approximation of k_d as a Function of Droplet Diameter
(Visually Measured d_p=0.3mm ± 0.1mm)

Expt. Run	$\phi = \frac{V_d}{V_T}$	Average d32(tf-to) mm	$\frac{K_d A}{V} = -\left(\frac{\ln \frac{C_o}{C_{o1}}}{(t-t_1)}\right)$	$k_{d\,expt.} = f(d_p)$ dp: 0.20mm	0.3mm	0.40mm
1	0.10	0.260	0.0279	9.30E-05	1.40E-04	1.86E-04
2	0.10	0.260	0.0322	1.07E-04	1.61E-04	2.15E-04
3	0.05	0.287	0.0334	1.11E-04	1.67E-04	2.23E-04
4	0.20	0.236	0.0086	2.87E-05	4.30E-05	5.73E-05
5	0.15	0.226	0.0134	4.47E-05	6.70E-05	8.93E-05
6	0.05	0.287	0.0359	1.20E-04	1.80E-04	2.39E-04

Note:

As shown in Table A6.17, $d3_2$ is the average of d_{32}=$f(t)$ between time period t_f-t_O shown in Table A6.17.

A.6.10. Calculation of k_d using the Penetration Theory

Table A6.19: Estimation of the Dispersed-phase Mass transfer coefficient using the Penetration Theory

Expt. Run	Volume Fraction ϕ	tf sec	t0 sec	$D_d = \frac{cm^2}{sec}$ Table5.4	$k_d = 2\left(\frac{D_d}{\pi(t_f - t_0)}\right)^{0.5}$ cm/sec
1	0.10	150	5.5	1.94E-07	4.1E-05
2	0.10	150	6.2	1.94E-07	4.1E-05
3	0.05	90	2.5	1.94E-07	5.3E-05
4	0.20	320	15.5	1.94E-07	2.8E-05
5	0.15	300	7.2	1.94E-07	2.9E-05
6	0.05	90	3.1	1.94E-07	5.3E-05

A.6.10. Calculation of k_d using Equation 1.11 (Based on d_{32}) where ϕ=0.05 and d=d_{32}

$\alpha = 0.2694$

$d = 0.0095$

$$f(t) = \frac{1}{\alpha \cdot t^{-0.7} + d}$$

$$\int_{20}^{90} f(t)\,dt = 2.642 \cdot 10^{3}$$

$$\int_{20}^{60} f(t)\,dt = 1.318 \cdot 10^{3}$$

$$\int_{20}^{30} f(t)\,dt = 263.92$$

slope=-0.0011 (from Figure 6.8)

Therefore from equation 6.4

$$k_d = -\frac{(slope)}{6}$$

$$\boxed{k_d = -\frac{(-0.0011)}{6} = 1.833E-04\,\frac{cm}{s}}$$

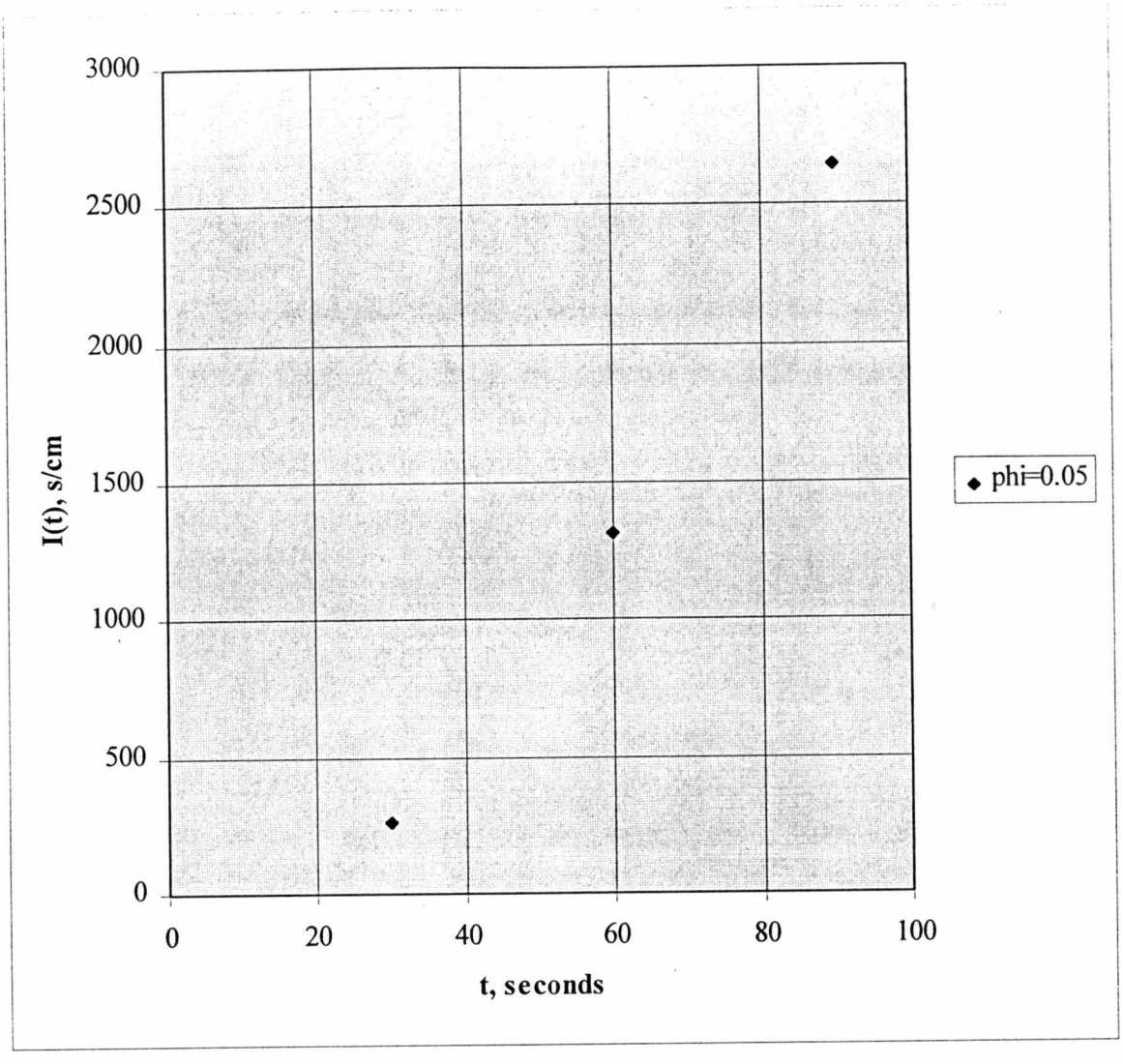

Figure A6.15: Plot of time t versus I(t) where $I(t) = \int_{20} \frac{1}{\alpha \cdot t^{-0.7} + d_{32}^{*}} dt$ for ϕ=0.05.

A.6.11. Calculation of k_d using Equation 1.11 (Based on d_{32}) where ϕ=0.10 and d=d_{32}

$\alpha := 0.2973$

$d := 0.0190$

$$f(t) := \frac{1}{\alpha \cdot t^{-0.7} + d}$$

$$\int_{20}^{150} f(t)\,dt = 3.876 \cdot 10^{3}$$

$$\int_{20}^{120} f(t)\,dt = 2.828 \cdot 10^{3}$$

$$\int_{20}^{90} f(t)\,dt = 1.843 \cdot 10^{3}$$

$$\int_{20}^{60} f(t)\,dt = 949.193$$

$$\int_{20}^{30} f(t)\,dt = 198.583$$

slope=-0.0010 (from Figure 6.9)

Therefore from equation 6.4

$$k_d = -\frac{(slope)}{6}$$

$$\boxed{k_d = -\frac{(-0.0010)}{6} = 1.6670E-04\,\frac{cm}{s}}$$

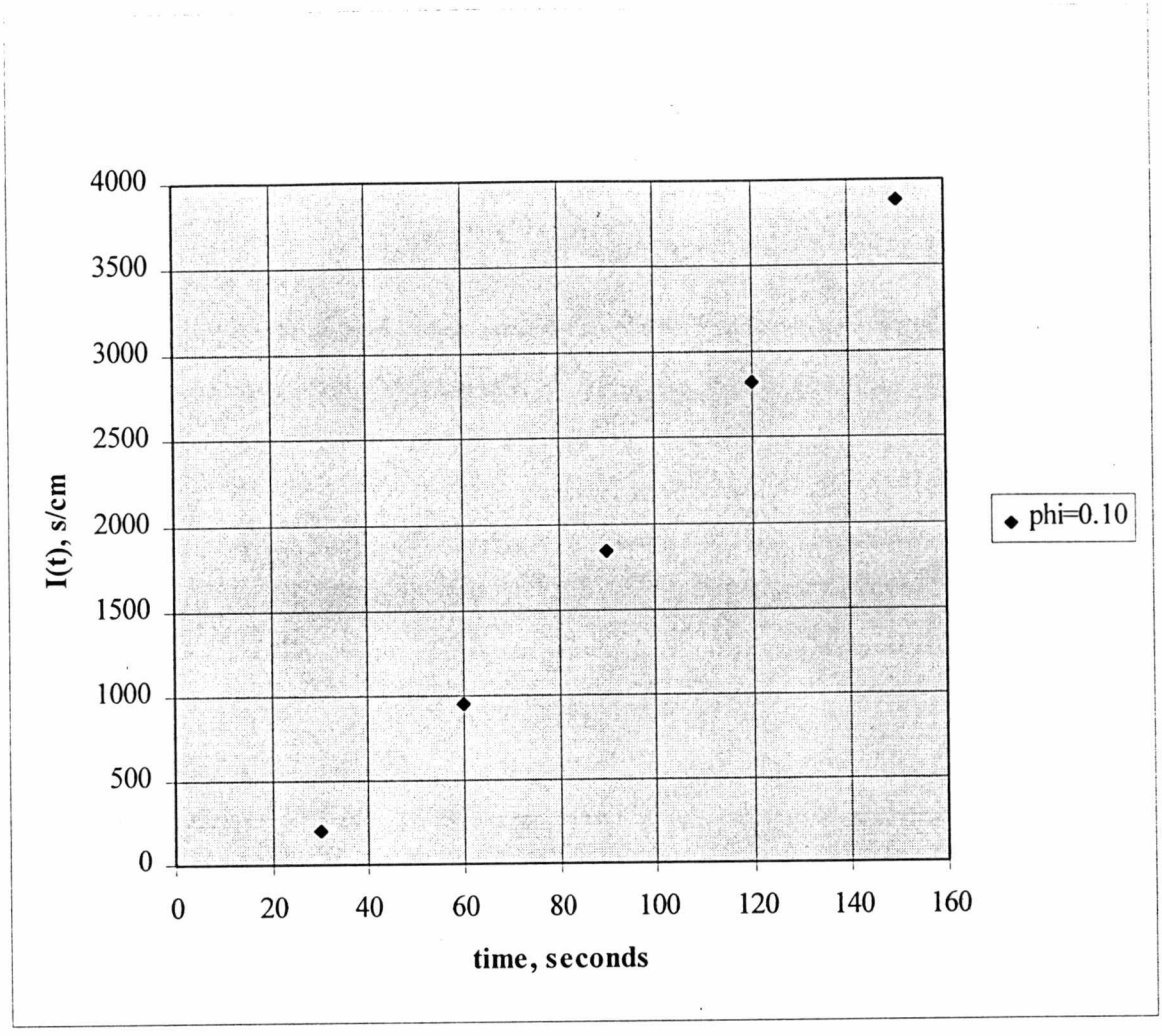

Figure A6.16: Plot of time t versus I(t) where $I(t) = \int_{20} \frac{1}{\alpha \cdot t^{-0.7} + d_{32}^{*}} dt$ for ϕ=0.10.

A.6.12. Calculation of k_d using Equation 1.11 where ϕ=0.15 and d=d_{32}

$\alpha := 0.3253$ $d := 0.0285$

$$f(t) := \frac{1}{\alpha \cdot t^{-0.7} + d}$$

$$\int_{20}^{300} f(t)\,dt = 7.086 \cdot 10^3 \qquad \int_{20}^{270} f(t)\,dt = 6.222 \cdot 10^3$$

$$\int_{20}^{240} f(t)\,dt = 5.37 \cdot 10^3 \qquad \int_{20}^{210} f(t)\,dt = 4.533 \cdot 10^3$$

$$\int_{20}^{180} f(t)\,dt = 3.714 \cdot 10^3 \qquad \int_{20}^{150} f(t)\,dt = 2.917 \cdot 10^3$$

$$\int_{20}^{120} f(t)\,dt = 2.148 \cdot 10^3 \qquad \int_{20}^{90} f(t)\,dt = 1.417 \cdot 10^3$$

$$\int_{20}^{60} f(t)\,dt = 741.955 \qquad \int_{20}^{30} f(t)\,dt = 159.166$$

slope=-0.0007 (from Figure 6.10)

Therefore from equation 6.4

$$k_d = -\frac{(slope)}{6}$$

$$\boxed{k_d = -\frac{(-0.0007)}{6} = 1.167E-04\,\frac{cm}{s}}$$

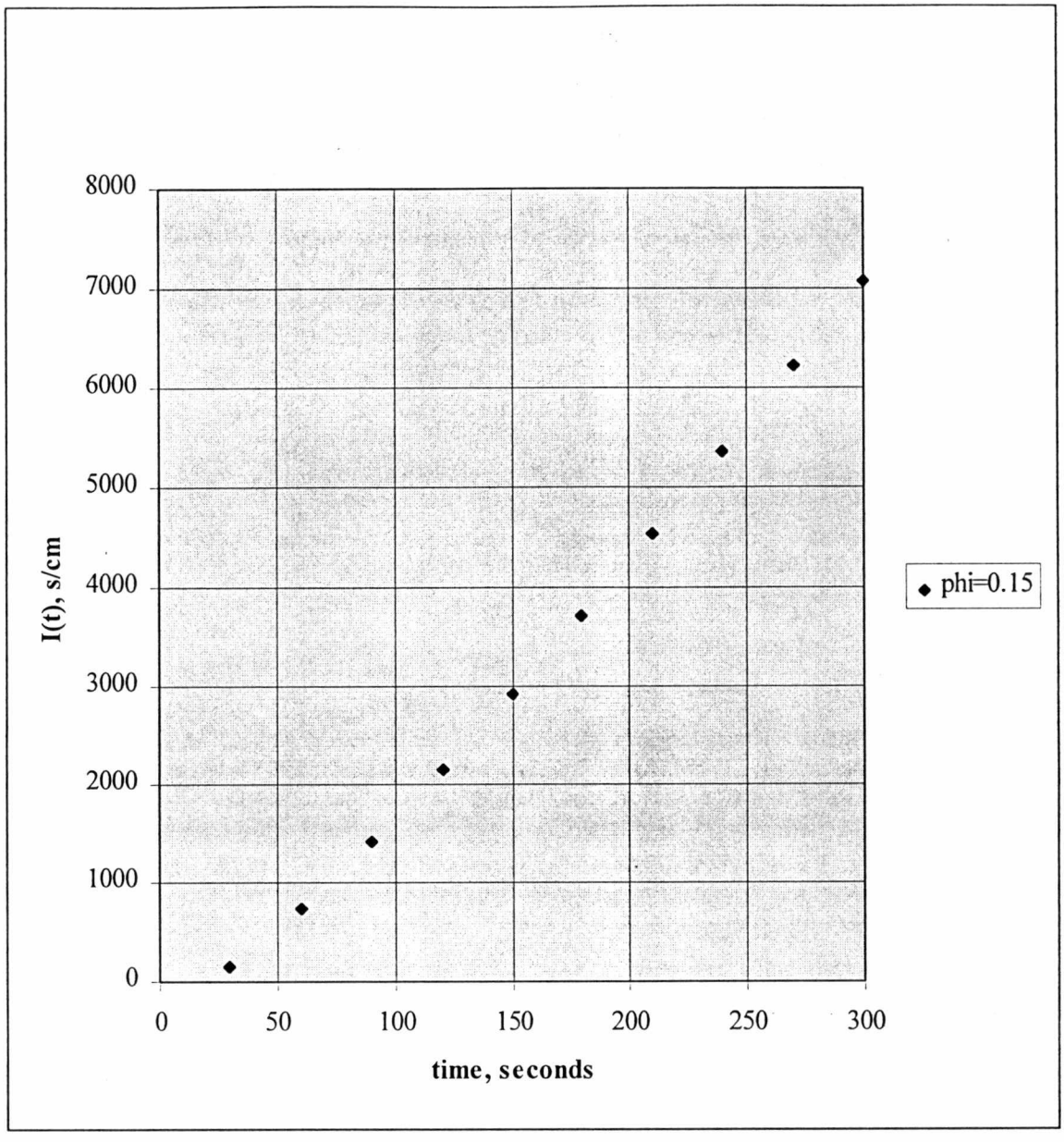

Figure A6.17: Plot of time t versus I(t) where $I(t) = \int_{20} \frac{1}{\alpha \cdot t^{-0.7} + d_{32}^{*}} dt$ for ϕ=0.15.

A.6.13. Calculation of k_d using Equation 1.11 where ϕ=0.20 and d=d_{32}

$\alpha := 0.3532$ $d := 0.038$

$$f(t) := \frac{1}{\alpha \cdot t^{-0.7} + d}$$

$$\int_{20}^{320} f(t)\,dt = 6.042 \cdot 10^3$$

$$\int_{20}^{300} f(t)\,dt = 5.592 \cdot 10^3$$

$$\int_{20}^{270} f(t)\,dt = 4.921 \cdot 10^3$$

$$\int_{20}^{240} f(t)\,dt = 4.259 \cdot 10^3$$

$$\int_{20}^{210} f(t)\,dt = 3.607 \cdot 10^3$$

$$\int_{20}^{180} f(t)\,dt = 2.966 \cdot 10^3$$

$$\int_{20}^{150} f(t)\,dt = 2.34 \cdot 10^3$$

$$\int_{20}^{120} f(t)\,dt = 1.733 \cdot 10^3$$

$$\int_{20}^{90} f(t)\,dt = 1.152 \cdot 10^3$$

$$\int_{20}^{60} f(t)\,dt = 609.238$$

$$\int_{20}^{30} f(t)\,dt = 132.83$$

slope=-0.0004 (from Figure 6.11)

Therefore from equation 6.4

$$k_d = -\frac{(slope)}{6}$$

$$\boxed{k_d = -\frac{-0.0004}{6} = 0.67E-04\,\frac{cm}{s}}$$

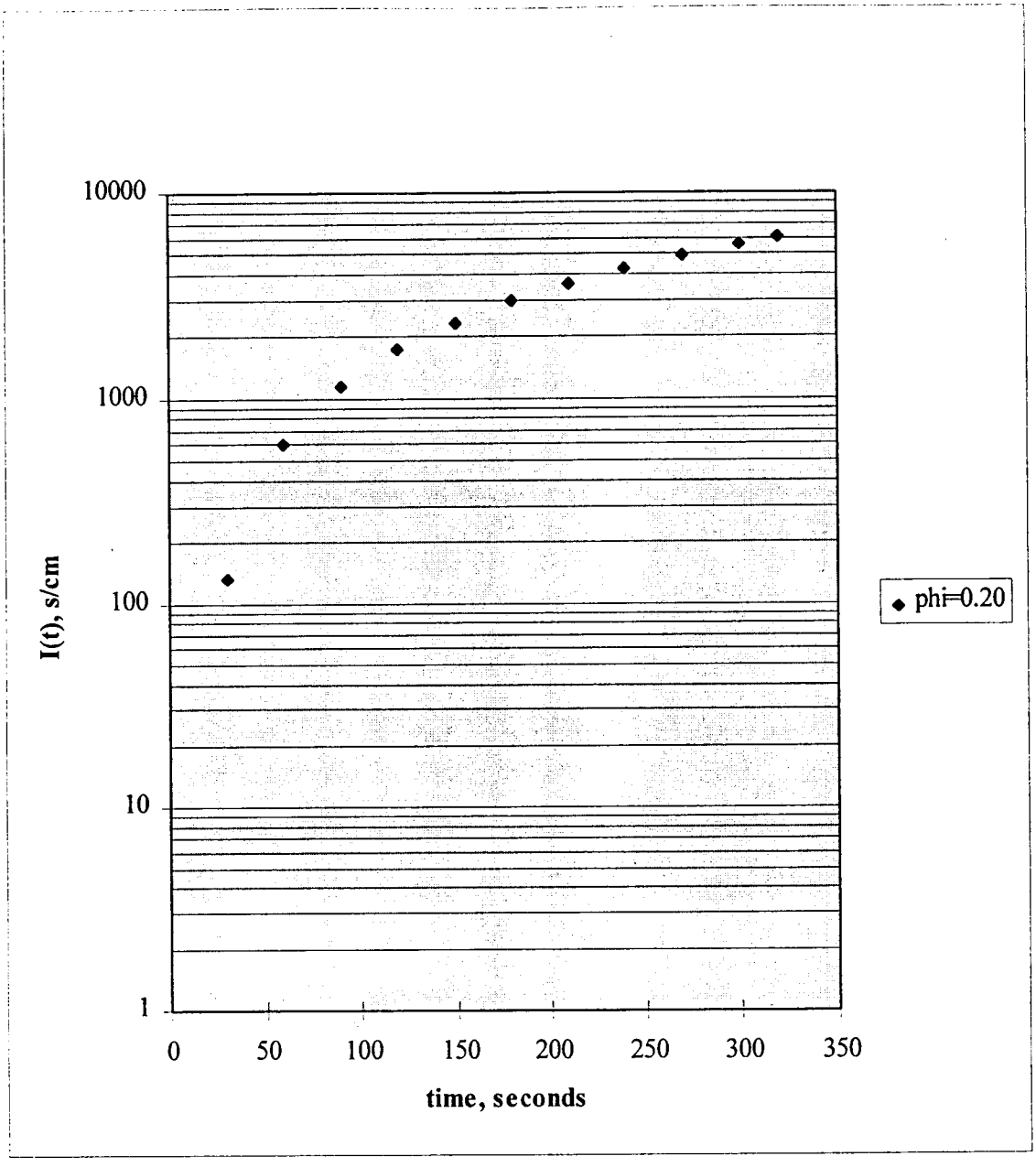

Figure A6.17: Plot of time t versus I(t) where $I(t) = \int_{20} \frac{1}{\alpha \cdot t^{-0.7} + d_{32}^{*}} dt$ for ϕ=0.20.

Table A6.20: Estimation of the Dispersed-phase Mass transfer coefficient using the Skelland and HuXien Model (1990)

Expt. Run	Diffusivit Dd Table3.4 cm^2/s	Volume Fraction $\phi = \frac{V_d}{V_T}$	Mean Viscosity μ_m P:g/cm-sec	Mean Density ρ_m g/cc	Final Transfer tf sec	$N_{Re_I} = \frac{\rho_m d_I^2 N}{\mu_m}$	$k_d = 5e-6\phi^{-0.0204}\sqrt{\frac{D_d}{t_f}}\left(\frac{d_I^2 N\rho_m}{\mu_m}\right)^{1.140}\left(\frac{\rho_c}{\Delta\rho}\right)^{0.518}$ cm/sec
1	1.94E-07	0.10	0.0211	1.0164	150	5172	1.2E-05
2	1.94E-07	0.10	0.0211	1.0164	150	5172	1.2E-05
3	1.94E-07	0.05	0.0187	1.0202	90	5862	1.87E-05
4	1.94E-07	0.20	0.0269	1.0088	320	4037	6.32E-06
5	1.94E-07	0.15	0.0238	1.0126	300	4569	7.56E-06
6	1.94E-07	0.05	0.0187	1.0202	90	5862	1.87E-05

Notes: N=250rpm dI=5.08cm density,viscosity from Table 3.2 Diffusivity from Table 3.3

Table A6.20: Estimation of the Dispersed-phase Mass transfer coefficient using the Skelland and HuXien Model (1990)

Expt. Run	Diffusivit Dd Table3.4 cm^2/s	Volume Fraction $\phi = \frac{V_d}{V_T}$	Mean Viscosity μ_m P:g/cm-sec	Mean Density ρ_m g/cc	Final Transfer tf sec	$N_{Re_I} = \frac{\rho_m d_I^2 N}{\mu_m}$	$k_d = 5e-6\phi^{-0.0204}\sqrt{\frac{D_d}{t_f}}\left(\frac{d_I^2 N\rho_m}{\mu_m}\right)^{1.140}\left(\frac{\rho_c}{\Delta\rho}\right)^{0.518}$ cm/sec
1	1.94E-07	0.10	0.0211	1.0164	150	5172	1.2E-05
2	1.94E-07	0.10	0.0211	1.0164	150	5172	1.2E-05
3	1.94E-07	0.05	0.0187	1.0202	90	5862	1.87E-05
4	1.94E-07	0.20	0.0269	1.0088	320	4037	6.32E-06
5	1.94E-07	0.15	0.0238	1.0126	300	4569	7.56E-06
6	1.94E-07	0.05	0.0187	1.0202	90	5862	1.87E-05

Notes: N=250rpm dI=5.08cm density,viscosity from Table 3.2 Diffusivity from Table 3.3

Table A6.21: Estimation of the Continuous-phase Mass Transfer Coefficient unsing the Skelland and Moeti (1990) Model

Expt. Run	Diffusivity cm^2/s Cont.	Volume Fraction	Viscosity P:g/cm-sec Cont.	Density, g/cc Cont.	Disp.	Nre 250 rpm	kc(dp=0.15mm) cm/sec
1	1.94E-07	0.10	0.0165	1.024	0.948	6658	3.52E-01
2	1.94E-07	0.10	0.0165	1.024	0.948	6658	3.52E-01
3	1.94E-07	0.05	0.0165	1.024	0.948	6658	4.98E-01
4	1.94E-07	0.20	0.0165	1.024	0.948	6658	2.49E-01
5	1.94E-07	0.15	0.0165	1.024	0.948	6658	2.88E-01
6	1.94E-07	0.05	0.0165	1.024	0.948	6658	4.98E-01

Equation Variables: N=250rpm dI=5.08cm density,viscosity from Table 3.2

Table A6.22: Summary of Dispersed-phase Mass transfer Coefficients as related to the Reynolds Number

			Dispersed-phase Mass Transfer Coefficient, cm/s					
Exp. Run	phi	Nrei	dp: 0.20mm	0.3mm	0.40mm	HuXien	Equation1.11	Penetration
1	0.10	5172	9.30E-05	1.40E-04	1.86E-04	1.24E-05	1.667E-04	4.13E-05
2	0.10	5172	1.07E-04	1.61E-04	2.15E-04	1.24E-05	1.667E-04	4.14E-05
3	0.05	5862	1.11E-04	1.67E-04	2.23E-04	1.87E-05	1.833E-04	5.31E-05
4	0.20	4037	2.87E-05	4.30E-05	5.73E-05	6.32E-06	6.667E-05	2.85E-05
5	0.15	4569	4.47E-05	6.70E-05	8.93E-05	7.56E-06	1.167E-04	2.91E-05
6	0.05	5862	1.20E-04	1.80E-04	2.39E-04	1.87E-05	1.833E-04	5.33E-05

A.6.13. Calculation of the Overall Mass Transfer Coefficient

$$\frac{k_c d_p}{D_c} = 1.237(10^{-5})\left(\frac{\mu_c}{\rho_c D_c}\right)^{1/3}\left(\frac{d_I^2 N \rho_c}{\mu_c}\right)^{2/3}\left(\frac{d_I N^2}{g}\right)^{5/12}\left(\frac{d_I}{d_p}\right)^{2}\left(\frac{d_p}{T}\right)^{1/2}\left(\frac{\rho_d d_p^2 g}{\sigma}\right)^{5/4}\phi^{-1/2}$$

(6.4)

The overall mass transfer coefficient, K is written in terms of k_c and k_d as

$$\frac{1}{K_d} = \frac{1}{k_d} + \frac{1}{mk_c} \quad ; \tag{6.5}$$

where, m is defined as

$$m = \frac{[Na_2SO_4]_{Aqueous}}{[Na_2SO_4]_{Organic}} \tag{6.6}$$

From Table 3.5, m ranges from 3.5 to 4.2. Since $k_c >> k_d$ as shown in Table 6.10 ,

$$K_d = k_d.$$

Table A6.23: Calculation of Overall Mass Transfer Coefficient

Expt. Run		Distribution Ratio* $m=[Na-]_d/[Na-]_c$	Mass Transfer Coefficient, cm/s		
			Moeti(1990) k_c(dp=0.3mm)	Experimental k_d(dp=0.3mm)	Overall K_d
1	0.10	4.160	3.52E-01	6.98E-05	6.97E-05
2	0.10	4.160	3.52E-01	8.05E-05	8.05E-05
3	0.05	4.160	4.98E-01	8.35E-05	8.35E-05
4	0.20	4.160	2.49E-01	2.15E-05	2.15E-05
5	0.15	4.160	2.88E-01	3.35E-05	3.35E-05
6	0.05	4.160	4.98E-01	8.98E-05	8.97E-05

VITA

Charlotte Mitcham Farmer was born in Macon, Georgia on August 6, 1964. She attended Meta T. Danforth Elementary School in Macon, Georgia and graduated from Brainerd High School in June, 1982. The following September she entered Tennessee Technological University and in May, 1987 received the degree of Bachelor of Science in Chemical Engineering. In January, 1991 she then entered The University of Tennessee Evening School and in December, 1996 received a Master of Science Degree in Chemical Engineering.

She is presently employed as a Innovation Project Manager within Corporate Development of Eastman Chemicals Company.